Calculation Methods in Geotechnics - Failure Mechanisms and Determination of Parameters

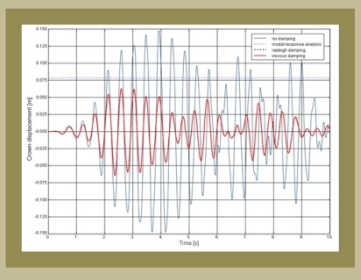

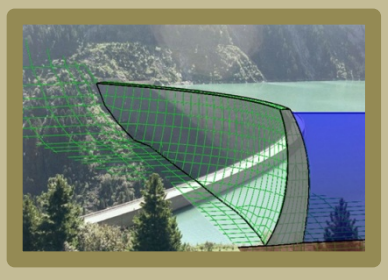

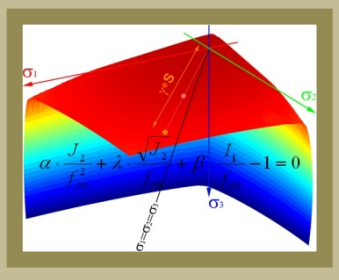

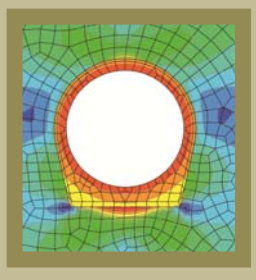

Compilation of Extended Abstracts
October 12th, 2011 – Salzburg, Austria

Table of Contents

Mechanisms of Progressive Failure in Brittle Argillaceous materials
The failure of Aznalcóllar Dam

A. Gens[1]
[1]Department of Geotechnical Engineering and Geosciences, Technical University of Catalonia, Jordi Girona 1-3, 08034 Barcelona, Spain
E-mail: antonio.gens@upc.edu

Abstract

This document presents a brief summary of the failure of Aznalcóllar dam, a catastrophic slide that caused one of the worst environmental disasters in Spain. The account includes a description of the failure and of the geometry and features of the slide and gives some information on the analyses carried out both of initiation of the failure and of the post-failure events. It was found that the main causes underlying the failure were the occurrence of progressive failure in the brittle foundation clay and the presence of very high pore water pressures in the foundation. The mechanism of the failure also explains the large post- failure movements (more than 50 m) that were responsible for the large spill of tailings.

Introduction

The Aznalcóllar tailings dam failed catastrophically in April 1998, causing one of the worst environmental disasters in Spain ever. The dam was part of a large open-cast mining complex that had been in operation for decades in the vicinity of Aznalcóllar village in the province of Seville, Spain. The tailings lagoon, which has an irregular hexagonal shape in plan view, was founded on a deposit of marine clays having a thickness of no less than 60 m in the centre of the lagoon. A plan view of the tailings deposit is given in Figure 1. A perimeter dam of increasing height was built over the years as the volume of tailings increased. The figure shows also a representative cross section of the dam, prior to the failure.

The confining embankment was conceived in the original design as a “downstream” construction rockfill dam. The embankment was built on top of a thin (4 m) upper granular alluvium overlying the marine clays (Fig. 2). An upstream blanket of Quaternary clay, covering the slope of the rockfill and connected to a shallow diaphragm wall, was designed to ensure the imperviousness of the embankment. As shown in Figure 1, the lagoon was divided into a larger Northern part and a smaller Southern one. An inner embankment or “jetty” was built to separate the two lagoons. Coarse pyroclastic tailings were mainly deposited in the Northern lagoon while finer pyritic slimes were deposited in the Southern lagoon. Tailings have been deposited in the lagoons since the beginning of 1978. The height and downstream extension of the embankment increased continuously for 20 years, as the accumulated volume of mine tailings increased. A safety evaluation was carried out in 1996 associated with a modified design that involved raising the height of the lagoon about 2 m above the original design.

The failure

Sometime during the early morning of the 25th of April, 1998 (when the eastern side of the embankment had a height of 28 m above the foundation) a failure took place involving a substantial section of the confining embankment. As a result, several millions of cubic metres of highly acid liquefied tailings poured into the Agrio and Guadiamar valleys. A twenty-four kilometre length of the Guadiamar River was affected by the mudflow. Figure 3 shows an aerial photograph of the breached embankment, the inundated valley and the partially emptied and eroded tailings. A detailed account is presented in [1] and [2].

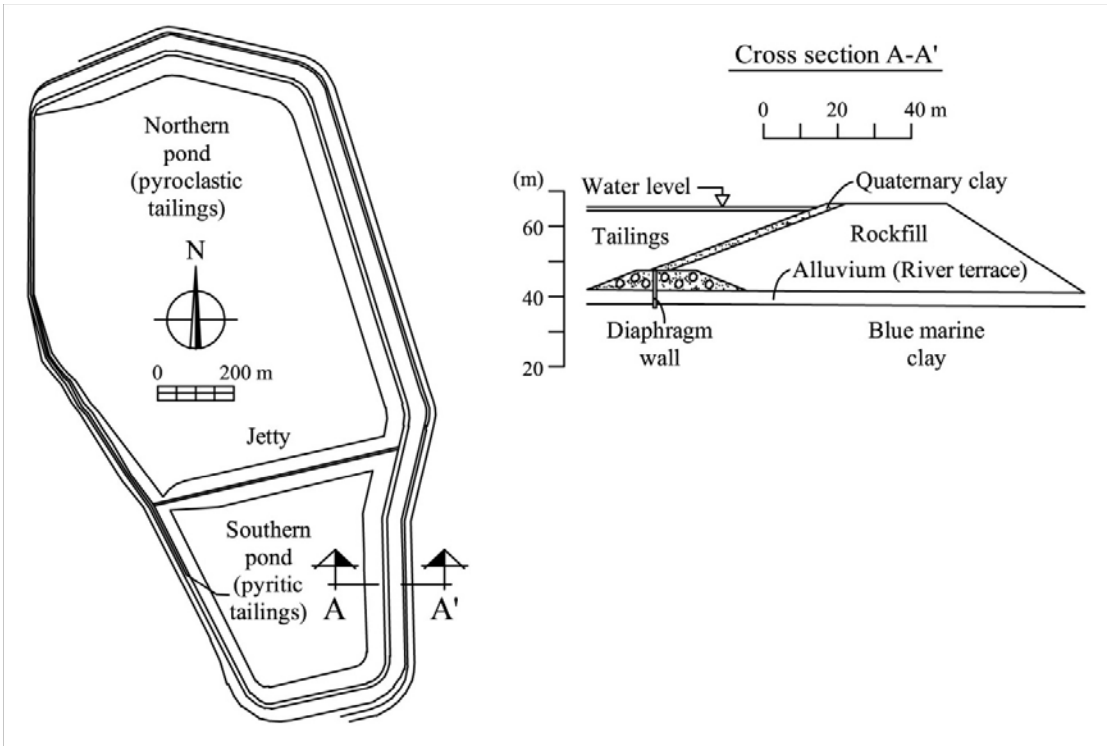

Figure 1: Plan view of the Aznalcóllar tailings deposit and representative cross section of the failed dam

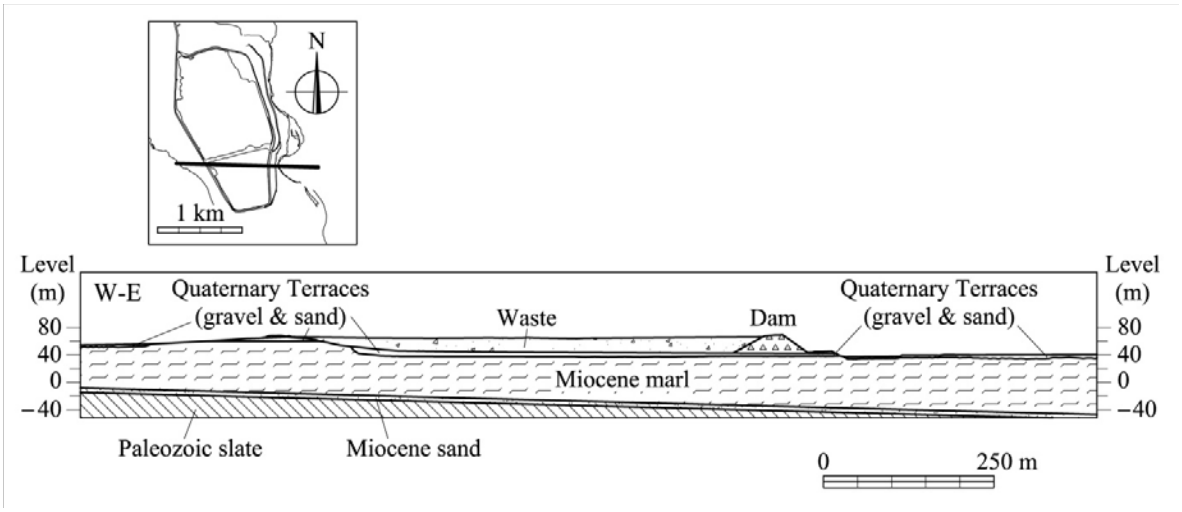

Figure 2: Cross-section of the tailings lagoon. Two stratigraphic discordances are observed: A lower one (high angle) between the Paleozoic substratum and the upper Miocene deposits, and an upper one (low angle), between the Miocene clays and the Quaternary deposits.

The breach in the embankment immediately north of the jetty which divided the Northern and Southern lagoons was a direct consequence of a deep translational slide, south of the breach, which displaced 600 m of embankment and its foundation towards the East. The failure surface was located inside the foundation blue clays. The displaced mass included the embankment, the alluvium terrace and about 10 m of the blue clay. Figure 4 shows the cross section of the slide at the position of Profile 4, defined by boreholes S4-1, S4-2 and S4-3. The boreholes located upstream of the embankment provided a precise position of the failure surface since the tailings were found in direct contact with the clay in some of them. In a number of boreholes it was also possible to identify the position of the sliding surface where a highly polished surface could be found.

Figure 3: A view of the breached dam a few hours after the failure.

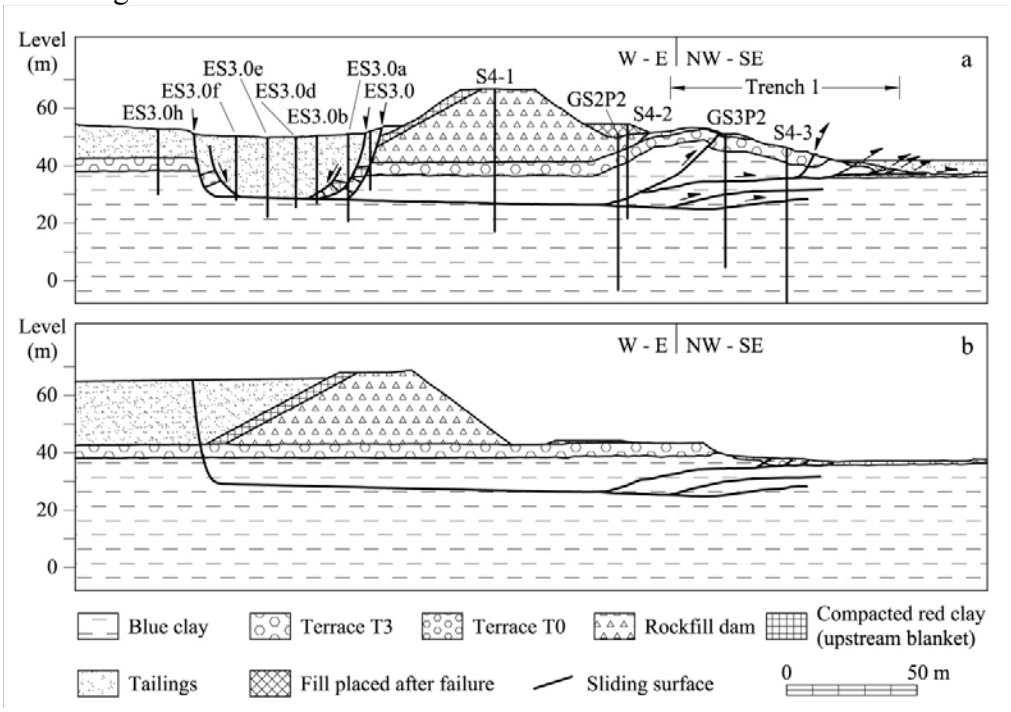

Figure 4: Cross-section of the slide at the position of Profile 4. (a) Geometry after the slide as interpreted from borehole results and surface topography, (b) Reconstruction of the position of the sliding surfaces before the failure.

Analysis of the failure

Finite element analysis

A large number of elastoplastic coupled flow-deformation analyses were performed, using the 2-D Plaxis code, with the purpose of increasing the understanding of the mechanisms leading to failure. Only some selected results are shown here. The process of dam construction and tailings impoundment was simulated in 11 steps. Each step was, in turn, divided into an undrained application of loading and a subsequent partial dissipation of the pore pressures until the next undrained unloading is applied. A total of 21 stages of calculation are thus defined. A Mohr-Coulomb elastic perfectly plastic model was adopted for all materials.

In a set of analysis a discontinuity with reduced strength characteristics was located at the position of the sliding plane. This involves an interesting issue because, if the reduced parameters chosen reproduce the final conditions, failure is predicted at a much earlier date (in phase 11, out of a maximum of 21). This result is consistent with previous findings, both in the simplified consolidation analysis and in the limit equilibrium calculation. It was necessary to adopt two sets of parameters: a "more resistant" set for the first part of the analysis, and a "weaker set" for subsequent calculations. This is not a procedure to simulate progressive failure, but it provides a strong indication of the need to reduce the available strength of the clay if the actual rupture mechanism is to be approximated. The following strength parameters were adopted for the analysis with a discontinuity plane:

Plane of discontinuity c' : variable between 1 kPa and 15 kPa; φ' = 21.5º

Clay above and below the critical plane c': 65 kPa; φ' = 24º (mass properties)

A drained cohesion, 15 kPa, was assumed to correspond to the initial phases and c' = 1 kPa was a further reduction of cohesion for the subsequent phases.

This FE analysis also provided data relating to the evolution of pore water pressures in the foundation. A profile of water pressures along the future failure plane is shown in Figure 5.

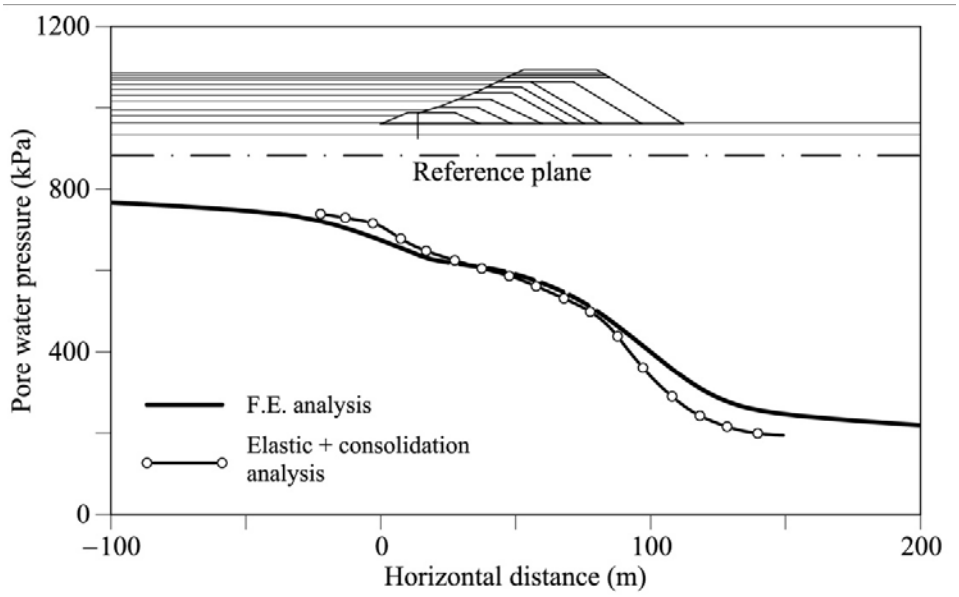

Figure 6: Distribution of pore water pressures along the failure surface (reference plane). Comparison of FE and simplified elastic-consolidation analysis. Horizontal coordinates start at the upstream toe.

The analysis also confirms that the shear deformations accumulate on the potential failure plane and they extend as the embankment construction advances (Figure 6a). The rupture mechanism, identified by means of the mesh deformation (Figure 6b) is similar to the actual failure mechanism described above. The failure phase was induced by a final reduction of strength parameters. Figure 6b shows the passive wedge developed at the distal end of the slide and a classic upstream active wedge (the model did not include the vertical jointing existing in the clay unit).
A new analysis fully incorporating progressive failure is currently being performed and it will be described in the oral presentation.

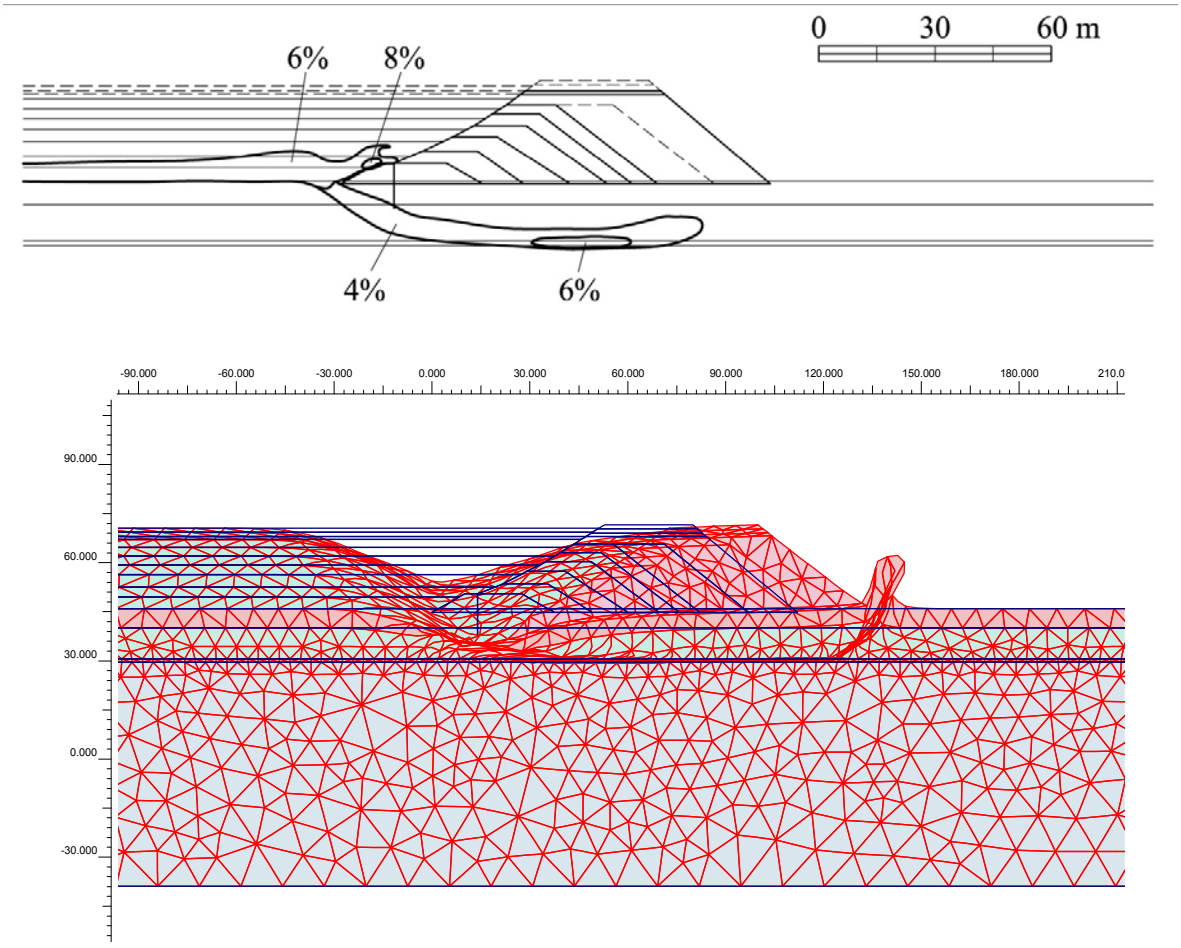

Figure 6: (a) Contours of accumulated shear deformations from the origin of calculations (maximum deformation: 22.35%); (b) Mesh deformation during the failure process.

Analysis post failure
An analysis of the dam and its foundation just after the onset of failure was also performed [3]

but the details are outside the scope of this Abstract. It can be mentioned, however, that the analysis of the dynamics of motion was able to reproduce in a robust manner several features of the failure including the distance travelled by the dam. The analysis provided information on several unknown aspects of the motion. It was found that the motion was rapid and it came to rest 15 seconds after the initiation. The calculated maximum velocity and acceleration (20 km/h and 0.14 g, respectively) provide key insights for a better understanding of the slide and, more importantly, of its consequences.

It has also been shown that the motion stopped because the driving force was reduced, due to the reduction in the level of the volume of liquefied tailings. This reduction is the consequence of the movement of the slide itself, which enlarged the basin being opened upstream of the dam. It is also interesting to realise that the (moderate) increase in resistance, offered by the passive wedge being developed at the distal extreme of the slide, played a very limited role in stopping the motion.

Conclusions

The Aznalcóllar failure is an unusual case of deep translational progressive failure involving the entire dam, which displaced a large distance (more than 50 m in the central part) as a rigid body and suffered only minor distortions. It is also interesting to note that the failure did not involve any shearing of the tailings or the rockfill bur it took place mostly in the foundation clay.

It is clear that the clay had a strong potential for progressive failure given its brittleness. In addition, the downstream construction of the embankment is a process that favours the development of this mechanism. The large quasi-horizontal displacement of the dam is another interesting feature of this failure, which has to be related to the evolution of driving and resisting forces, once the failure has initiated. The brittleness of the clay and the low residual friction angle indicate that, once the failure has initiated, there is a potential for an accelerated motion due to the progressive loss of clay strength.

A second contributing factor to the failure was the fact that in the design potentially high water pressures due to the undrained loading of the foundation clay. The low permeability of the clay led to very limited dissipation of pore pressures over the twenty years of dam construction.

Acknowledgements

The contribution of E.E. Alonso, co-author of the report on the failure, is gratefully acknowledged. Thanks are also due to my colleagues J. Alcoverro, A. Lloret, C. López, J. Moya and E. Romero for their assistance during the investigation on the Azanalcóllar dam failure.

.

References

Alonso, E. E., Gens, A. (2006). Aznalcóllar dam failure. Part 1: Field observations and material properties. Géotechnique, Vol. 56, pp. 165–183

Gens, A., Alonso, E. E., (2006) Aznalcóllar dam failure. Part 2: Stability conditions and failure mechanism. Géotechnique, Vol. 56, pp. 185–201

Alonso, E. E., Gens, A. (2006). Aznalcóllar dam failure. Part 3: Dynamics of the motion. Géotechnique, Vol. 56, pp. 203–210

From the interaction of material parameters and calculation approaches

R. Poisel [1], K. Mair am Tinkhof [1], and A. Preh [1]
[1] Institute for Geotechnics, Vienna University of Technology, Karlsplatz 13, A-1040 Wien, Austria
E-mail: rainer.poisel@tuwien.ac.at

Abstract

Geotechnics falls back on empirical, semi empirical, conventional approaches (usually limit equilibrium equations) and various numerical models. Back calculations of real failures often show the dependence of material parameters from the mechanical model used. This fact is generally called „model factor“. That means that especially in rock mechanics there are no universally valid parameters of a certain material, but the parameters depend on the mechanical model. This fact is demonstrated with the help of the rock slope failure mechanisms “sliding of a block” and “block toppling“.

Introduction

Investigations of the stability of a structure need models
- of the structure (e.g. a model of the failure mechanism),
- of the behaviour of the material (e.g. a model of the material strength) and
- of the load.

Usually these models are set up independently from each other. Taking the examples of rock slope failure mechanisms “sliding of a block” and “toppling”, it is shown that the model of the behaviour of the material (i.e. the friction angle) is dependent on the model of the structure.

Analytical stability investigations

Sliding of a block

The friction angle of a joint between two blocks can be determined by increasing the dip of the joint between two blocks until the upper block slides (“tilt test”; Fig 1).

The angle of friction of the joint between the two blocks follows from the condition for limit equilibrium (Fig. 1):

$$N = 0 \;\Rightarrow\; G \cdot \cos\alpha \cdot \tan\varphi_s - G \cdot \sin\alpha = 0 \;\Rightarrow\; \boldsymbol{\varphi_s = \alpha} \qquad (1)$$

Toppling of a single block

Toppling of a single block occurs if the base friction angle is high enough to prevent sliding and if the following condition for limit equilibrium is satisfied (Fig 2):

$$M = 0 \;\Rightarrow\; -G \cdot \sin\alpha \cdot h/2 + G \cdot \cos\alpha \cdot b/2 = 0 \;\Rightarrow\; \boldsymbol{\alpha = \arctan(b/h)} \qquad (2)$$

Equation (2) means that the center of gravity has to lie outside the base for toppling taking place.

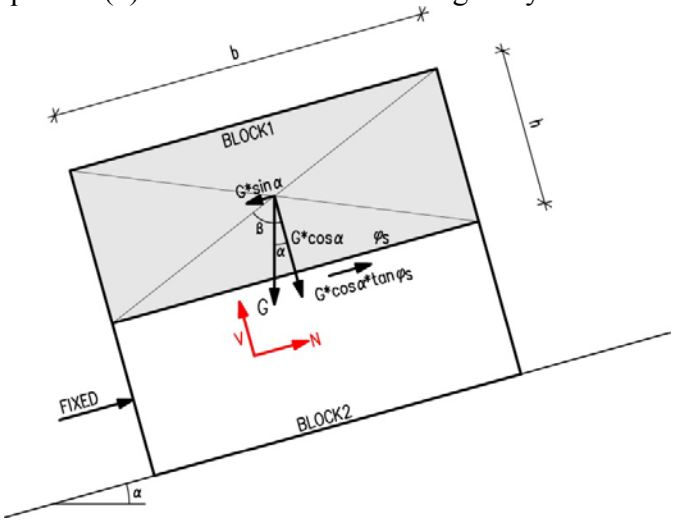

Figure 1: Forces acting on a block lying on an inclined plane

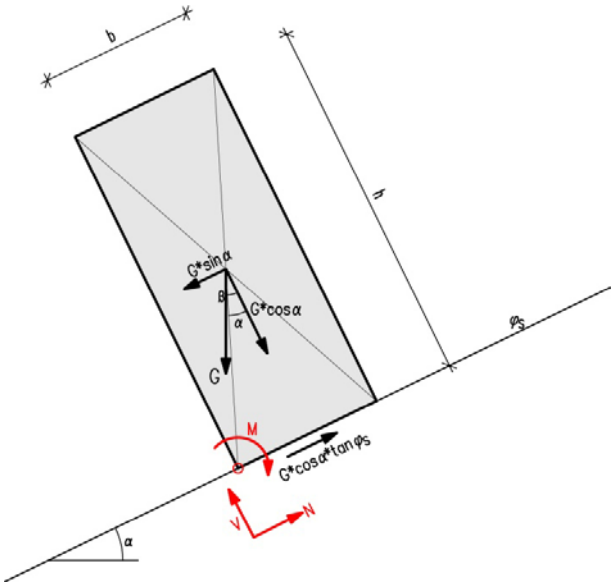

Figure 2: Forces acting on a toppling block

Toppling of two blocks

Increasing the dip of the base plane of two blocks leaning against each other (Fig 3), the friction angle of the joint between the two blocks is determined by evaluating the conditions for limit equilibrium [1]:

Upper block:

Sliding: $N = 0 \;\Rightarrow\; G \cdot \sin\alpha - P - (G \cdot \cos\alpha - P \cdot \tan\varphi_t) \cdot \tan\varphi_s = 0$ (3)

(4)

Toppling: $M = 0 \Rightarrow \mathrm{P} \cdot \mathrm{h_P} - G \cdot \sin\alpha \cdot h/2 + G \cdot \cos\alpha \cdot b/2 = 0$

Lower block:
Sliding: $N = 0 \Rightarrow G \cdot \sin\alpha + P - (G \cdot \cos\alpha + P \cdot \tan\varphi_t) \cdot \tan\varphi_s = 0$ (5)

Toppling: $M = 0 \Rightarrow -\mathrm{P} \cdot \mathrm{h_P} + P \cdot \tan\varphi_t \cdot b - G \cdot \sin\alpha \cdot h/2 + G \cdot \cos\alpha \cdot b/2 = 0$ (6)

Toppling condition for two blocks:
(4)-(6) $2 \cdot \mathrm{P} \cdot \mathrm{h_P} - P \cdot \tan\varphi_t \cdot b = 0 \Rightarrow \boldsymbol{\varphi_t = \arctan(2h_P / b)}$ (7)

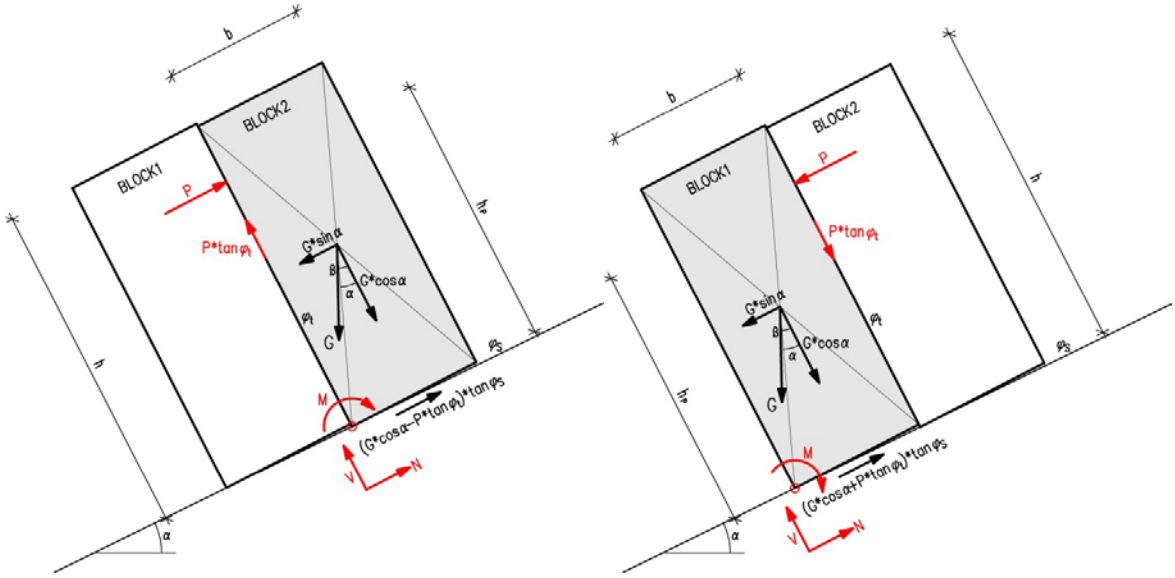

Figure 3: Forces acting on two toppling blocks (left: forces on upper block, right: forces on lower block)

Applying this model of toppling blocks, the point of application of P, h_P, is unknown. Generally it is assumed that h_P equals h [3].

Laboratory experiments

Sliding and toppling tests were performed in the laboratory using two blocks of conglomerate and two blocks of sandstone. The base of the blocks was a wooden board mounted on a hinge, thus making increasing dip angles possible (Figures 4 and 5).

In both tests the lower block was fixed on the wooden board in order to avoid sliding of the lower block. Then the dip of the board was increased, until either the upper block began to slide downwards or both blocks toppled.

Table 1 shows the properties of the blocks and the dip angles of the board when sliding (α_s), toppling of one block (α_{t1}) and toppling of two blocks (α_{t2}) occurred.

[1] Table 1: Properties of the blocks used and results of laboratory experiments

Samples	**block height [cm]**	**block width [cm]**	**material density [kg/m³]**	**sliding angle α_s [°]**	**toppling angle 1 block α_{t1} [°]**	**toppling angle 2 blocks α_{t2} [°]**
Conglomerate	15,0	7,3	2460	29,0	25,5	33,0
Sandstone	20,0	7,0	2030	26,0	25,0	34,0

Figure 4: Sliding of a block (tilt test); left: conglomerate; right: sandstone

Figure 5: Toppling of two blocks; left: conglomerate; right: sandstone

Back calculation of the friction angle between blocks

Sliding of the upper conglomerate block on the lower conglomerate block took place when the dip of the contact plane α_s exceeded 29° (Table 1). Sliding of the upper sandstone block on the lower sandstone block took place when the dip of the contact plane α_s exceeded 26°. Following Equation (1) the friction angle of the contact plane between the conglomerate blocks is 29° and the friction angle of the contact plane between the sandstone blocks is 26° back calculated by the sliding tests (Table 2).

Following Equation (7) the friction angle of the contact plane between the conglomerate blocks is 76° and the friction angle of the contact plane between the sandstone blocks is 75° back calculated by the toppling tests.
The discrepancy between the friction angles back calculated from sliding and toppling tests is reduced when h_P is assumed to be smaller than h in the analytical model or when the numerical model UDEC [2] is used. Assuming h_P to be e.g. h/2 yields friction angles of the contact planes between the blocks of 64°. In a UDEC model of the toppling tests the conglomerate blocks topple at a dip of the base plane α_{t2} of 33°, when the friction angle of the contact plane φ_t is 41°, and the sandstone blocks topple at a dip of the base plane α_{t2} of 34°, when the friction angle of the contact plane φ_t is 38°. However, the friction angles determined by sliding tests and by toppling tests do not coincide.

[2] Table 2: Back calculation results

Samples	**sliding angle** α_s [°]	**toppling angle 2 blocks** α_{t2} [°]	**friction angle sliding** φ_s **analytical** [°]	**friction angle toppling** φ_t **analytical** $h_P = h$ [°]	**friction angle toppling** φ_t **analytical** $h_P = h/2$ [°]	**friction angle toppling** φ_t **UDEC** [°]
Conglomerate	29,0	33,0	29,0	76,0	64,1	41,0
Sandstone	26,0	34,0	26,0	75,0	63,5	38,0

Conclusion

The simple examples of the rock slope failure mechanisms “sliding of a block” and “toppling” show that the friction angles back calculated from sliding and toppling tests using the same blocks and the same contact planes do not coincide. Thus, they reveal that the model of rock behaviour (i.e. the friction angle) is dependent on the model of the structure (i.e. on the mechanical model of the failure mechanism) and cannot be determined as a certain value. There is no “friction angle” of a certain type of rock valid for every failure mechanism. Every material (rock) has different friction angles for different models of the structure (e.g. for different failure mechanisms).

In other words, models agree with reality only to a limited extent. Thus the deviations of the

model of the structure, of the material behaviour and of the load from reality have to compensate each other in order to make agreement with reality possible. As different models of the structure have different deviations from reality, the models of material behaviour have to have different deviations from reality as well. Thus, friction angles determined by sliding of a block are different from friction angles determined by toppling blocks.

References

Goodman R.E., Bray J.W. (1976). Toppling of rock slopes. Proc. of the Specialty Conference on Rock Engineering for Foundations and Slopes ASCE/Boulder, Colorado, pp. 201-234.

Itasca (2011). UDEC: Universal Distinct Element Code, version 5.0, User's guide. Minneapolis: Itasca Consulting Group.

Wyllie D., Mah C. (2004). Rock slope engineering. Spon Press, London.

The new RVS 09.01.42 (Tunnel structures in soft soil under built-up areas)
Design Concept and Benchmark

M. Brandtner[1], M. Hofmann[2], P. Hölzl[3], E. Saurer[4] and H. Walter[5]
[1] IGT Geotechnik und Tunnelbau ZT-GmbH, Salzburg, Austria
[2] ALPINE BeMo Tunnelling GmbH, Innsbruck, Austria
[3] PCD ZT-GmbH, Wien, Austria
[4] ILF Consulting Engineers, Rum/Innsbruck, Austria
[5] Ingenieurkonsulent f. Bauingenieurwesen, Dr.-A.-Altmann-Str. 24, 5020 Salzburg, Austria

E-mail: hw@zthw.at

Abstract

The new issue of RVS 09.01.42 follows the semi-probabilistic design concept of the Eurocode. Standard cases (2-D finite element analyses of tunnel cross sections applying non-linear constitutive relations for the ground and linear elastic material laws for the support) should be analysed using Design Approach DA 2* of EN 1997-1. Additional specifications deal with situations where Design Approach DA 3 has to be applied for ultimate limit state analyses. Finally, suggestions are made in RVS 09.01.42 how to tackle problems when the support is modelled using constitutive relations with implicit limitation of the stress level at high strains.
In order to gain insight into the effects of different design methodologies and Design Approaches a simple benchmark has been studied: The analysis of a bedded circular tunnel lining has been chosen and nonlinear constitutive relations for concrete have been adopted from EN 1992-1-1 and EN 1992-2.
The design methodologies of these codes for ultimate limit state analysis were compared with the procedure suggested in RVS 09.01.42 by means of a parameter study of the benchmark problem. The procedure specified in EN 1992-2 proved to be most conservative. EN 1992-1-1 is somewhat less conservative (by up to 15 % in terms of the maximum characteristic distributed load). With higher bedding stiffness and higher amount of reinforcement the differences decrease. The suggested procedure in RVS 09.01.42 is still less conservative, by another 5 to 15 %. This result is surprising given that the product of all safety factors is identical with EN 1992-1-1. A good match between RVS 09.01.42 and EN 1992-1-1 was obtained by reduction of the ultimate strain in addition to strength.

Motivation

The Austrian guideline RVS 09.01.42 “Tunnel structures in soft soil under built-up areas” 0 is currently being revised. At the time of the previous issue in 2004 0, Eurocode 7 0 was about to be published, but many aspects of the practical application of the semi-probabilistic safety concept were still under discussion. As partial safety factors were already introduced at that time for concrete and steel design this previous issue contained already some regulations concerning tunnel analysis and design for cyclic excavation based on the partial safety factor concept. It was already obvious that the concept proposed in Eurocode 7 0 has its limitations in connection with

numerical methods using nonlinear constitutive laws for both soil and support. In the meanwhile experience and expertise in the application of the partial safety factor concept in general, and the three design approaches of EN 1997-1 0 in particular, have increased. The strengths and limitations of each of the design approaches have become obvious.
Whereas nonlinear constitutive relations for soil have been used already for decades, combining them with nonlinear material laws for the support has been restricted to comparatively few applications. These applications have remained beyond the scope of standards and guidelines. Using nonlinear material laws for the support allows redistribution of forces from highly stressed parts of the support structure to less stressed parts. This may result in a more economic design. However, care has to be taken that a reasonable level of safety is maintained. With the re-design of RVS 09.01.42 0 these advanced techniques should be dealt with, maintaining an appropriate level of safety in accordance with the semi-probabilistic concept of the Eurocodes 0-0 being the first goal.
For retaining structures, which include tunnel linings in the broadest sense, Design Approach DA 2* is the most practical for standard cases. The asterisk indicates that effects of actions, and not the actions itself, are multiplied by a safety factor. It involves the least work in the transition to the Eurocodes. This procedure is also intended as standard in the Austrian guideline RVS 09.01.42 “Tunnel structures in soft soil under built-up areas” in the 2004 issue. However, it is not directly applicable in the case of constitutive laws for the support which limit the possible stress level. Possible remedies have been suggested, but their effect on the safety (in comparison with the established Design Approaches) still needs clarification. To this end, a simple benchmark has been devised and investigated to some depth.

Specifications for Analysis and Design in RVS 09.01.42

History of RVS 09.01.42
Up to 2004, use of the conventional safety concept with global safety factors was specified in RVS 9.32 (the former name of RVS 09.01.42). NATM tunnels were usually investigated by analyzing representative 2D plane strain sections, for the ground linear elastic – perfectly plastic constitutive laws like the Mohr-Coulomb-model were applied. For the shotcrete – frequently the most important means of support – beam elements with linear-elastic material behaviour were employed. For the friction angle and cohesion of the ground nominal values were utilized. Different values of stiffness of young and mature shotcrete were suggested. The reinforcement was designed according to 0 with a global safety factor on internal forces.
Starting with the 2004-issue 0, it was distinguished between partial safety factors on actions and partial safety factors on resistances for ultimate limit state design. Additionally, a separate serviceability limit state design was introduced. In accordance with the specifications for retaining structures in Eurocode 7 0 and the National Annex 0, use of Design Approach DA 2* has been specified. Failure of the soil is governed by strength parameters, which are hardly dependent on the dead load of the ground. Amplification of the dead load directly by a factor does not result in additional safety. Since active soil pressure and soil resistance is a result of the analysis, the boundary between active and passive regions cannot be known in advance. Compared with the pre-2004-issues of RVS 9.32 0 the required amount of reinforcement decreased slightly.
Experience with both the pre-2004-issues and the 2004-issue suggests a sufficient level of safety. The authors are not aware of any damage to a shotcrete lining which could be attributed to

insufficient safety margins in the design of the reinforcement.

Current version of RVS 09.01.42
In the current versions two aspects of the design have been paid more attention to:

- The stability of an unsupported face which is dominated by the shear parameters of the ground. Here application of Design Approach 3 is suggested in the guideline.
- Numerical tools in combination with non-linear material laws for support which implicitly confine the allowable stress level of the support do not allow the application of DA 2* any more: Internal forces cannot be increased beyond the inherent limits of the material law; amplification works only within the elastic range of the material description. As a remedy, one can either use Design Approach 3 where the partial safety factor on permanent (geotechnical) actions is 1.0. (Variable actions can be increased directly by a factor of 1.5/1.35 = 1.11.) This option is also specified in Appendix A of ÖNORM B 1997-1-1 0, with the restriction that relatively conservative values for the partial safety factors on friction angle and cohesion of the ground are used. This option is primarily focused on failure of the ground (GEO) 0. If possible failure of the support is predominant (STR) the only remaining option appears to be applying an overall safety factor on the strength parameters of the support.

In the current issue of RVS 09.01.42 0 it has been specified, that both types of failure should be investigated, and that the global safety factor on the support strength parameters should be chosen as $\gamma_R \cdot \gamma_E$, where γ_R is the partial safety factor on the support strength parameters and γ_E is the partial safety factor on effects of actions.
These specifications are plausible and appear to guarantee a reasonable safety level. In order to gain more insight into the effects of different assumptions, the RVS-specifications had to be compared with specifications directly in the Eurocodes. As a first step, a simple benchmark has been devised.

Benchmark

General Design
It is not an easy task to find an example which allows straight-forward comparison of different design methodologies if nonlinear constitutive relations for both ground and support are used. (Either DA 3 cannot be used because the shear strength of the ground is not considered, or the failure criterion in shear prevents direct application of partial safety factors on dead load.) A simple way to cover at least some ground-support-interaction is a collapse load analysis for the secondary lining of a typical tunnel cross section. In the chosen example the lining is circular, and bedded by radial springs with constant stiffness in compression and no stiffness in tension. The lining is loaded by a constant distributed load in vertical direction, see Figure 1. Stiffness and strength of the support (i.e. the secondary tunnel lining) interact with the stiffness of the ground. The strength parameters of the ground do not affect the results. The analysis is performed using different software packages.

Geometry
The geometry of the structural model is given in Figure 1.
Geometric parameters are given in Table 1.

[3] Table 1: Geometry / Parameters

Geometry / Parameters	**Unit**	**Value**
Secondary lining thickness h	cm	40
Tunnel radius R (to lining centerline)	m	5.0
Reinforcement a_s per face	cm^2	3.85
Concrete cover (to center of reinforcement)	cm	5.0

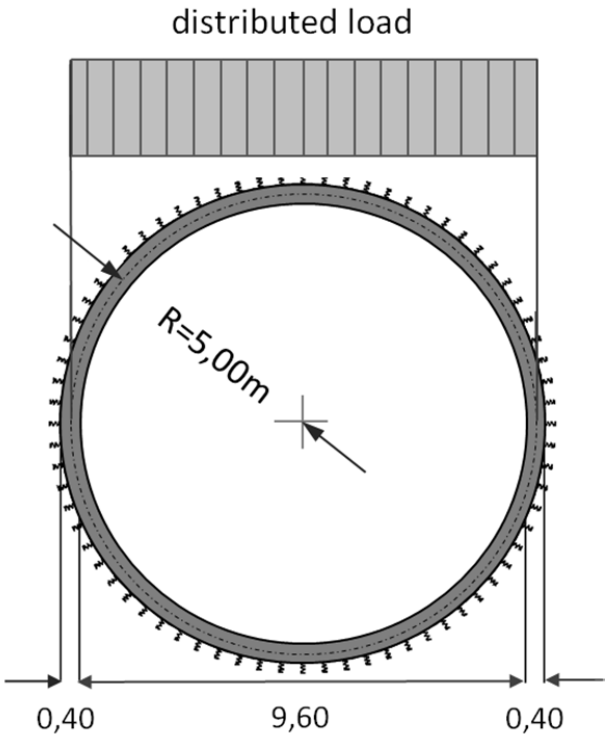

Figure 1: Structural model, bedding and ground pressure

Material and bedding properties
Used material properties for concrete grade C25/30 are given in Table 2.

[4] Table 2: Material properties for concrete grade C25/30

Properties	**Unit**	**Value**
Young's modulus E_{cm}	GPa	31
Mean compressive strength f_{cm}	MPa	33
Characteristic cylinder strength f_{ck}	MPa	25
Design strength f_{cd}	MPa	16.67
Mean tensile strength f_{ctm}	MPa	2.6

Both, the concrete tensile strength and the effects of tension stiffening are neglected in a first run. Material properties for reinforcement (steel grade B550B) are given in Table 3.

[5] Table 3: Material properties for reinforcement B550B

Properties	**Unit**	**Value**
Young's modulus E_s	GPa	200
Yield strength f_{yk}	MPa	550
Design yield strength f_{yd}	MPa	478
Min value of ratio k $(=f_t/f_y)_k$	-	1.08
Strain at maximum load ε_{uk}	%	≥ 5.0

The lining is bedded with springs in radial direction having a bedding stiffness of k_S=20 MN/m³.

Load
Only a constant, vertical load is applied to the structure, acting over the tunnel diameter on the projected length (see Figure 1). Dead loads are neglected.

Design methodologies
Design Approach DA3 according to Eurocode 7 0 is not suitable for this problem type (no effect of ground shear strength on the results). As a consequence, mainly design methodologies suggested by Eurocode 2 are applied for the analysis, such as:

Methodology according to EN1992-1-1, clause 5.8.6 0 (the only clause in this standard which deals with ultimate limit states in conjunction with non-linear analysis)

Nonlinear procedure according to EN1992-2, clause 5.7 0. In this procedure an overall safety factor $\gamma_O = 1.27$ is used.

Both procedures are based on the stress-strain-relation of 0, clause 3.1.5, and not on the parabola-rectangle-diagram, 0, clause 3.1.7.
Additionally, the method stipulated in RVS 09.01.42 0 (double reduction of material strength) is investigated. In this case, the procedure according to 0, clause 5.8.6, is applied, but with further reduction of the strength parameters. For details see 0-0.

Stress-strain relationship of concrete
Depending on the design methodology different stress-strain relationships for concrete are needed:

- Stress-strain relationship for structural analysis according to EN 1992-1-1 0, clause 5.8.6. (σ_{NL1} in Figure 2). In equation (3.14) and for the determination of the ratio k, the mean compressive strength f_{cm} is replaced with the design compressive strength f_{cd}. Furthermore, E_{cm} will be replaced with $E_{cd} = E_{cm}/\gamma_{CE}$ (see Table 4 for safety factors).
- Stress-strain relationship according to EN 1992-2 0, clause 5.7 (σ_{NL2} in Figure 2).The methodology according to EN 1992-2, clause 5.7 is based on the stress-strain relationship following equation (3.14) with replacement of f_{cm} in equation (3.14) and the k-value by γ_{cf} f_{ck} ($\gamma_{cf} = 1.1\ \gamma_S/\gamma_C$).
- Doubly reduced strength parameters according to RVS 09.01.42 0, chapter 5 (σ_{NL3} in Figure 2). The characteristic support properties are reduced with factor $\gamma_R \cdot \gamma_E$ where γ_R represents the partial factor of safety (material) according to relevant standards and γ_E a factor according to RVS 09.01.42, clause 5.2.

[6] Table 4: Safety factors applied for stress-strain relationship of concrete

Safety factors		**Value**
γ_{CE}		1.2
$\gamma_{cf} = 1.1\ \gamma_S/\gamma_C$		0.843
with	γ_S (partial factor of safety for reinforcement)	1.15
	γ_C (partial factor of safety for concrete)	1.5
$\gamma_R \cdot \gamma_E$		2.025
with	$\gamma_R = \gamma_C$ (partial factor of safety for concrete)	1.5
	γ_E (partial factor of safety for permanent actions)	1.35

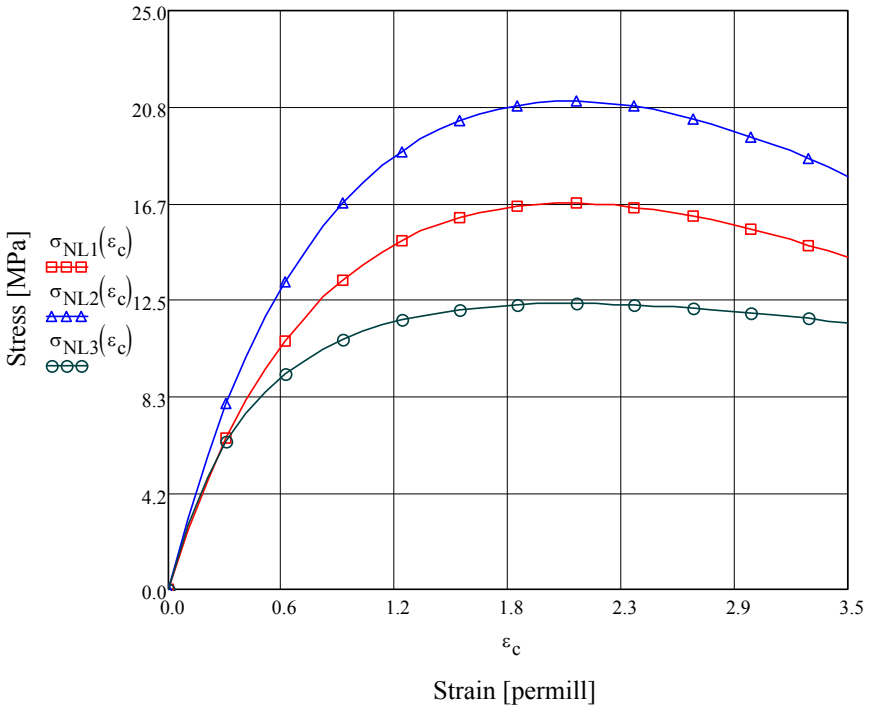

Figure 2: Stress-strain relationship of concrete under compression.

The benchmark is checked for ultimate limit state (ULS) only - serviceability state checks (such as limitations for crack width, stresses, deformation) are not accounted for.

Software packages, discretization

Four finite element programs have been employed to carry out the test. In all of them the model is discretized with beam elements. Bedding is simulated using radial springs (active only in compression).

Two of the packages handle material nonlinearities by numerically integrating the stresses in thickness direction over a number of layers. Another two packages use a flexibility based approach, handling the nonlinearity based on the relationship between moment and curvature. To

ensure that nonlinearity of concrete and steel is treated correctly in all programs, a simple test on a cantilever beam with a moment and an axial force at the free end has been carried out. The programs used in this benchmark are listed below; all of them passed this check.

- Program M (layered beams)
- Program Z (layered beams)
- Program S (flexibility based approach)
- Program C (flexibility based approach)

In all packages two-node beams are chosen, except in program M, which offers three-node beam elements as well. The model has an equal amount of nodes.
The number of layers and the layer thicknesses for the benchmark are different in programs M and Z and have been chosen according to previous experience with those packages (17 concrete layers with varying thickness in program M, 20 concrete layers with constant thickness in program Z). In both programs the reinforcement layers have been modelled as thin steel layers. The results obtained with programs M and Z were close enough to each other that one can assume that the integration over the thickness is accurate enough. All analyses are load driven.

First Results

In a first step results had to be obtained for the case without tension stiffening. It was found that the resulting ultimate load strongly depends on the mesh size which was chosen in a first guess according to experience. It turned out that the mesh dependency is mainly caused by the distance of integration points from the location of extreme bending moments. To achieve better comparability afterwards the secondary lining has always been divided into 60 beam elements (programs Z, S and C) and 30 beam elements (program M) and 60 springs. Care was taken that in all models one integration point is situated at the uppermost point of the ceiling (extremum of the bending moment).

With the adjusted mesh defaults, the following ultimate limit loads have been determined for characteristic material strength (f_{cm}, f_{yk}):

[7] Table 5: Ultimate Distributed Load without Tension Stiffening

Program	**Unit**	**Ultimate Load**
M	kPa	540
Z	kPa	530
S	kPa	298
C	kPa -	500

It appears that programs with a flexibility based approach have problems to overcome a certain point when approaching the ultimate limit state. The results of programs which are based on layered beam formulation are similar.

In a next step tension stiffening was taken into account. The left graph in Figure 3 shows a first definition of tension vs. strain, which was confirmed by all participants to be a practical assumption.

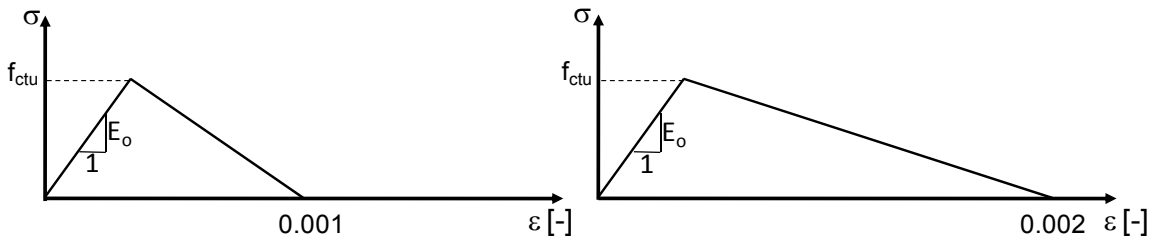

Figure 3: Assumptions for tension softening

Surprisingly all of the programs had problems to obtain convergence and it was necessary to change the tensile region of the stress strain curve according to the curve depicted in the right graph of Figure 3.
A detailed examination of the development of the relation between moment and axial force showed that all the programs had difficulties to overcome the beginning of fracturing. This seems to be a difficulty for structures with low reinforcement in general.

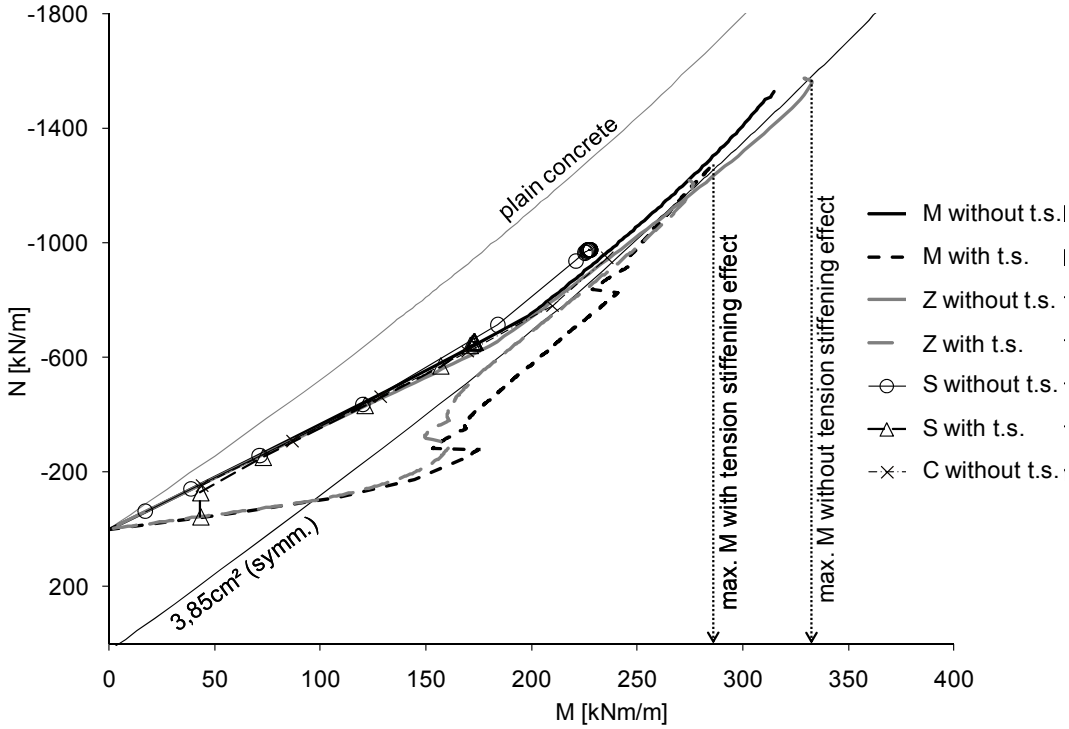

Figure 4: Development of M-N relation with and without tension stiffening (t.s.) for different FE codes M, Z, S and C.

Normally one would assume that with tension stiffening the capacity of structures will increase, but in this case without tension stiffening a higher ultimate load has been obtained (Figure 4). With no physical explanation at hand the authors assume that the differences are caused by numerical instability only. It was decided to neglect tension stiffening in the following benchmark analyses.
Another interesting aspect is that the load-displacement curves do not show a typical plateau due

to yielding; they have only a slight curvature and obviously exhibit brittle failure characteristics. This view is corroborated by the fact that failure occurs in the relatively small compression zone: As soon as all layers in the compression zone have reached the descending branch of the stress-strain-relation the failure load of the beam is reached.
It should be mentioned, that shear failure was not investigated, since in all programs shear is handled linearly.

Comparison of Design Methodologies

In order to follow the primary purpose of the benchmark a comparison of the requirements of EN 1992-1-1 (section 5.8.6), EN 1992-2 (Section 5.7) and the suggested variant of DA 2 specified in the new version of RVS 09.01.42 was conducted.
To get an overview, a range of possible values of the bedding stiffness and of the amount of reinforcement has been studied. The two programs M and Z with a layered-beam-approach have been used and mean values of their results have been calculated; tension stiffening effects have been neglected. Table 6 summarizes results obtained with the three approaches. For easier assessment, the characteristic values of the applied pressure p_k have been compared, and not the obtained (average) pressure just before failure, p_{ult}:
EN 1992-1-1: $p_k = p_{ult} / \gamma_E = p_{ult} / 1.35$
EN 1992-2: $p_k = p_{ult} / \gamma_E / \gamma_O = p_{ult} / 1.35 / 1.27$
RVS: $p_k = p_{ult}$

[8] Table 6: Calculated maximum characteristic distributed load in [kN/m²]

A_S [cm²/m]	3.85			7.7			20.0
Bedding [kN/m³]	4000	20000	100000	4000	20000	100000	20000
EN 1992-1-1	124	255	481	149	282	537	362
EN 1992-2	108	220	429	127	248	483	330
RVS	142	287	515	162	318	565	396
RVS, red.ε_{cu}	129	256	492	140	285	544	368
Linear elastic	12.3	25.1	74	24.2	49	136.5	118

There is an additional line referring to "RVS, red. ε_{cu}" which will be discussed later.
As already mentioned, the values in the table result from the average of results of codes Z and M. The maximum difference between the results was approx. 5 percent.
From Table 6 and Figure 5 it is obvious, that the procedure according to EN 1992-2 yields the most conservative results. A possible cause for the difference might be, that the different value for α_{CC} (the recommended value is 1.0 in EN 1992-1-1 and 0.85 in EN 1992-2) does not affect the procedure described in clause 5.7.
Surprisingly, the results of EN 1992-1-1 and RVS differ (up to around 15 %) despite using the same product of partial safety factors.

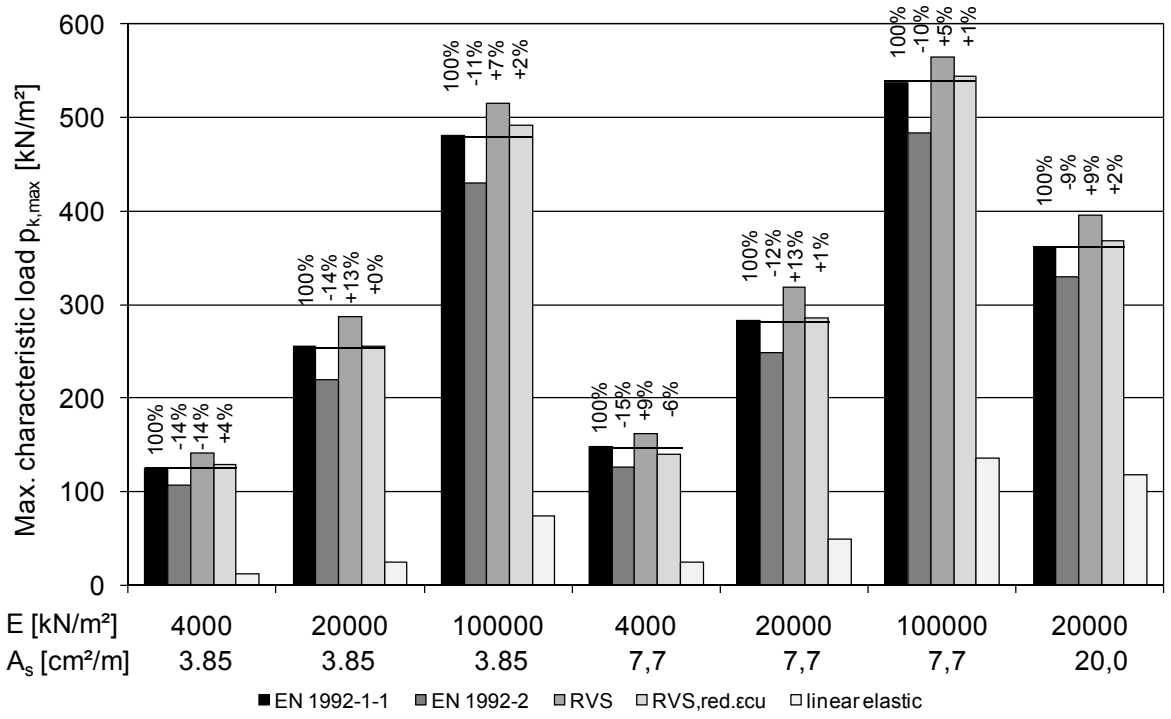

Figure 5: – Comparison of results.

The analyses for the RVS-procedure were repeated with the same safety factors, but additional reduction of the ultimate compressive strain of the concrete, ε_{cu}. Again the factor $\gamma_E = 1.35$ was applied to ε_{cu} , resulting in a limitation of 2.59 ‰ instead of 3.50 ‰. Application of this value resulted in the distributed loads in the sixth line of Table 6 which are in the range of 5% of the results for the procedure of EN 1992-1-1. A possible explanation for the relative strong influence of ε_{cu} (whereas a reduction of ε_{c1} had almost no effect on the ultimate load) is the effect of the shape of the stress-strain-relation in compression on the moment carrying capacity of each cross section (larger lever arm of the resultant compressive force). With increasing stiffness of the bedding the relative differences between the procedures decrease (except for one case), as well as the eccentricity M/N in the cross section. The differences also have a decreasing tendency with increasing amount of reinforcement.
The calculated values were also compared with the design according to EN 1992-1-1 using relation 3.1.7 for cross sectional forces and moments from a linear elastic analysis using the same amount of reinforcement as in the nonlinear analyses. As can be seen from Table 6 and Figure 5 the difference between linear and nonlinear analyses is huge: With low reinforcement, the linear elastic analysis allows only about 10 to 20 percent of the load. With higher reinforcement and higher bedding stiffness the differences decrease, but are still in the range of 70 % and above.

Conclusions

The new issue of RVS 09.01.42 is closer related to the Eurocodes than the previous issue of 2004. New specifications deal with the applicability of the Design Approaches of EN 1997-1, also in connection with nonlinear constitutive models for support. Because experience with the

new specifications and suggestions is limited, a simple benchmark problem has been defined. It allows the comparison of design procedures specified in EN 1992-1-1 and EN 1992-2 for nonlinear analyses with the corresponding specifications in RVS 09.01.42.
Some of the most interesting or surprising results are summarized below:

1. Despite the simplicity of the benchmark considerably different ultimate loads (under load control) are obtained if different engineers tackle the problem with different software packages. The differences in ultimate load can be easily 50 % and more. Only after scrutiny and elimination of all sources of discrepancies the results of programs M and Z (both using layered beams) agreed within about 5 %.
2. The descending branch of the stress-strain-relation of concrete in compression governs the overall load-displacement curve: Only a slightly nonlinear curve can be observed, the failure of the structure appears brittle in the analyses. It should be pointed out that no horizontal load was applied.
3. Modelling Tension Stiffening with the help of a softening branch of the stress-strain-relation in tension appears to be very difficult to handle with finite element simulations. Neglecting Tension Stiffening resulted in higher ultimate loads although the opposite had to be expected.
4. The result obtained by the design procedure specified in EN 1992-1-1 and EN 1992-2, respectively differ by up to 15 %. Results with EN 1992-2 are more conservative, the differences increase with increasing eccentricity of the axial force.
5. The procedure suggested in RVS 09.01.42 is even less conservative than EN 1992-1-1 unless not only the strength parameters, but also the ultimate strain (before failure) are reduced. Again, the differences increase with increasing eccentricity of the axial force.
6. Compared with a linear elastic analysis and design according to EN 1992-1-1, clause 3.1.7, the ultimate load is at least 70 % higher using the fully nonlinear model. This was true for all variants of the parameters of the benchmark studied.

Limitations of the benchmark problem are

1. No effect of the shear strength of the soil, therefore no comparison with DA 3 of EN 1997-1 is possible.
2. Just different design methodologies and approaches based on the semi-probabilistic concept of the Eurocodes have been compared. A fully probabilistic investigation is missing.
3. Time dependent behaviour of support and ground has been neglected.

Other types of benchmark, e.g. for face stability analysis or for shotcrete as support, have to be undertaken in order to generalise the findings.

References

RVS 09.01.42 (2011)., Tunnel structures in soft soil under built-up areas, to be published.
RVS 9.32 (2004) Statisch-konstruktive Richtlinie Geschlossene Bauweise im Lockergestein unter Bebauung.
ÖNORM EN 1997-1 (2009-05-15). Eurocode 7, Geotechnical Design - Part 1: General rules.
ÖNORM B 1997-1-1 (2010-03-15). Eurocode 7, Geotechnical Design, National specifications

concerning ÖNORM EN 1997-1 and national supplements.
ÖNORM EN 1992-1-1 (2009-07-01). Eurocode 2: Design of concrete structures - Part 1-1: General rules and rules for buildings.
ÖNORM B 1992-1-1 (2007-02-01). Eurocode 2: Design of concrete structures -Part 1-1: General rules and rules for buildings. National specifications concerning ÖNORM EN 1992-1-1, national comments and national supplements.
ÖNORM EN 1992-2 (2007-09-01). Eurocode 2: Design of concrete structures — Part 2: Concrete bridges — Design and detailing rules.
ÖNORM B 1992-2 (2008-08-01) Eurocode 2: Design of concrete structures — Part 2: Concrete bridges — Design and detailing rules. National specifications concerning ÖNORM EN 1992-2, national comments and national supplements.
ÖNORM B 4200-4 (1984). Reinforced concrete structures – analysis and design.
Walter, H. (2006). Design of the primary support of the NATM excavation of the metro station Taborstraße in Vienna based on a nonlinear 3-D-FE-model. Felsbau 24 Nr.2, p. 38-51.
Walter, H. (2007). Implicit ULS Design using Advanced Constitutive Laws within the Framework of Eurocode 7.In: J. Eberhardsteiner et.al. (eds.), ECCOMAS Thematic Conference on Computational Methods in Tunnelling (EURO:TUN 2007), Vienna, Austria, 2007.

Application of Computational Methods for the Design of Rock Caverns

K. Grossauer[1] and H. Wannenmacher[2]
[1] Amberg Engineering Ltd., Trockenloostrasse 21, CH-8105 Regensdorf-Watt, Switzerland
E-mail: kgrossauer@amberg.ch
[2] Amberg Engineering Ltd., Rheinstr 4, CH-7320 Sargans , Switzerland
E-mail: hwannenmacher@amberg.ch

Abstract

The application of computational methods is essential for the design in underground engineering. This extended abstract shows two different examples featuring the choice of the calculation model and the application of a brittle failure criterion.
The first example highlights the choice of the calculation model by means of a shallow cavern, and shows the impact of the calculation with a homogeneous model with smeared rock parameters, and an explicit modelling of joints on the results.
The second example focuses on the calculations for deep seated caverns in competent ground conditions. Two different strength criteria for modelling shear behaviour as well as brittle rock mass behaviour are applied. The results of both models are analysed and compared to previous experience in similar conditions.

Introduction

Computational methods are nowadays an essential part for the design of underground facilities. The reliability of these methods, however, depends on a number of factors for which the determination and consideration in modelling have a decisive influence on the outcome.
This included the choice of the calculation method – continuum or discontinuum model for example – as well as the type of rock mass modelling and consideration of support measures.
These two different aspects are demonstrated and discussed with two examples.

Shallow situated cavern – case history 1

The Waferfab manufacturing facility is situated on the western valley flank of the St. Gallen Rhine valley at the foot of the Gonzen. The facility includes surface office buildings as well as underground manufacturing caverns, connected by two service tunnels on different access levels of the cavern.
The underground structure is mainly located within the Quinten formation, a fine-grained to compact, thick-bedded limestone, and within the upper limb of the of the Gonzen fold according to 0.
Due to the safety and transport requirements a shallow location with an overburden ranging from 20-70m above the main cavern diminishing to 7m at the end of the ”Litho cavern” was emphasized for construction. The dimensions of the main production cavern are 100m*18m*18m (l-s-h) while the “Litho cavern” (56m*18m*10m) is situated perpendicular to the main

production cavern.

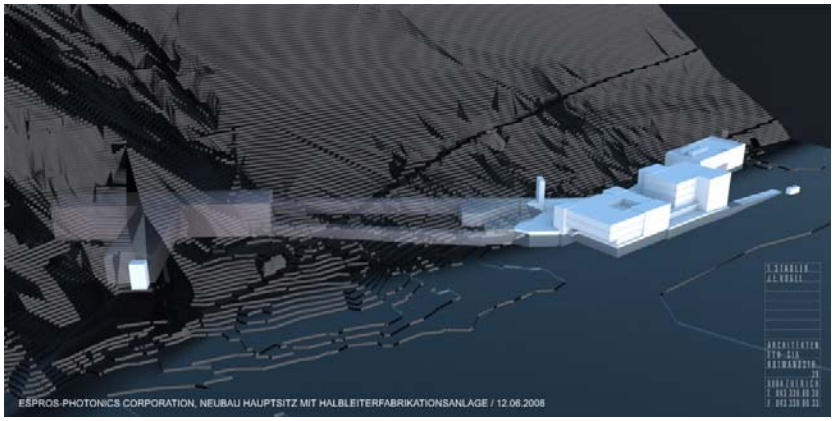

Figure 1: Situation of the Waferfab facility

Rock Mass and Rock Mass Behaviour

The Quintner limestone shows a widely differing rock mass behaviour within the area, including gravitational and stress induced block failure at higher stress regimes, buckling as well as spalling phenomena's at bifurbications or pillars at abandoned chambers of the mine.

The bedding of the lower Quinten limestone principally dips towards East (081/26). Two major joint systems are present, j1 (235/75) is parallel with major fault zones and j2 (155/88) perpendicular to the fold axis.

During the excavation of caverns some open joints parallel to j2 with apertures ranging from minor centimetres up to 30cm were encountered. The open joints, properly related to large tectonic events, resulted in large and sudden gravitational block falls concurring with the excavation.

Continuum vs. Discontinuum Modelling

The construction of caverns with spans larger than 10m is limited by the arching effect of the crown, which leads to partial opening of the face and immediate support installation to restore the clamping stress within the arch. The primary cavern support consists of grouted rock bolts and fibreglass bolts with lengths varying from 8 to 10 meters as well as a single shell reinforced sprayed concrete lining with a thickness of 20 cm. The geotechnical design included some primary analyses of potential key blocks. The rock mass shows an uneven distribution of the mean block size ranging from several cubic meters to block sizes of 0.41 m^3 with decreasing depth of the cavern. The Joint Condition Factor was determined between 1.5 and 2 resulting in GSI values ranging from 70 to 80 in the front part of the production cavern and 40 to 60 backwards. The shape of the blocks changes from cubic, platy shapes to cubic forms in the reverse part as well.

Figure 2: Rock mass conditions in the front part (left) and backwards (right) of the cavern

The importance of the modelling approach is highlighted by utilizing two section of the cavern focusing on the two rock mass types, differing mainly on the block volume. The parameters for the homogenised, smeared rock mass model were elaborated by scaling the intact rock parameters considering the GSI value, according to 0, and are summarised with Table 1.

[9] Table 1: Rock mass parameters for the homogenised model.

Young's Modulus [GPa]	25
Tensile Strength [MPa]	0.9
Friction angle [°]	39
Cohesion [MPa]	8

The representation of the explicit discontinuities of the blocky structure was modelled using Goodman's joint element method (JFEM), a program routine recently offered by Rocscience within the program package phase 2, version 7. No reduction of intact rock parameters, as used with the continuum approach, was considered for this modelling approach. To account for the strength of the discontinuities cohesion and friction were kept identical for both sections investigated. The parameters of the intact rock and discontinuities are as follows.

Table 2: Rock discontinuity parameters for the discrete model.

	intact rock	bedding planes	joint set 1 and 2
Young's Modulus [GPa]	40		
UCS *[MPa]	110		
Tensile Strength [MPa]	8	0.9	0
mi [-]	12		
Friction angle [°]		39	30
Cohesion [MPa]		8	0
Normal stiffness [MPa/m]		100'000	30'000
Shear stiffness [MPa/m]		10'000	5'500

The effect of the local open joints within the first section is considered by low lateral confinement of K0=0.3 for both modelling approaches. The confinement for the section 2 is

slightly higher K0=0.4 (since the direct influence of the open joints is not that obvious as for section 1. As stated before, the knowledge of the lateral confinement is of high importance for key block analyses, but can be treated of minor importance since only the differences of the modelling approaches are discussed.
For comparison of the rock mass behaviour only single partial face excavation was considered, to avoid the influence of the support interacting with the rock mass. The continuum modelling shows only minor deformation rates due to excavation of the first partial face considered for the comparison.

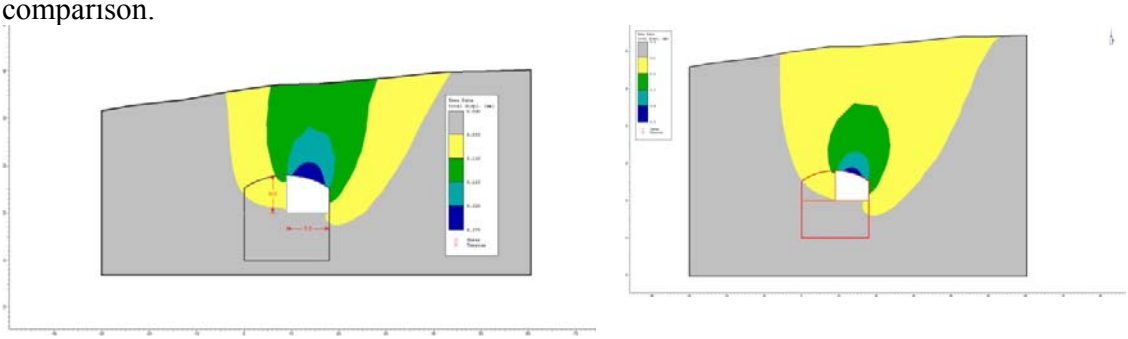

Figure 3. Displacement of the cavern section 1 (left) and section 2 (right)

The modelling of discrete rock masses emphasises a much higher skill of the geotechnical engineer, since parameters on the strength and stiffness are hardly available for the modelling. The output of such models is always affected of some certain degree of inaccuracy due to the lack of defined input parameters. Even utilizing simple models as the JFEM by rocscience give more accurate information and reliability on the expected rock mass behaviour. The disturbance of the rock mass evaluated by adjacent extensometer readings reaches up to 4 – 6 m in the crown, which matches the modelling of the discontinuum approach with higher accuracy then the continuum model shows.

Brittle Failure Rock Mass Behaviour – case history 2

Spalling and Strain Bursting

For hard rock material extensile crack initiation is the primary form of damage, even under pure compression (e.g. 0 and 0). Under low confinement, the propagation of extension cracks leads to spalling observed around hard rock openings at depth. Damage initiation has certain sensitivity to confining stress. As demonstrated by 0, 0, and 0 the damage initiation threshold is related to frictional characteristics so that

$$\sigma_{1,crit} = A(UCSi) + B\sigma_3 \qquad (1)$$

where A = 0.33 – 0.50 for most non-porous and non-foliated rocks and B = 1.4 to 2.6.
The empirical Hoek-Brown (HB) criteria for scaling the unconfined strength of a rock mass and estimating the confinement-strength relationship, latest modified version 0, is of limited reliability for undisturbed hard rock masses (GSI>75) and maybe of mixed success for GSI 65-75, as suggested by 0. The HB criterion does not adequately account for brittle damage, crack propagation and the inhibition of frictional strength development in near-excavation

environments.
The range of spalling limit recommended by 0 is based on σ_1/σ_3 rations ranging from 7 to 10 at the point of intersection with the initiation threshold.

Range of Application Limits for Spalling
Spalling commonly occurs for a ratio of compressive to tensile strength UCSi/T above 15 and GSI value higher than 65 (even with moderate jointing with GSI = 65 to 75 provided stresses are high enough for full joint closure). The lower limit for spalling is a combined function of these two indicators. In the lower portion of this range of combined limits, spalling or shearing is possible and dual analysis with GSI and the new spalling approach would be recommended.

[10] Table 3: Model selection based on strength ratio and rock mass quality, after 0.

Ratio *UCSi/T*	GSI <55	GSI 55 to 65	GSI 65 to 80	GSI >80
<8	*GSI*	*GSI*	*GSI*	*GSI*
9 to 15	*GSI*	*GSI*	*GSI*	*GSI/SP*
15 to 20	*GSI*	*GSI/SP*	*SP/GSI*	*SP*
>20	*GSI*	*GSI/SP*	*SP*	*SP*

Simplified Brittle Behaviour Analysis of Deep Seated Caverns
A simplified approach for the consideration of spalling behaviour is applied to the numerical analysis of a hydropower project with two caverns situated in massive and rock mass with a height of overburden of approximately 650 m. The initial stress conditions are estimated horizontal stresses at cavern level being around 2 times higher the vertical ones. A GSI value is estimated to 85 and the UCSi/T ratio is calculated to 13.3. The entire set of rock mass parameters are summarised in Table 4.
According to the brittle failure theory as briefly discussed above, the situation with the two caverns could be analysed following the GSI or the brittle failure approach.

[11] Table 4: Rock Mass Parameters

Rock Mass Parameters			mean value
Young's Modulus	E_{rm}	[MPa]	43'000
Specific weight	γ	[kN/m^3]	27
Poisson's ratio	ν	[-]	0.33
GSI	-	[-]	85
Friction angle	φ	[°]	49
Cohesion	c	[MPa]	13
Vertical stress	σ_v	[MPa]	18
Horizontal / Vertical stress ratio	-	[-]	2.14

The analysis is done in a simplified way utilising the 2D FE code Phase2 (version 7) and the rock mass is modelled elastically. The stress points resulting from the calculation are plotted versus the tri-linear failure criterion (see red line in Figure 4) featuring damage initiation criterion (blue

line), spalling limit (green line) and Hoek-Brown strength criterion (shear failure). Stress points being above the damage initiation and above the spalling criterion are assigned to spalling failure (see red points in below figure, right hand side). Damage initiation occurs for stress points above the corresponding criterion and not being assigned to spalling failure (blue points). The remaining stress points indicate either still elastic behaviour or shear failure if plotted outside the shear failure criterion.
Compared to a shear failure analysis the utilisation of the tri-linear criterion for the consideration of brittle rock mass behaviour, even when very simplified modelled as shown here, yields good results which capture the actual behaviour more realistically.

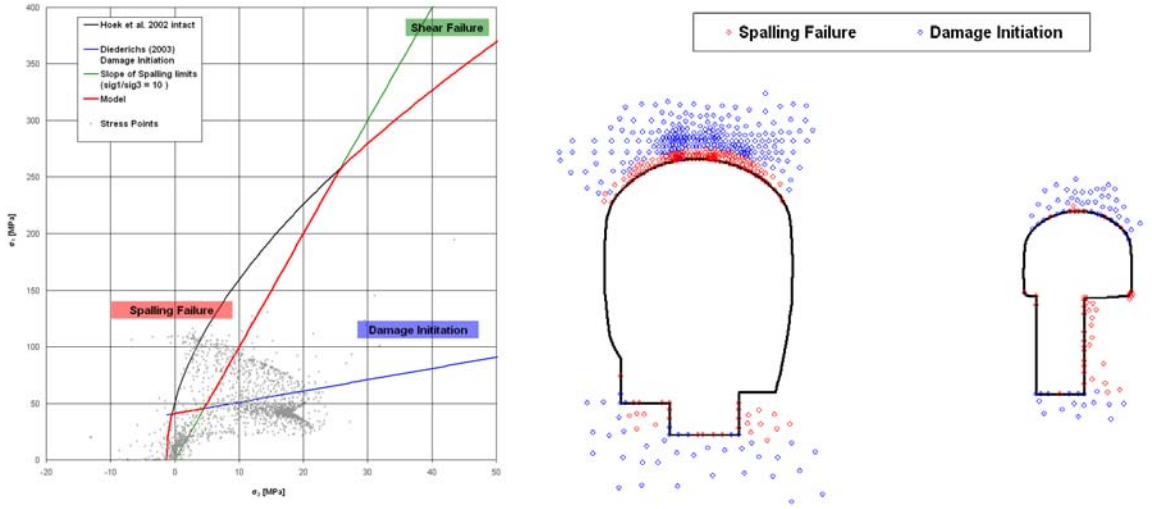

Figure 4. Stress points plotted in tri-linear failure criterion (left) and demonstration of spalling failure (red points) and damage initiation (blue points) in the cross section (right).

Conclusion

Computational methods can provide substantial support for the design of underground caverns. To capture the ground response realistically proper modelling techniques are required. Two case histories have been shown featuring the issue of continuum versus discontinuum models as well as brittle rock mass behaviour. Both situations show that even with simple models the ground behaviour can be captured more realistically.

References

Pfiffner, A. 2009. Geologie der Alpen. First ed. Haupt, Bern.

Cai, M., Kaiser, P.K., Uno, H., Tasaka, Y., Minami, M., 2004. Estimation of rock mass deformation modulus and strength of jointed hard rock masses using the GSI System. Int. J. Rock Mech. Min. Sci. 41 (1), 3-19.

Stacey, T.R. 1981. A simple extension strain criterion for fracture in brittle rock. Int. J. of Fracture, 18: 469-474.

Tapponier, P. and Brace, W.F. 1976. Development of stress induced micro cracks in Westerly

granite. Int. J. Rock Mech. &Min. Sci. and Geomech. Absrt., 13: 103-112.
Diederichs, M.S. 2003. Rock fracture and collapse under low confinement conditions. Rock Mechanics and Rock Engineering. 36 (5) pg 339-381.
Diederichs, M.S. 2000. Instability of hard rock masses: the role of tensile damage and relaxation. PhD., U.Waterloo. 566p.
Brace, W.F., Paulding, B.W. & Scholz, C. 1966. Dilatancy in the fracture of crystalline rocks. Journal of Geophysical Research, 71 (16): 3939-3953.
Diederichs, M.S. and Carvalho, JL 2007. A modified approach for prediction of strength and post yield behaviour for high GSI rock masses in strong, brittle ground. 1st Canada/U.S. Rock Mech. Symp. 2007, Taylor & Francis Ltd, Vancouver, 249-257.
Hoek, E, Carranza-Torres, CT, Corkum, B. 2002. Hoek-Brown failure criterion-2002 edition. Proc.5th North American Rock Mech. Symp., Toronto, 267–73.
Hoek E, Diederichs MS, Empirical estimation of rock mass modulus. International Journal of Rock Mechanics and Mining Sciences 43, 2006, p. 203-215.

Decisive Parameters for the Design of Power Plant Caverns

E. Saurer and Th. Marcher
ILF Consulting Engineers, Feldkreuzstrasse 3, A-6063 Rum / Innsbruck, Austria
E-mail: erich.saurer@ilf.com

Abstract

The demand on pumped storage plants for energy storage and covering peak current has been increasing significantly during the last years. Simultaneously, standards for environmentally and ecologically friendly design of power plants are set at higher levels. As a consequence power plant cavern with cross-sectional areas of >1500 m² are executed by an increasing number.
From a rock mechanics perspective, challenges concerning excavation and support systems for such caverns arise. Even though preferred geological boundary conditions in sound rock may be given, plastic zones in rock are developing causing rearrangement of stresses and thus deformation up to several centimeters. This tendency is supported by the tight arrangement of tunnels, galleries and shafts required for operation and maintenance as well as the distance between powerhouse and transformer caverns, which shall be as small as possible. Still, the rock pillar between the two caverns has to fulfill design requirements in terms of strength and stiffness.
In this technical note, some dependencies with respect to decisive parameters for the design of power plant caverns are presented. The dependencies include size of the cavern, geology, excavation and support measures and resulting deformation. The data on which the dependencies are based on result from data collected in design project of ILF as well as from literature.

Introduction

With the increasing demand on renewable energies the requirements of pumped storage plants (PSP) are growing. Already today's power production requires certain availability of storage capacity due to the time lag between production and demand. However with increasing capacity of renewable energies, such as solar and wind power plants, the requirements concerning production and storage capacities of PSP rise. Therefore the number of PSP under construction is growing. In order to design economically and to consider all required boundary conditions, it is common practice to place machines and transformers in underground caverns. As a consequence of the above mentioned tendencies in terms of capacity, the requirements concerning size of caverns grow simultaneously. From a rock mechanics perspective, this implies that excavation and support of caverns in rock get more challenging. This is not only due to the size of caverns or complexity of access tunnels but also due to tighter schedules for design and construction. When starting a project, in order to get a first idea of requirements and deformation tendencies, it would be useful to have a tool for a first assessment of geometry, support and deformation behavior of the required power cavern.
In this paper, some correlations concerning decisive parameters for the preliminary design of power caverns are presented. These correlations may provide a first idea concerning required size of a cavern as a function of the required capacity as well as concerning support as a function of

rock properties.

Decisive Parameters and their Influence on Cavern Design

Parameter Identification

The main parameters taken into account in this study are summarized below:

- total capacity of the PSP: Here, the maximum capacity for power production is considered
- length (L), width (W) and height (H)
  - area of the cavern (W x L)
  - cross-sectional area of the cavern (W x H)
  - volume of the cavern (W x L x H)
- overburden h above the cavern
- stiffness rock and rock mass: Limited by the availability of the number of data sets, here the properties of rock and rock mass considered are E_{int} and E_{rm} where index *int* denotes intact rock and *rm* denotes rock mass.
- strength of rock and rock mass: In analogy to the stiffness, the unconfined compression strength (UCS) of intact rock and rock mass are denoted by UCS_{int} and UCS_{rm} respectively.

Although the anisotropy of the rock mass is considered to be important, this parameter has not been considered due to the lack of available of data.

Shape of Cross Section

The most common shapes for the design of caverns are shown in Fig 1.

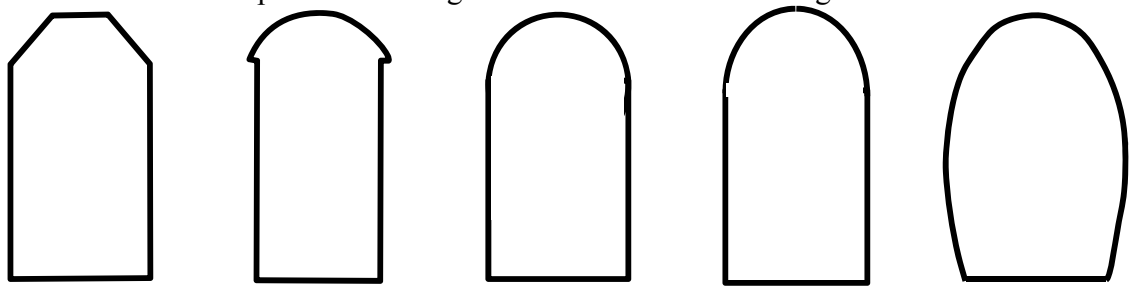

Figure 1: Common shapes of caverns; (a) trapezoidal; (b) mushroom; (c) circular shape; (d) bullet shape; (e) horse shoe

The choice of the shape to be considered for a particular cavern cannot be related directly to the above mentioned parameters. Neither the height nor rock strength shows a clear correlation with the cavern shape. In fact the optimum shape of the cavern is the one with minimum moment in the concrete lining. A correlation might be found when relating anisotropy to the vertical stress and strength of rock mass. At this stage, the database is not sufficiently filled to return significant results.

Correlations between Capacity and Cavern Dimensions

In the first place, correlations between capacity and geometry of the cavern have been analyzed (see Fig. 2). While correlation of cavern height may be correlated from the capacity, it has been found that for the cross sectional area (B x H) and the area of the cavern (L x B) dimensions cannot be correlated separately. Then again, the correlation between the capacity and the entire volume of the cavern is promising. Therefore, the remaining parameter may be derived from this correlation.

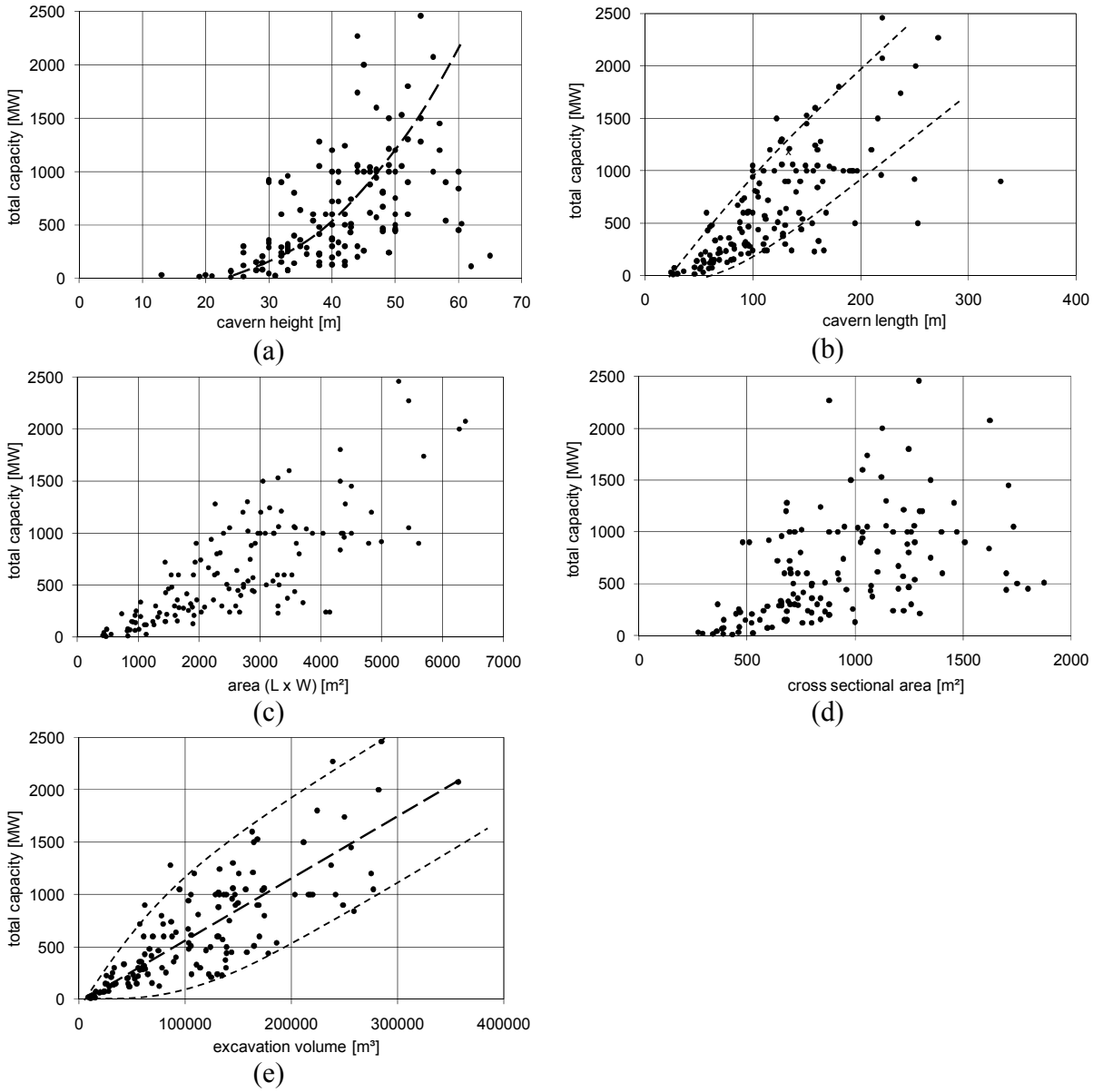

Figure 2: Correlations between total capacity and dimensions of PSP caverns. Dots represent data from literature and own projects, lines denote interpretation of mean values and ranges.

Correlations between Rock Properties and Support

Some correlations between stiffness and strength of rock mass and the anchor grid size and anchor length are shown in Fig. 3. Black dots denote passive anchors whereas white dots represent prestressed anchors.

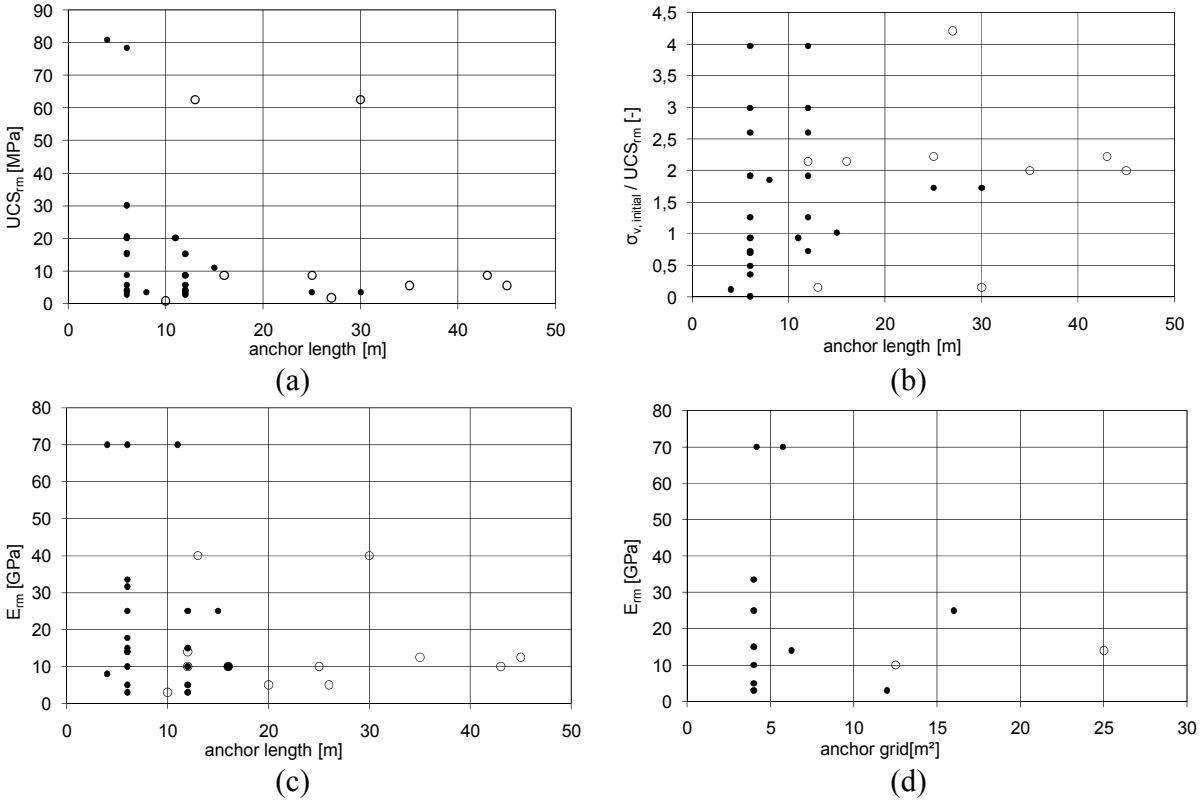

Figure 3 (a)-(d): Correlations between of the rock mass properties and supporting anchors

Correlation between Rock Properties, Cavern Dimensions and Deformations

In Fig. 4, vertical deformation normalized by the width of the cavern is plotted against the stiffness and the strength of rock mass, respectively.

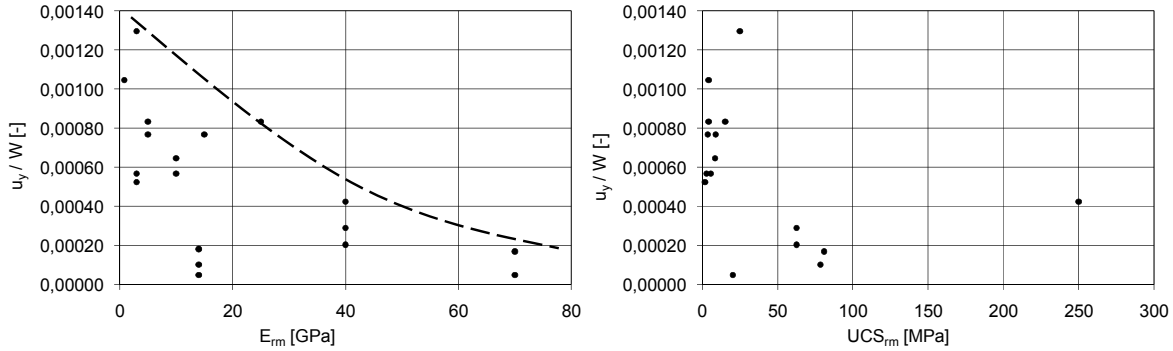

Figure 4: Vertical deformation u_y normalized by the width W of the cavern plotted against the stiffness (a) and the strength of rock mass (b).

Conclusion

Based on literature and own projects, a data set to evaluate decisive parameters for power plant caverns is presented. Some dependencies and correlations between decisive parameters have been investigated. Correlations between total capacity and geometry of the main cavern may be used as a first assessment at an early design stage for power storage plants or may serve to cross check defined geometries.
Furthermore, correlations between geometry and rock properties have been analyzed with respect to expected deformation (i.e. convergence). Some dependencies between support of shotcrete, anchor length and grid are presented as function of rock properties and cavern size.
Due to the decreasing number of available data sets with increasing complexity of parameters and results the significance of resulting parameters is decreasing. The data shown here represent an overview of possible dependencies and is a first step towards a more detailed study. Continuous collection and implementation of decisive parameters, in particular rock properties, support systems and measured deformation, into the database will further increase the significance of the dependencies.
The authors are aware of the fact and would like to point out that the presented correlations will never replace a fundamental analysis of each particular cavern design. However it may be useful to get a first idea and to check the cavern design at an early stage of a project.

Acknowledgements

The support by Mr. Benjamin Santeler concerning the literature review and collection of data is kindly acknowledged.

References

Abraham K.H., Barth St., Bräutigam F., Hereth A., Müller L, Pahl A., Rescher O.-J. (1974). Vergleich von Statik, Spannungsoptik und Messungen beim Bau der Kaverne Waldeck II: Rock Mechanics, Suppl. 3, 143-166.

Börker M., Ammon C., Frey D. (2010). Zugangsstollen I für Kraftwerke Linth-Limmern: Tunnel 8 Schweiz.

Dünser Ch., Vorauer J., Beer G. (2004). Effiziente 3-D numerische Simulation im Tunnel und Kavernenbau: Beton- und Stahlbetonbau 99 Heft 2.

Fava A.R., Ricca A. (1997). A new design for a large cavern in the alps Int. J. Rock Mech. Min. Sci.34: 3-4 paper No. 078.

Freitag M., Larcher M., Blauhut A. (2011). Das Pumpspeicherkraftwerk (PSKW) Reißeck II: Geomechanik und Tunnelbau 4 Nr. 2.

Hönisch K. (2010). The world´s underground hydro power plants in 2010: International water power & dam construction yearbook 2010

Jenni H., Mayer C.M. (2010). Kraftwerk-Projekt Linthal 2015: Tunnel 8 Schweiz

Kessler E., Kocher B. (1976). Felsmechanische Berechnung des Etappenausbruches einer Kaverne: Seperatdruck aus „Schweizer Baublatt“ Nr. 6 Zürich.

Köhler H. (1973). Pumpspeicherwerk Waldeck II – Maschinenkaverne und Triebwasserleitung: PORR Nachrichten Nr. 55

Lee Y.N., Suh Y.H., Kim D.Y., Jue K.S. (1997). Stress and deformation behaviour of oil storage caverns during excavation: Int. J. Rock Mech. & Min. Sci. 34 3-4 paper No. 305 Korea.

Lux K.-H., Hou Z., Düsterloh U. (1999). Neue Aspekte zum Tragverhalten von Salzkavernen und zu ihrem geotechnischen Sicherheitsnachweis Teil 2: Beispielrechnung mit dem neuen Stoffmodell: Erdöl Erdgas Kohle 115. Jahrgang Heft 4

Marclay R., Hohberg J.M., John M., Marcher T. (2010). The new Linth-Limmern hydro-power plant – design of caverns under 500m overburden: Rock Mechanics in Civil and Environmental Engineering

Netzer E., Pürer E. (2006). Pumpspeicherwerk Kops II – Geologie Planung und Felsmechanik der Maschinenkaverne: Felsbau 24 Nr. 1

Phienwej N., Anwar S. (2005). Rock mass characterization for the underground cavern design of Khiritharn pumped storage scheme: Geotechnical and Geological Engineering 23 175-197 Thailand

Porzig R., Barow U., Reichenspurner P. (2001). Pumpspeicherwerk Goldisthal – Auffahrung und Sicherung der Kavernen und der Stollensysteme: Felsbau 19 Nr. 5

Pöttler R. (1988). Finite Elemente – Anwendung in der Baupraxis – Rechnergestützte Berechnung (FEM). und Konstruktion (CAD). Erfahrungen derzeitiger Stand Tendenzen: Stabilitätsuntersuchung von Salzkavernen Ruhr-Universiät Bochum

Pöttler R. (1992). Die Standsicherheitsuntersuchung für die Kaverne der englischen Überleitungsstelle im Kanaltunnel: Bautechnik 69 Heft 11.

Schnetzer H., Gerstner R. (2011). Triebwasserstollen Kopswerk II – Bauarbeiten Druckstollen und Nebenanlagen: Geomechanik und Tunnelbau 4 Nr. 2.

Vigl A., Barwart Ch. (2011). Triebwasserstollen Kopswerk II – geomechanische und bautechnische Planung: Geomechanik und Tunnelbau 4 Nr. 2.

Westermayr H. (2006). Pumpspeicherwerk Kops II – Ausbruch und Sicherung der Maschinenkaverne: Felsbau 24 Nr. 1.

Wittke W. (1974). Neues Entwurfskonzept für untertägige Hohlräume in klüftigem Fels: Deutsche Fassung des Vortrags „New Design Concept for Underground Openings in Jointed Rock“ zum Symposium über numerische Methoden in der Bodenmechanik und Felsmechanik Karlsruhe.

Wisser E. (1982). Der Bau des Kavernenkrafthauses Langenegg: Bauingenieur 57 185-192.

Umrüstung der Schachtanlage Konrad
Kalibrierung von Gebirgsparametern für numerische Prognoseberechnungen

S.C. Möller[1], L. te Kamp[2], M. Polster[3] und G. Eilers[4]

[1] CDM Consult GmbH, Motorstr. 5, 70499 Stuttgart
[2] ITASCA Consultants GmbH, Leithestrasse 111, 45886 Gelsenkirchen
[3] Deutsche Gesellschaft zum Bau und Betrieb von Endlagern für Abfallstoffe mbH (DBE), Eschenstrasse 55, 31224 Peine
[4] Bundesamt für Strahlenschutz (BfS), Willy-Brandt-Str. 5, 38226 Salzgitter

E-mail: sven.moeller@cdm.com

Kurzbeschreibung

Im Rahmen der Errichtung eines Endlagers für radioaktive Abfälle mit vernachlässigbarer Wärmeentwicklung im früheren Eisenerzbergwerk Konrad sind auf der 850 m-Sohle z.T. Neuauffahrungen von Strecken, sowie auch Aufweitungen von Bestandsstrecken vorgesehen.
Für die Nachweise von Standsicherheit und Gebrauchstauglichkeit von Gebirge und Ausbausystem werden räumliche numerische Berechnungen durchgeführt. Die Berechnungen werden in Anlehnung an die Beobachtungsmethode als Prognose- und Kalibrierungsmodell vorgesehen. Als Grundlage für die im Folgenden beschriebenen numerischen Prognoseberechnungen werden vorhandene Langzeitmessungen aus den Bestandstrecken der Grube Konrad be-rücksichtigt und der Ermittlung von repräsentativen Berechnungskennwerten zugrunde gelegt.

Einleitung

Das Bundesamt für Strahlenschutz ist in Vertretung der Bundesrepublik Deutschland als Bauherr und Betreiber verantwortlich für die Umrüstung des ehemaligen Eisenerzbergwerkes Konrad in Salzgitter zum Endlager Konrad für schwach- und mittelradioaktive Abfälle mit vernachlässigbarer Wärmentwicklung. Die Deutsche Gesellschaft zum Bau und Betrieb von Endlagern für Abfallstoffe (DBE) führt als beauftragter Dritter diese Umrüstung durch.
Für die Erweiterung der bestehenden Grubenbaue und für die Auffahrung von neuen Grubenbauen auf der 2. Sohle (850 m-Sohle) sind die Nachweise der Standsicherheit und Gebrauchstauglichkeit von Gebirge und Ausbausystem für die Bauzustände und für den Endzustand (= Ende der Nutzungsdauer) unter Berücksichtigung der vorliegenden geologischen Verhältnisse und der geomechanischen Eigenschaften des anstehenden Gebirges zu führen. Als Nutzungsdauer wird ein Zeitraum von ca. 40 Jahren berücksichtigt.
In Abhängigkeit der geforderten Nachweise für den Bauzustand und den Endzustand (Betriebsdauer), werden für die numerischen Berechnungen aus vorliegenden geotechnischen Messungen jeweils gesonderte Berechnungskennwerte durch Kalibrierung abgeleitet. Die Berechnungskennwerte für den Endzustand berücksichtigen hierbei das rheologische Gebirgsverhalten bzw. standzeitabhängige Prozesse während der Betriebsdauer.

Baumaßnahme

Im Rahmen des Umbaus der Grube Konrad zum Endlagers für radioaktive Abfälle mit vernachlässigbarer Wärmeentwicklung [1] werden für die erforderliche Infrastruktur und den späteren Transport von Gebinden mit radioaktivem Abfall sowohl bestehende Grubenbaue erweitert als auch neue Strecken aufgefahren. Wie in Abbildung 1 dargestellt, beinhaltet die

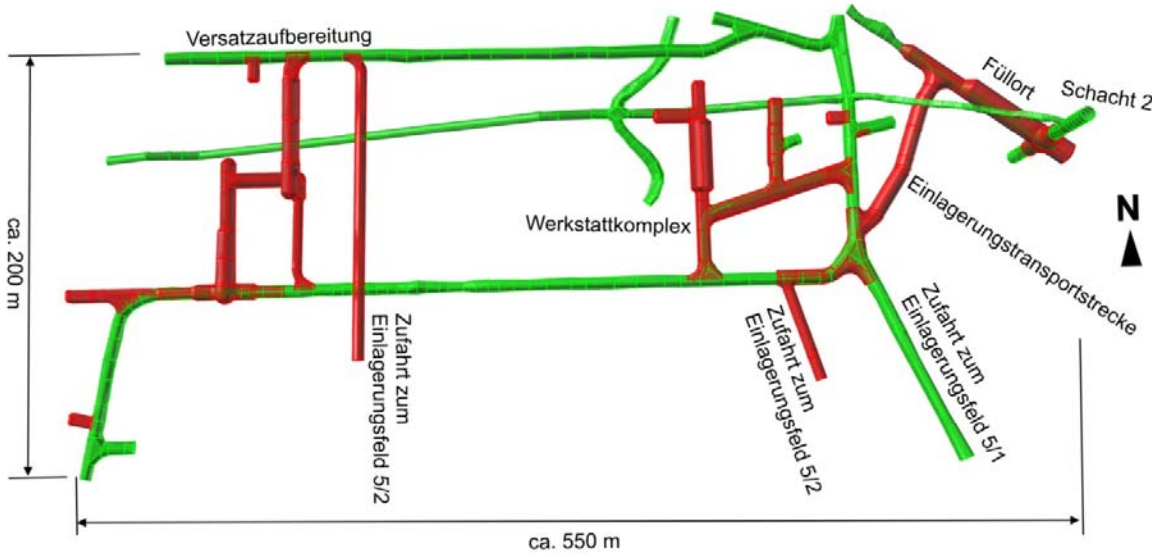

Abbildung 1: Grundriss der 850 m-Sohle (Ausschnitt) mit bestehenden Grubenbaue (grün) und Baumaßnahmen (rot)

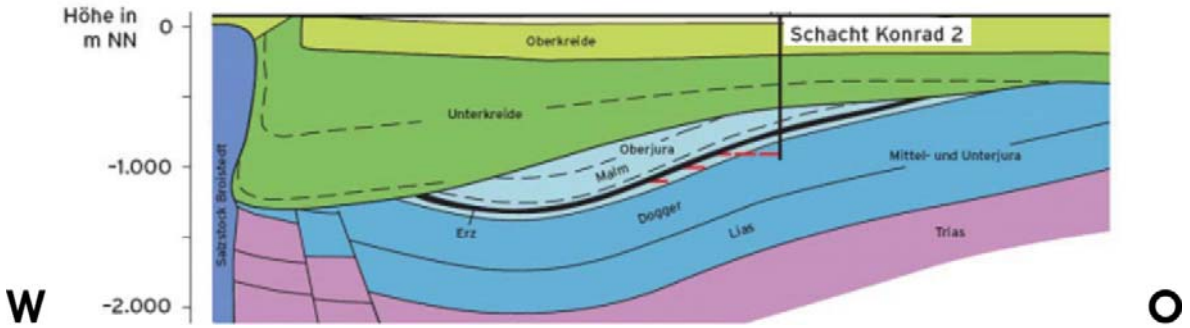

Abbildung 2: Geologischer West-Ost-Schnitt mit Schacht Konrad 2 [1]

Baumaßnahme im östlichen Teil der 2. Sohle die Ertüchtigung und Aufweitung des Schachtes Konrad 2, die Füllortaufweitung inkl. der zugehörigen Schachtglocke, die Neuauffahrung der Einlagerungstransportstrecke und die Errichtung eines Werkstattkomplexes, was sowohl Neuauffahrungen als auch Streckenaufweitungen erfordert. Im westlichen Teil werden zur Erstellung einer Versatzaufbereitungsanlage überwiegend Neuauffahrungen vorgenommen.

Geologie und Tektonik

Die Schachtanlage Konrad schließt die im Oberen Jura (Malm) liegende Erzlagerstätte auf (s.

Abbildung 2). Die Gesteinsschichten des Oberjura werden von den sehr gering wasserdurchlässigen Ton- und Mergelgesteinen der Unterkreide, der Oberkreide und vom Quartär überdeckt. Die Schichten der Unterkreide bilden dabei die wichtigste geologische Barriere des späteren Endlagers [1].

Im Nahbereich von Schacht 2 stehen auf der 850 m-Sohle die zum Malm gehörenden Gesteine des Oberen, Mittleren und Unteren Korallenoolithes an (s. Abbildung 3). Die vorliegenden stratigraphischen Einheiten lassen sich petrographisch in Anlehnung an [2] in überwiegend kalksteinartige und überwiegend tonsteinartige Gesteine einteilen, wobei die Kalksteine in Bezug auf ihre Steifigkeits- und Festigkeitseigenschaften generell steifer und standfester als

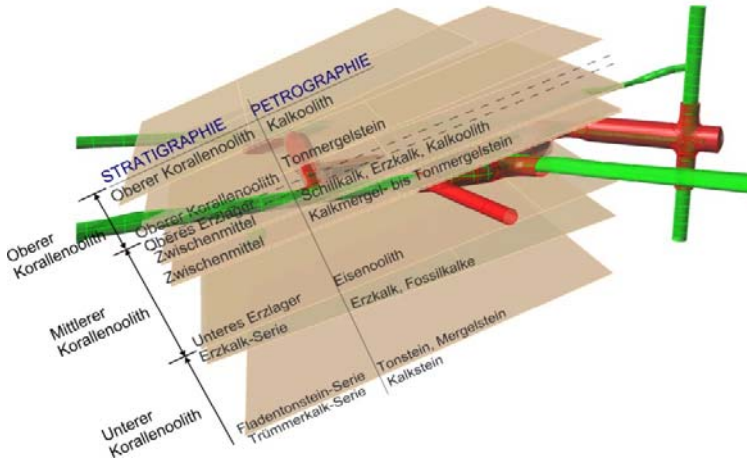

Abbildung 3: Geologische Einheiten auf der 850 m-Sohle im Nahbereich von Schacht 2

die Tonsteine sind. Während die derzeit vorliegenden Bestandsstrecken in den Kalksteinen meist als mittel- bis gering verformbar und standsicher einzustufen sind, wird insbesondere bei den Gesteinen der Fladentonstein-Serie im Zusammenhang mit der durchzuführenden Baumaßnahme mit druckhaften Gebirgsverhältnissen gerechnet. Zusätzlich zur geologischen Schichtenfolge wurden im Bereich der 850 m-Sohle mehrere tektonische Elemente (Großklüfte und Störungen) kartiert; teilweise wurden Versatzweiten im dm- bis m-Bereich festgestellt.

Modellbildung und numerische Modellierung

Abbildung 4 zeigt die vorgesehenen Modellbereiche zur numerischen Modellierung der Baumaßnahmen auf der 850 m-Sohle. Aufgrund der großen räumlichen Ausdehnung werden 6 unterschiedliche Modellbereiche vorgesehen. Im schachtnahen Bereich überlappen sich diese teilweise. Die Modellgrößen umfassen Modellbereiche mit einer mittleren Kantenlänge von ca. 130 m bei einer mittleren Gesamtzonenanzahl pro Modell von ca. 3 Mio. Der rechentechnisch benötigte Arbeitsspeicher beträgt in etwa 15 bis 20 GB, die Dauer einer Rechenphase (Bauzwischenzustand) liegt unter Verwendung von 24 parallelgeschalteten 2,9-GHz-Prozessoren bei ca. 6 bis 8 h. Da die Berechnungen in Anlehnung an die Beobachtungsmethode als Prognose- und baubegleitendes Kalibrierungsmodell vorgesehen werden, ist es wichtig, dass die Berechnungsdauern im Hinblick auf die Bauausführung gering gehalten werden. Bei größeren

Abweichungen zwischen Prognoseberechnungen und baubegleitenden

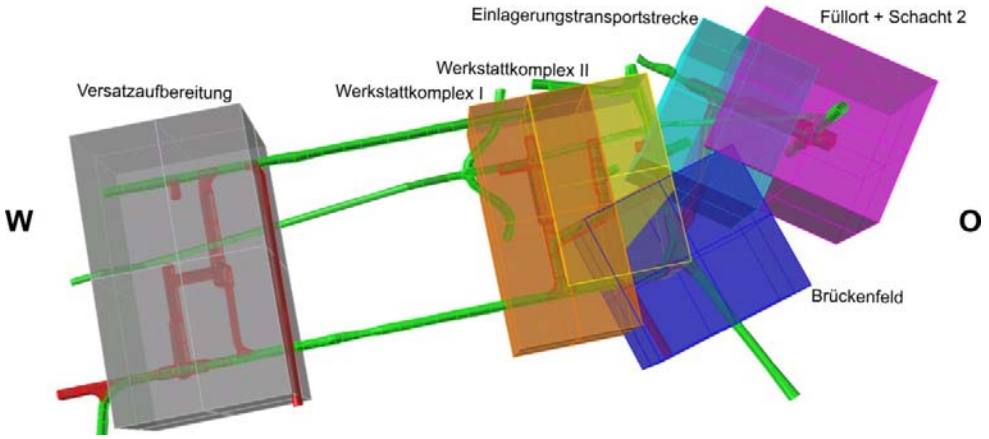

Abbildung 4: Modellbereiche für die Baumaßnahmen auf der 2. Sohle

Messungen ist geplant, das numerische Berechnungsmodell zeitnah an den Ergebnissen des geotechnischen Messprogramms zu kalibrieren. Die Überprüfung des Tragverhaltens, die Entscheidung über den weiteren Bauablauf sowie die endgültige Dimensionierung des Ausbaus kann somit baubegleitend angepasst werden.

Verwendetes Stoffmodell zur Beschreibung des Gebirgsverhaltens

Zur Abbildung des Gebirgsverhaltens wird ein elasto-plastisches Stoffmodell mit einer Festigkeitsanisotropie zur Berücksichtigung der Schichtung und Entfestigung im Nachbruchbereich (strain softening) gewählt. Der elastische Verformungsanteil wird als isotrop, linear-elastisch (Hooke) modelliert. Für den plastischen Anteil wird die Mohr-Coulomb'sche Scherfestigkeit sowie eine Begrenzung der Zugspannungen (tension cut-off) verwendet. Zur Berücksichtigung der Anisotropie der Festigkeit, wird hierbei zwischen Matrix- und Schichtungsfestigkeit unterschieden.

Zur Berücksichtigung des Restfestigkeitsverhaltens des Gebirges wird im vorliegenden Stoffmodell zusätzlich zur Spitzenscherfestigkeit, sowohl auf der Matrix als auch auf der Schichtung, eine von den akkumulierten plastischen Dehnungen abhängige Entfestigung bis zu einer Restscherfestigkeit berücksichtigt. Wie in Abbildung 5 dargestellt, erfolgt die Scher-und Zugentfestigung in linearer Abhängigkeit von definierten Entfestigungsparametern (□s und □t). Für Matrix und Schichtung werden hierbei gesonderte Entfestigungsparameter verwendet. Weitere Angaben zur Implementierung des Festigkeitsverhaltens sind in [5] enthalten.

Kalibrierung von Berechnungskennwerten

Entsprechend der lokal angetroffenen Geologie findet eine Einteilung der Modelle (Abbildung 4) in geotechnische Homogenbereiche statt. Hierbei werden auf Basis der stratigraphisch-petrographischen Einteilung gemäß Abbildung 3 Homogenbereiche festgelegt, für die jeweils Berechnungsparameter abgeleitet werden. Für die Ableitung dieser, das Gebirgsverhalten repräsentierenden Berechnungsparameter werden Konvergenz- und Extensometermessungen aus den entsprechenden stratigraphischen Einheiten, bzw. aus vergleichbaren geotechnischen Homogenbereichen herangezogen.

Die Auswertung von geotechnischen Messungen [3], [4] zeigt, dass für den Nahbereich des

Schachtes 2 auf der 850 m-Sohle keine vollständigen Langzeitmessungen mit Nullmessungen unmittelbar nach Streckenauffahrung dokumentiert sind. Für die vorliegenden Höhen- und Konvergenzmessungen liegen die entsprechenden Nullmessungen mehrere Jahre nach Streckenauffahrung. Aus diesem Grunde wird bei der Auswertung von Konvergenz- und Extensometermessungen als Grundlage für die Parameterkalibrierungen auf Stationen in vergleichbaren Strecken zurückgegriffen. Es werden dabei solche Stationen gewählt, welche sich hinsichtlich Stratigraphie und Petrographie in gleicher geologischer Einheit befinden. Zusätzlich wird geprüft, inwieweit bei den gewählten Stationen Streckengeometrie,

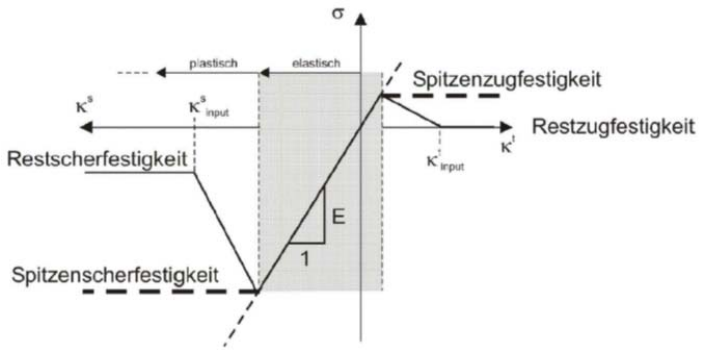

Abbildung 5: Scher- und Zugentfestigung in Abhängigkeit von Entfestigungsparametern

Messungen ist geplant, das numerische Berechnungsmodell zeitnah an den Ergebnissen des geotechnischen Messprogramms zu kalibrieren. Die Überprüfung des Tragverhaltens, die Entscheidung über den weiteren Bauablauf sowie die endgültige Dimensionierung des Ausbaus kann somit baubegleitend angepasst werden.

Auswertung von Konvergenzmessungen als Grundlage für Parameterkalibrierungen

In Abbildung 6 wird exemplarisch die Situation an einer, für die Gesteine des Unteren Erzlagers repräsentativen Konvergenzstation 128209 aus dem Versuchsfeld 5/1 dargestellt. Für diesen Teil der Grube liegen langjährige Messreihen von bis zu 20 Jahren vor. Abbildung 7 zeigt die zugehörigen Konvergenzverläufe für horizontale und vertikale Konvergenzen sowie den zeitlichen Verlauf der Konvergenzraten. Aus Abbildung 7 ist ersichtlich, dass

- die größten gemessenen Konvergenzen in den ersten Jahren auftreten,
- die Konvergenzraten danach mit der Standzeit abnehmen, jedoch selbst nach langer Standzeit noch Konvergenzraten > 0 vorliegen,
- die vertikalen Konvergenzen größer sind als die horizontalen (typisches Verhältnis in dieser stratigrafischen Einheit: vertikal/horizontal = ca. 1,5 bis 2,0).

Aufgrund der o.g. Charakteristika wird bei der Auswertung der Konvergenzmessungen eine Unterteilung in die Phasen 0, I, II und III gemäß Abbildung 7 vorgenommen. Bei der Phase 0 handelt es sich um messtechnisch nicht erfassbare Konvergenzen, welche durch Vorentspannung im Gebirge und durch den zeitlich nacheilenden Einbau der Messstationen bedingt sind. Phase I berücksichtigt quasi sofort auftretende Konvergenzen ab dem Zeitpunkt der Auffahrung bis wenige Monate. Phase II berücksichtigt einen Zeitraum mit abnehmenden Konvergenzraten ab wenigen Monaten bis wenige Jahre, Phase III quasi konstante bzw. nur noch geringfügig abnehmende Konvergenzraten ab einer Zeit von wenigen Jahren.

Ort:	02YEA82R001
Koordinaten:	Rechts: 3596597,3 Hoch: 5782244,1 NN: -722,3
Benachbarte Messpunkte:	80,0 m nördl., PP 1802
Installation:	14.03.1989
Streckenauffahrung:	13.03.1989
Streckenquerschnitt:	34,1 m²
Ausbauart:	Spreizhülsenanker und Maschendraht
Stratigraphie:	Mittlerer Korallenoolith, Unteres Erzlager
Petrographie:	Eisenoolith, Kalkstein mit Tonsteinlagen und Sandsteinspuren
Tektonik:	keine

Besonderheiten:

- 17.01.2003: Messpunkt 4 erneuert.

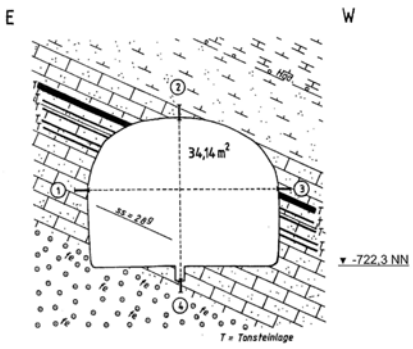

Abbildung 6: Repräsentativer Querschnitt mit Konvergenzmessstation 128209 aus [3]

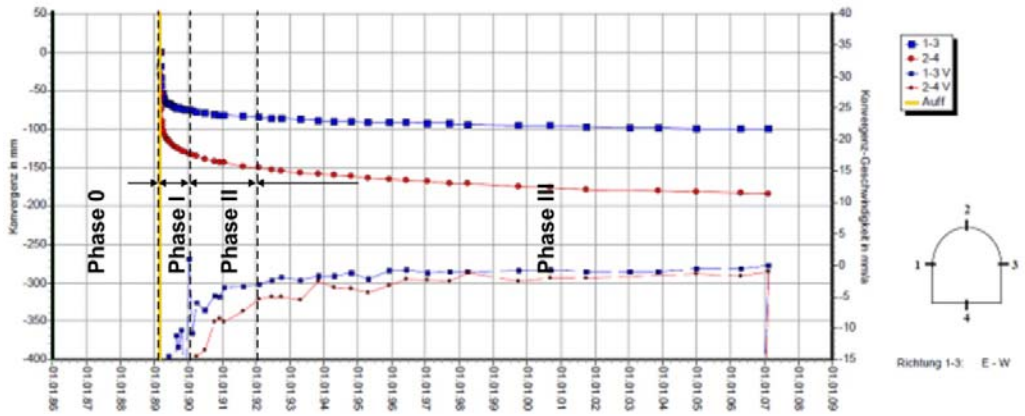

Abbildung 7: Konvergenzverlauf (exemplarisch gewählte Konvergenzmessstation 128209)

Konvergenzen „Bauzustand“

Die Kalibrierung der Berechnungsparameter für die Dauer des Bauzustands erfolgt auf Grundlage der Konvergenzen in den Phasen 0 bis II. Der nicht messbare Anteil der Phase 0 wird hierbei mit 50% Vorentspannung als Verdoppelung der Phasen I und II angenommen. Die Konvergenzen „Bauzustand“ k_{BZ} ergeben sich dann mit Gleichung (1) zu

$$k_{BZ} = k_{Phase\,0} + k_{Phase\,I} + k_{Phase\,II} \quad \text{, mit} \tag{1}$$

$$k_{Phase\,0} = k_{Phase\,I} + k_{Phase\,II} \tag{2}$$

Konvergenzen „Endzustand“

Zur Berücksichtigung von rheologischen Gebirgseigenschaften und standzeitabhängiger Prozesse, wie beispielsweise Verwitterung oder Entfestigung im Laufe der Betriebsdauer, werden gesonderte Kalibrierungen durchgeführt. Als Grundlage für die Parameterkalibrierungen „Betriebsdauer“ (Endzustand) werden dafür die durchschnittlichen jährlichen Konvergenzraten der Phase III auf eine Betriebsdauer von 40 Jahren extrapoliert. Die Berücksichtigung der rheologischen Prozesse erfolgt hierbei durch Herabsetzen der Scherfestigkeitsparameter, sodass sich in Bezug auf die Konvergenzmessungen vergleichbare Konvergenzbeträge ergeben. Gleichzeitig wird auch das Verhältnis von vertikalen zu horizontalen Konvergenzen gemäß Konvergenzmessungen berücksichtigt. Die relevanten Konvergenzen während der Betriebsdauer

bzw. Endzustand k_{EZ} ergeben sich dann mit Gleichung (3) zu

$$k_{EZ} = k_{\text{Phase III, t=40a}} \quad . \tag{3}$$

Die insgesamt zu berücksichtigenden Konvergenzen k_{ges} aus „Bauzustand“ und „Endzustand“ ergeben sich mit Gleichung (4) zu

$$k_{ges} = k_{\text{Phase 0}} + k_{\text{Phase I}} + k_{\text{Phase II}} + k_{\text{Phase III, t=40a}} \quad . \tag{4}$$

Schlussfolgerung

Für das beschriebene Vorgehen zur Ableitung von repräsentativen Berechnungskennwerten zur Beschreibung des Gebirgsverhaltens wurden mehr als hundert Konvergenzmessstationen ausgewertet. Für die 8 stratigraphischen Einheiten aus Abbildung 3 wurden hiervon insgesamt 24 Stationen als Grundlage für die Kalibrierung herangezogen. Als Ergebnis der durchgeführten Parameterkalibrierungen liegen nunmehr 10 Parametersätze (jeweils Bauzustand/Endzustand) für insgesamt 5 definierte geotechnische Homogenbereiche vor. Die Kalibrierungen erfolgten an 2D, bzw. 3D-Modellen (im Falle streckenparallelen Einfallens der Schichtung) unter Berücksichtigung eines elasto-plastischen Stoffmodells mit anisotropem Festigkeitsverhalten und Entfestigung.
Die ermittelten Parametersätze wurden anhand dreidimensionaler Rückrechnung des Ist-Zustandes der Bestandsstrecken auf Plausibilität überprüft. Zusätzliche Plausibilitätskontrollen erfolgten durch einen Abgleich mit Ergebnissen diverser ingenieurgeologischer Untersuchungen. Hierbei ergaben sich gute Übereinstimmungen zwischen berechneten und gemessenen Befunden zur Tiefe und Ausprägung der Auflockerungszone, Größe der Ankerlasten, sowie auch Übereinstimmung zu den im Labor bestimmten Gesteinsparametern. Auf dieser Basis kann das beschriebene Vorgehen zur Ableitung von Berechnungskennwerten als zutreffend und praktikabel bewertet werden.

Quellenangabe

[1] Bundesamt für Strahlenschutz, Endlager Konrad, Wissen schafft Vertrauen, Nov. 2009
[2] DBE, Schachtanlage Konrad, Geomechanisches Normalprofil, Januar 2009.
[3] DBE, Schachtanlage Konrad, Konvergenzmessungen im Grubengebäude - Messepoche 03/2007 bis 03/2008, Januar 2009.
[4] DBE, Konrad, Auswertung von Höhenmessungen unter Tage im Zeitraum von 1990 bis 2005, Juli 2007.
[5] ITASCA Consultants, FLAC3D, Version 4.0 Manuals, Minnesota, USA, 12/2009

Predicting the stability of large excavations at Heathrow Terminal 5

D. Potts[1], N. Kovacevic[2] and D. Hight[2]
[1] Department of Civil and Environmental Engineering, Imperial College, London, UK
[2] Geotechnical Consulting Group, London, UK
E-mail: d.potts@imperial.ac.uk

Abstract

This paper describes the results of finite element analyses of the temporary slope geometries in London Clay at London Heathrow Airport's Terminal 5. The aims of the analyses were to examine the times before failures developed, and to identify the failure mechanisms involved. The brittle behaviour of the London Clay was modelled, and the effects of progressive failure were taken into account. The analyses fall into the category of Class A predictions, and were used in the assessment of how long temporary slopes to deep excavations could be left open before backfilling, and how the slopes should be monitored.

Introduction

The majority of the below-ground construction at London Heathrow Airport's new Terminal 5 (T5) was carried out in open-cut excavations made in the London Clay Formation which underlies Terrace Gravels. There was a need to adopt slopes that were as steep as possible, to minimise the excavation and backfill volumes, but which would be stable for periods up to 6 months. Temporary slope geometries were selected on the basis of experience and precedents for other, usually shallower, short-term slopes cut in the London Clay.

It is extremely difficult to assess the stability of temporary slopes cut in stiff overconsolidated plastic clays, such as London Clay, partly because they are brittle and prone to progressive failure. Nevertheless, it is still common to design these slopes using limit equilibrium (LE) methods of analysis. However progressive failure is a strain–dependent phenomenon, and thus conventional LE stability analyses are not well suited for stability problems of this kind. In this respect finite element (FE) analyses are far superior. They do not impose a predetermined failure mechanism, and can assess operational strengths rationally on the basis of the development and distribution of strain within the slope.

Progressive failure can now be modelled using advanced numerical techniques and these have been used to analyse the role of progressive failure in London Clay slopes both in the short- and long-term [5,8]. The scale of the excavations at T5 (see Figure 1) justified the use of these state-of-the-art techniques to take into account the effects of progressive failure in assessing the stand-up time of the temporary slopes.

The FE analyses were carried out on a 'standard' stepped section involving a series of 5m high 1V:1H slopes in the London Clay, with 5m wide gently sloping berms (1V:20H) between, and a

maximum depth of 20m (Figure 2). Given the different excavation depths at T5, shallower excavation depths (approximately 15m and 10m) having the same section were also analysed.

Figure 1: Plan view of excavations at Terminal 5

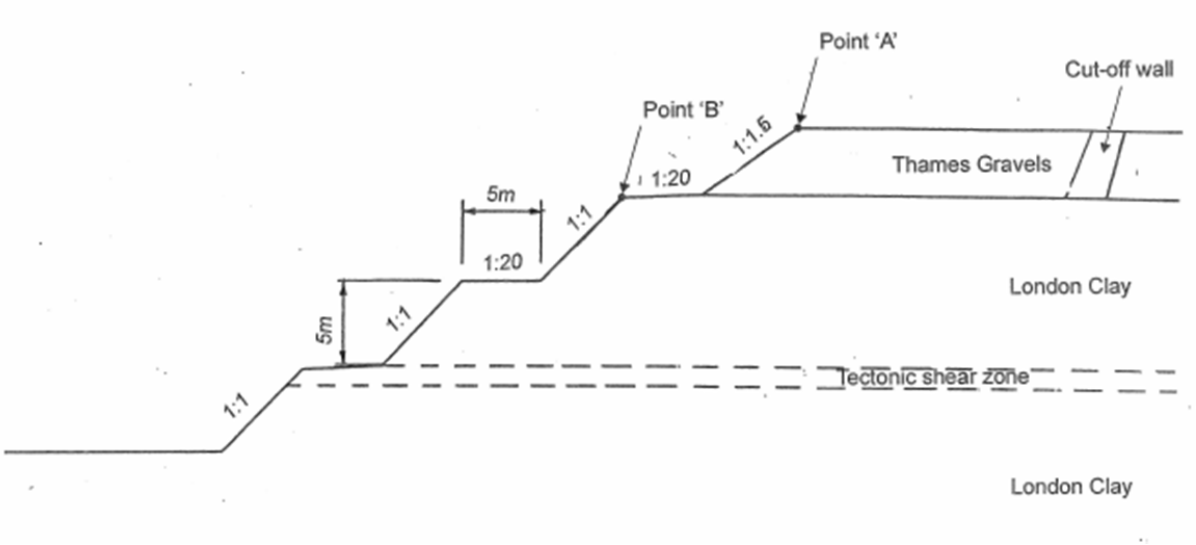

Figure 2: 'Standard' section

Ground Conditions

Ground conditions at Terminal 5 are discussed in detail elsewhere [1,4]. Approximately 4m of Terrace Gravels overlie the London Clay. Below a depth of 45m the London Clay is stiffer and much stronger. The ground water table was in the Terrace Gravels, 2m below the ground surface. Based on site measurements a hydrostatic distribution of pore water pressures was adopted in the London Clay, there being no evidence of under-drainage.

Soil Models and Model Parameters

The soil models employed in the analyses are described in some detail by [4]. Whereas the Terrace Gravels were modelled as a linear elastic perfectly plastic material, the London Clay was characterised by a generalised non-linear elastic strain-softening plastic model of the Mohr-Coulomb type in which effective stress shear strength parameters c' and ϕ' vary according to the plastic deviatoric strain invariant. Pre-peak behaviour is formulated by a non-linear elastic model of the form described by [2] in which the secant shear and bulk moduli depend on both the current strain and stress levels.

The analyses were coupled, i.e. they involved consolidation/swelling, and it was therefore necessary to specify permeability, k. Two alternatives were adopted in the parametric study. In the first, profiles of vertical and horizontal permeability, based on experimental and field measurements, were selected. These were assumed to remain constant throughout an analysis. Alternatively the permeability was assumed to be isotropic and to vary with mean effective stress, p', according to a non-linear relationship of the form proposed by [6]:

$$k = k_0.e^{(-b.p')} \qquad (1)$$

where k_0 is the permeability at zero mean effective stress in m/s and b is a parameter which has dimensions (m^2/kN).

The model parameters used in the analyses are the same as those used in the back-analyses of the failed temporary slopes at Prospect Park and Wraysbury Reservoir [3].

Finite Element Analysis

The FE analyses were carried out using the computer code ICFEP. To represent the cross section being analysed (Figure 2), the FE mesh shown in Figure 3 was developed.

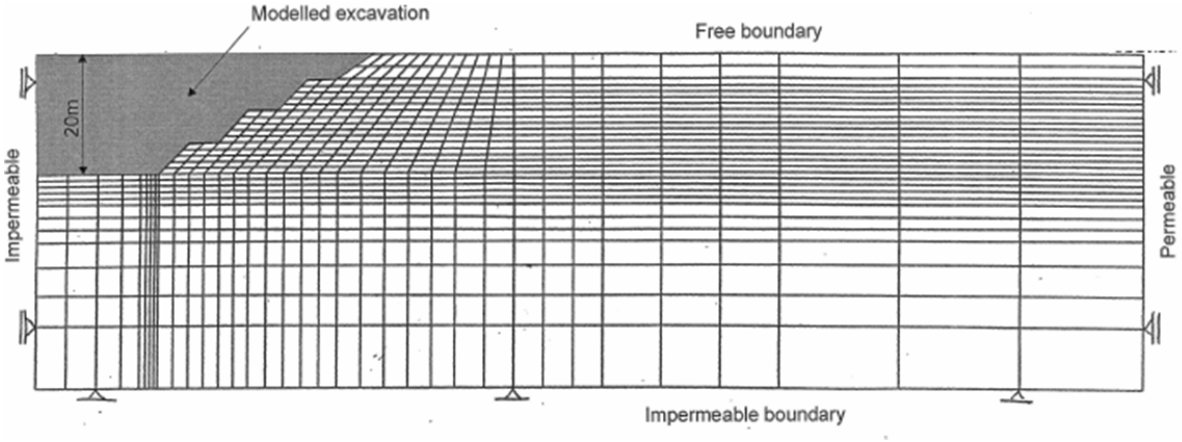

Figure 3: Finite element mesh used in the analyses

Plane strain eight-noded isoparametric elements with 'reduced' 2x2 integration were used. All eight nodes of an element had both displacement and pore water pressure degrees of freedom. A modified Newton-Raphson approach with a sub-stepping stress point algorithm was used to solve the finite element equations [6].

No horizontal displacement was allowed on the vertical boundaries, whereas the bottom boundary was fixed in both the vertical and horizontal directions. The bentonite cut-off wall, assumed to be 20m back from the top of slope (see Figure 2), was used to model de-watering of the Terrace Gravels. The far end vertical boundary was assumed to be permeable (a source of water), while the near end vertical boundary was assumed to be the axis of symmetry, and as such was impermeable (no flow). The bottom boundary was deep (55m), and assumed to be impermeable.

Excavation was simulated by removing layers of elements from the mesh at a uniform rate. Swelling of the London Clay (the Terrace Gravels was modelled as a drained material) was allowed during excavation, keeping a specified pore water pressure (suction) at the excavation boundary. Swelling was simulated in the FE analyses by applying increments of time, t. The time increments during excavation were small enough (typically 0.01 years) for there to be no significant amount of swelling in materials with relatively low permeabilities (such as the London Clay). Subsequently, after excavation was completed, the time steps were increased (typically to 0.1 years). However, when collapse was approached, the time steps were reduced again.

Results of the Analyses

The FE analyses of the temporary slopes at T5 were carried out to investigate the time before there was overall failure and to identify the failure mechanism involved. However in some cases, prior to overall failure local instability involving the berms was predicted and these were of more immediate concern at T5. The FE analyse were performed on a parametric basis with a range of factors considered, including:

- The width and depth of the excavation
- The initial value of the coefficient of earth pressure at rest, K_o
- The initial permeability profile of the London Clay and the way it changed as the clay swelled
- The pore water boundary conditions, that is, the average suction operating at the exposed surface of the London Clay.

A full description of these analyses and the results obtained can be found in [4]. Only a selection of the results is presented here.

Results from the base case analysis are presented in Figures 4 and 5. The predicted displacement vectors and pore water pressure contours immediately after excavation are given in Figure 4. These plots indicate that the slope was stable and that excavation of the London Clay has given

rise to depressed pore water pressures. The incremental displacement vectors and the contours of deviatoric plastic strain at the last stable increment of the analyses (i.e. 6.7 years after excavation) are shown in Figure 5. These indicate a deep seated failure mechanism that was initiated from the toe of the slope. Figure 5b implies that the role of progressive failure was substantial as it shows that the operational strength along the predicted base rupture surface was at residual (the plastic shear strain contour is in excess of 15%) whereas the operational strength was still pre peak on that part of the rupture surface near to the original ground surface.

Results from the parametric study indicate that the most influential soil properties and conditions on the results were the K_o profile, the permeability profile and the hydraulic boundary conditions (i.e. the average suction operating at the exposed surface of the London Clay)

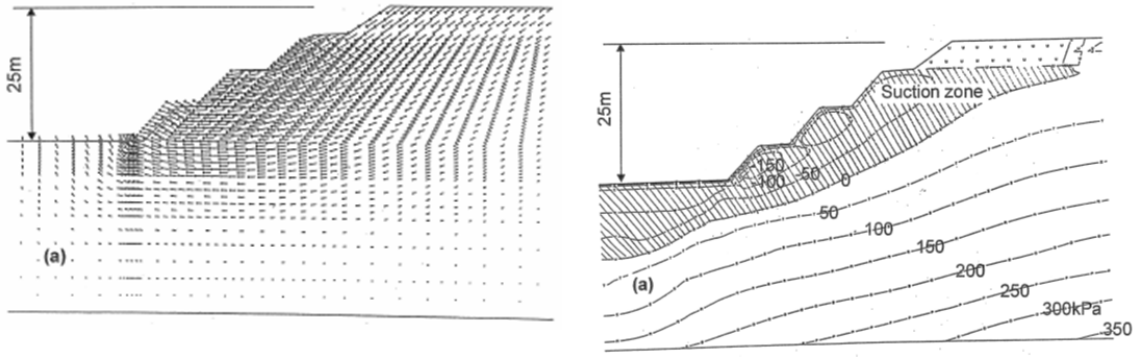

Figure 4: (a) displacement vectors and (b) contours of pore water pressure at the end of excavation

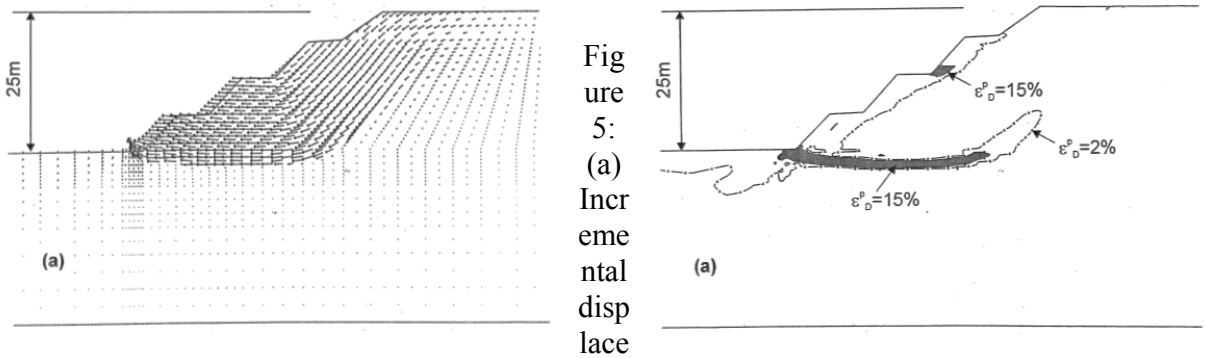

Figure 5: (a) Incremental displacement vectors and (b) contours of plastic shear strain just prior to collapse

Conclusions

Sensitivity studies, using reasonable bounds to K_0, in situ permeabilities, and surface suction conditions, showed that the slopes were stable in the short-term immediately after excavation. However, the time to failure of the slopes and the form of the failure, whether shallow or deep-seated, was determined by a combination of the assumed permeability profile and whether or not allowances were made for increases in permeability as the clay swelled, the average surface

suction, the in situ K_0 profile and the depth of excavation.

When deep-seated failures were predicted the slip surface developed from the toe of the slope and involved the formation of a basal shear. The slip surface penetrated less deeply into the slope when the K_0 profile was reduced. The risk of a deep-seated failure developing within the required stand-up time reduced as the depth of excavation reduced since the formation of a basal shear was delayed. Any superficial failures involved the first berm from the top.

Not surprisingly, the time to failure was influenced most by the assumptions regarding permeability, although what was surprising was the magnitude of the effect on the time to deep-seated failures of allowing for an increase in permeability as the clay swelled. Results of analyses using the non-linear permeability model, which captured the effects of swelling, were regarded as the more reliable. These showed that:

- If a condition of zero suction was maintained at the exposed surface of the London Clay, superficial berm failures would occur 0.2 years after excavation.
- If an average suction of 25 kPa was maintained at the exposed surface of the London Clay a deep-seated failure would develop first after 1.11 years. A basal shear zone was predicted to occur approximately 0.2 years after excavation and to be accompanied by an identifiable increase in movements.
- The adoption of a uniform slope, as opposed to a bermed slope, would have increased the risk of a deep-seated failure.
- If the K_0 profile was lower than that deduced from the ground investigation then the risk of shallow failures would have been reduced.

On the basis of the back analyses of temporary slope failures at two sites near to Heathrow [3] it was considered reasonable to expect an average suction of 25kPa to apply. It was therefore concluded that deep-seated failures would not occur at Heathrow during the required 6 month period when the cuts would be open. No deep-seated failures have been reported. However, shallow berm failures did occur and were generally associated with water ponding on the berm or running down the cut face.

The results suggest the potential usefulness of suction measurements, together with displacement monitoring, as a means of monitoring and controlling temporary cut slope behaviour at T5. Inclinometers were installed to determine if and when a basal shear zone developed, evident as a location of concentrated movements at the level of the toe of the slope. Suctions were also monitored as a check on whether the assumption of an average surface suction of 25kPa was reasonable.

References

Hight, D.W., McMillan, F., Powell, J.J.M, Jardine, R.J. and Allenou, C.P. (2003), 'Some characteristics of London Clay', *Int. Workshop on Characterisation and Engineering Properties of Natural Soils*, Singapore, Tan et al (eds), Vol.2, 81-908.

Jardine, R.J., Potts, D.M., Fourie, A.B. and Burland, J.B. (1986), 'Studies of the influence of non-linear stress-strain characteristics in soil-structure interaction', *Geotechnique*, Vol.36, No.3,

377-396.

Kovacevic, N., Hight, D.W. and Potts, D.M. (2004), 'Temporary slope stability in London Clay - back analyses of two case histories', *Advances in geotechnical engineering*, The Skempton Conference, London, Jardine et al (eds), Vol.3, 1-14.

Kovacevic, N., Hight, D.W. and Potts, D.M. (2007), 'Predicting the stand-up time of temporary London Clay slopes at Terminal 5, Heathrow Airport', *Geotechnique*, Vol.57, No.1, 63-74.

Potts, D.M., Kovacevic, N. and Vaughan, P.R. (1997), 'Delayed collapse of cut slopes in stiff plastic clay', *Geotechnique*, Vol.47, No.5, 953-982.

Potts, D.M. and Zdravkovic, L. (1999), 'Finite element analysis in geotechnical engineering: Theory', London, Thomas Telford.

Vaughan, P.R. (1994), 'Assumption, prediction and reality in geotechnical engineering', *Geotechnique*, Vol.44, No.4, 573-603.

Vaughan, P.R., Kovacevic, N. And Potts, D.M. (2004), 'Then and now: some comments on the design and analysis of slopes and embankments', *Advances in geotechnical engineering*, The Skempton Conference, London, Jardine et al (eds), Vol.3, 15-64.

Stability analysis with FEM: strain softening vs. strength reduction approach

I .N. Hamdhan[1, 2] and H. F. Schweiger[1]
[1] Institute of Soil Mechanic and Foundation Engineering, Graz University of Technology, Graz, Austria
[2] Department of Civil Engineering, National Institute of Technology, Bandung, Indonesia
E-mail: indra.hamdhan@TUGraz.at

Abstract

In slope stability analysis, a progressive failure can occur due to a reduction of strength with increasing strain. This paper examines slope stability analysis with strain softening behaviour and their comparison with the strength reduction approach applying the finite element method. The results show that failure mechanisms obtained by both approaches are almost identical. The ratio between peak and reduced strength in strain softening behaviour is correlated with the factor of safety (FOS) in strength reduction technique.

For strain softening materials, it cannot be assumed that a safety factor (FOS) greater than one based on peak shear strength means stability, because deformations may lead to a local loss of strength, requiring mobilization of additional strength at other points along the slip surface. This mechanism leads to additional movement and further strain softening. Therefore, if the peak strength is mobilized anywhere along the failure surface, a slope in strain softening materials is at risk of progressive failure. Analysis of slope stability was done by the finite element method using the Mohr Coulomb failure criterion and an advanced Multilaminate model. In the proposed paper, the Multilaminate model for soil, enhanced with a non-local formulation as regularisation method, and a simple Mohr Coulomb model in invariant formulation are compared.

Introduction

The finite element method is an established numerical technique for solving boundary value problems in geotechnical engineering. Whereas in the past emphasis was put on calculating displacements and stresses under working load conditions the method is increasingly being applied to ultimate limit state calculations such as slope stability analysis because of its ability and flexibility. One of the advantages of finite element method as compared to traditional methods such as limit equilibrium methods is that no assumption of the shape and location of critical failure surfaces has to be made.

The main objective of this paper is to evaluate and to compare the failure mechanism of a simple slope obtained by a strain softening and strength reduction approach respectively and to check the influence of the stress path followed on the calculated factor of safety. Analysis of slope stability was performed by using a Mohr Coulomb and a Multilaminate model.

Shear Strength Reduction Technique

The shear strength reduction technique is considered the most widely used method in slope stability analysis using the finite element method. It works well when a simple Mohr Coulomb model, which is a linear elastic perfect plastic model, where soil parameters are assumed to be constant during all stages of soil loading and unloading, is employed.

The principle of the shear strength reduction technique in finite element analysis is to simultaneously reduce c and tanφ in small increments until failure occurs in the numerical analysis. If shear strength parameters at failure are c_r and φ_r, the factor of safety (FOS) can be defined as:

$$FOS = \frac{\tan\varphi}{\tan\varphi_r} = \frac{c}{c_r} \tag{1}$$

Multilaminate Model with Strain Softening

In Multilaminate model, the constitutive behaviour is formulated on so called sampling planes (e.g. Schweiger *et al*., 2009). The analysis presented in this paper use the Multilaminate model with a linear strain softening formulation as developed by Galavi, 2007. In this formulation, the peak strength on a plane is reached at a certain strain level ($\varepsilon_{di,\ peak}$) followed by softening to a residual value $\varepsilon_{di,\ res}$ (**Figure 1** and **2**).

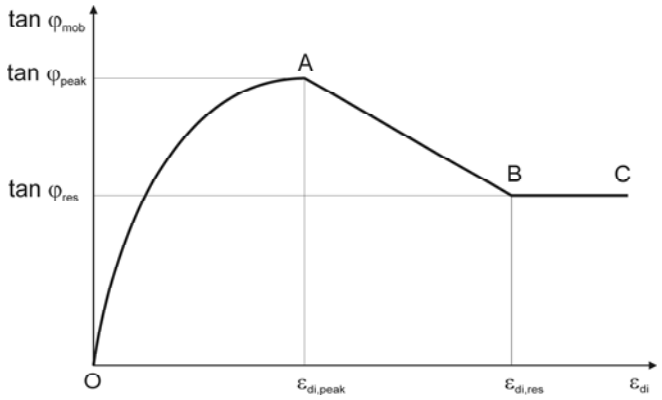

Figure 1: Relation between mobilized friction angle and damage strain on each sampling plane.

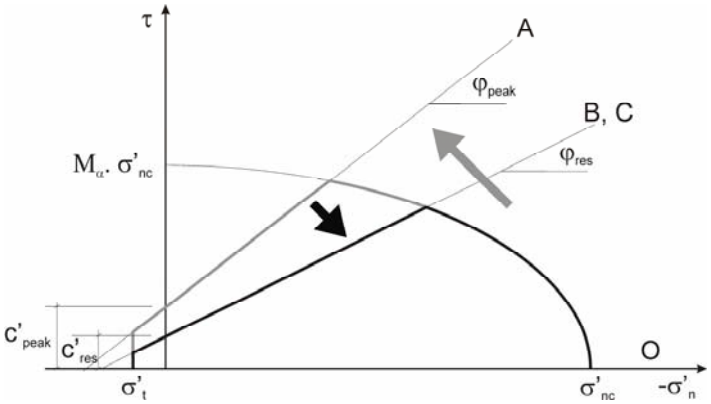

Figure 2: Deviatoric hardening and softening on a sampling plane.

Linear softening on integration planes is defined as:

$$\tan\varphi'_{mob} = -m_{soft,\varphi}\left(\varepsilon_{di} - \varepsilon_{di,peak}\right) + \tan\varphi'_{peak} \quad (2)$$

$$c'_{mob} = -m_{soft,c}\left(\varepsilon_{di} - \varepsilon_{di,peak}\right) + c'_{peak} \quad (3)$$

m_{soft} is the softening rate parameter that governs the reduction of the strength parameters on the sampling plane whereas in general cohesion degrades faster than the friction angle which reaches residual values after significant plastic deformation. Consequently, two independent softening rate parameters for cohesion ($m_{soft,c}$) and friction angle ($m_{soft,\varphi}$) have been introduced into the model.

Numerical Modelling of Slope Stability

In this section, slope stability analysis will be evaluated using four different methods to calculate the factor of safety (FOS):

1. Analysis with strain softening behaviour.
   In this method, slope stability analysis is carried out using the Multilaminate model with two different ratios of peak / residual strength (ratio of 1.1 and 1.3).
2. Analysis with reduced strength.
   In this method, slope stability analysis is carried out using the Multilaminate model with reduced strength. This reduced strength is obtained from two different ratios of peak / residual strength (ratio of 1.1 and 1.3)
3. Analysis with strength reduction in one step.
   In this method, slope stability analysis is carried out using the Multilaminate model with peak strength in the beginning of calculation. After the peak strength is reached, the material is changed to reduced strength. This leads to a stress state violating the strength criterion and thus to a redistribution of stresses. This reduced strength is also obtained from two different ratios of peak / residual strength (ratio of 1.1 and 1.3)
4. Analysis with “standard” strength reduction technique using the MC-criterion.
   In this method, slope stability analysis is carried out using the Mohr Coulomb model with the

load obtained from the analysis with strain softening behaviour.

All analyses are performed utilizing the FE-code PLAXIS (Brinkgreve *et al*., 2008),

Geometry, Finite Element Mesh and Material Properties
A simple geometry of a slope with homogeneous soil has been chosen. The slope is 10 m high and has a 1:2 gradient (horizontal to vertical). The geometry and finite element mesh used are shown in **Figure 3**. 458 15-noded elements have been used.

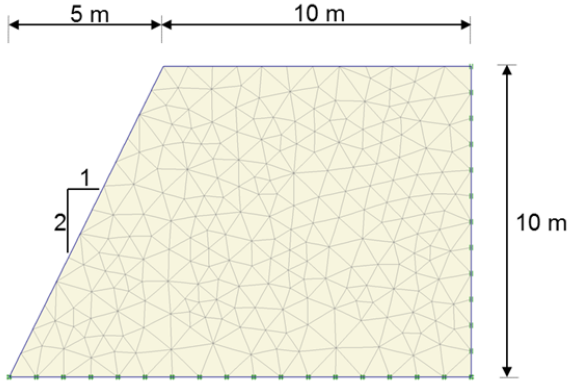

Figure 3: Geometry and finite element mesh of slope

The soil parameters for the Mohr Coulomb and the Multilaminate model are given in **Table 1** and **Table 2**.

Table 1: Input Parameters for Mohr Coulomb (MC) Model

Description	***Symbol***	**Unit**	**Value**
Unit weight	γ	kN/m^3	20
Young modulus	E	(kPa)	10000
Poisson's ratio	ν	(-)	0.35
Cohesion	c	(kPa)	30
Friction angle	φ	(^{o})	35

Table 2: Input Parameters for Multilaminate (ML) Model

Description	**Symbol**	**Unit**	**Value**
unit weight	γ	kN/m^3	20
Reference oedometer modulus	$E_{oed_{ref}}$	(kPa)	10000
Reference young modulus for unloading and reloading	$E_{ur_{ref}}$	(kPa)	30000
Poisson's ratio	ν'	(-)	0.25
Peak cohesion	c'_{peak}	(kPa)	30
Peak friction angle	φ'_{peak}	(^{o})	35

Reduced cohesion (ratio of 1.1)	$c'_{res1.1}$	(kPa)	27.27
Reduced friction angle (ratio of 1.1)	$\varphi'_{res1.1}$	(°)	32.48
Reduced cohesion (ratio of 1.3)	$c'_{res1.3}$	(kPa)	23.08
Reduced friction angle (ratio of 1.3)	$\varphi'_{res1.3}$	(°)	28.31
Softening rate parameters for cohesion	$m_{soft,\,c}$	(-)	2.75
Softening rate parameters for friction angle	$m_{soft,\,\varphi}$	(-)	0.064

Boundary Conditions

In the analysis with the Multilaminate model, a prescribed displacement of 4 m width with a constant rate was imposed on the top of the slope. In Mohr Coulomb analysis, a load is imposed on the slope surface (**Figure 4**). The amount of loading is obtained from the residual force of the result of the Multilaminate model considering strain softening behaviour.

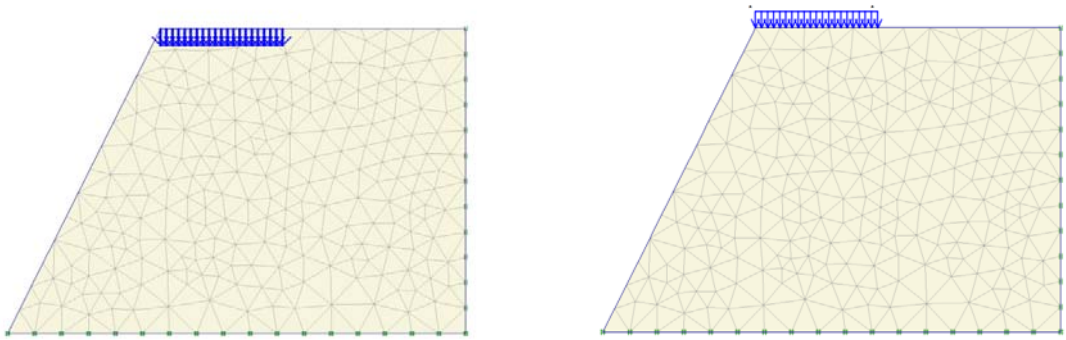

a) Prescribed displacement input in ML. b) Load input in MC.

Figure 4: Loading conditions for the slope.

Results

By applying the same ratio between peak and reduced strength (R) using the Multilaminate Model almost identical residual vertical forces are obtained whatever method is used (strain softening, reduced strength and change of strength in one step). The difference is only 2.5% with R = 1.1 and 11% with R = 1.3.

In the analysis slope stability with strain softening using the Multilaminate model with a ratio equal to 1.1, the residual vertical force at the surface of the slope is equal to 328.81 kN/m or 82.2 kN/m^2 (load along 4m at the surface). This value is applied as a load in the Mohr Coulomb model and gives a FOS of 1.08. When the ratio is increased to 1.3, the residual vertical force at the surface of the slope is equal to 231.30 kN/m or 57.8 kN/m^2 (load along 4m at the surface). If this value is applied as a load in the Mohr Coulomb model, a FOS of 1.21 is obtained. It should be mentioned that due to the formulation of the Multilaminate model, the strength is slightly higher as compared to the Mohr Coulomb model (with the some value for φ') and therefore some differences have to be expected.

All four different methods of calculation of the safety factor investigated (ML with strain softening, ML with reduced strength, ML with change of strength in one step and MC with

strength reduction technique) seem to convergence to similar failure mechanisms and factors of safety. **Figure 5** and **6** show the vertical force – total displacement curves at the control point (A, B and C) of the top surface and failure mechanism for all analyses.

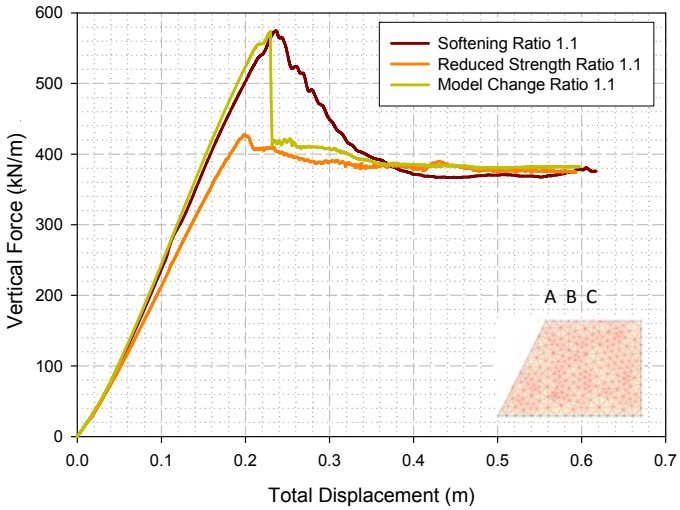

a) Vertical force vs. total displacement

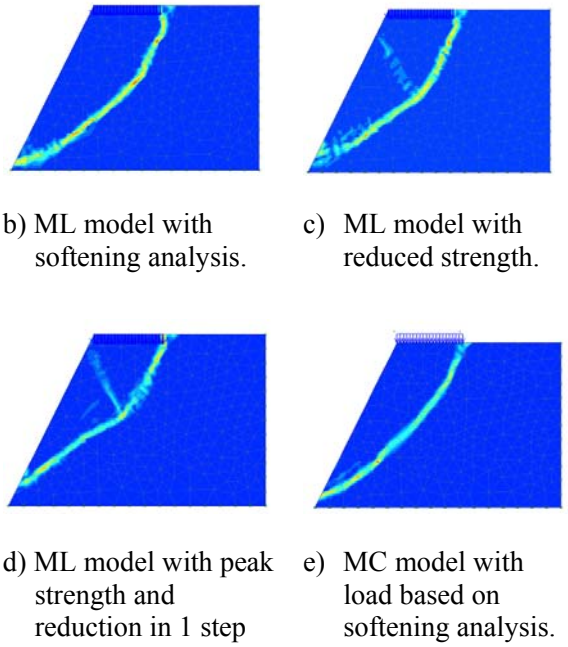

b) ML model with softening analysis.

c) ML model with reduced strength.

d) ML model with peak strength and reduction in 1 step

e) MC model with load based on softening analysis.

Figure 5: Analysis of slope stability with ratio peak / reduced strength equal to 1.1.

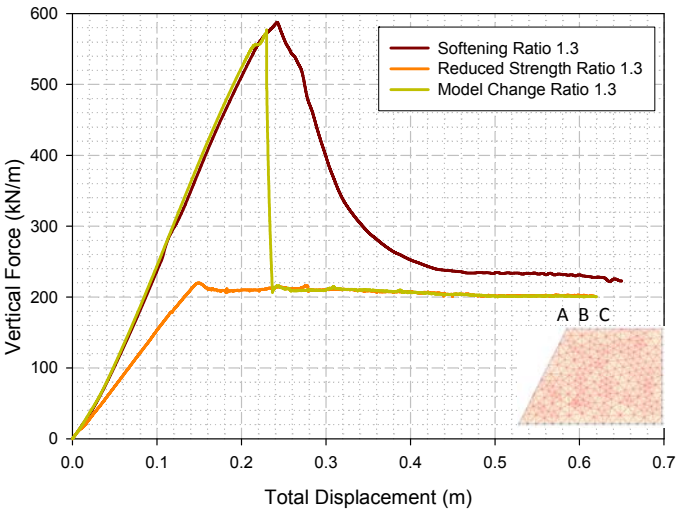

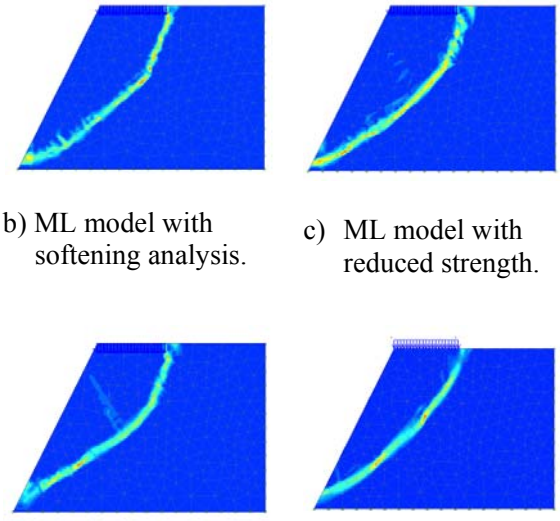

b) ML model with softening analysis.

c) ML model with reduced strength.

d) ML model with peak

e) MC model with

a) Vertical force vs. total displacement	strength and reduction in 1 step	load based on softening analysis.

Figure 6: Analysis of slope stability with ratio peak / reduced strength equal to 1.3.

Conclusion

Slope stability analysis based on the finite element method has been performed. Different methods of analysis with the Multilaminate model, namely (1) strain softening, (2) reduced strength from start of analysis, and (3) strength reduction in a single step to residual, yield very similar results with respect to failure mechanisms and factors of safety (FOS). Ratio of peak / residual strength in Multilaminate model with strain softening behaviour is close to FOS from strength reduction technique obtained from the Mohr Coulomb failure criterion.

Based on these (preliminary) studies it could be concluded (at least for such simple cases as considered here) that the stress paths followed are not crucial for calculating failure mechanisms and factors of safety. However, it is pointed out that only drained conditions and Mohr Coulomb type failure criteria have been considered so far.

References

Brinkgreve, R.B.J., Broere, W., and Waterman, D. (2008). Plaxis, user's manual. The Netherlands.

Conte, E., Silvestri, F., and Troncone, A. (2010). Stability analysis of slopes in soils with strain-softening behaviour. Computers and Geotechnics, Vol. 37, pp. 710-722.

Galavi, V. (2007). A Multilaminate model for structured clay incorporating inherent anisotropy and strain softening. PhD. Thesis, Graz University of Technology, Graz, Austria.

Matsui, T., and San, K., C. (1992). Finite element slope stability analysis by shear strength reduction technique. Soils and Foundation, Vol. 32 (1), pp. 59-70.

Schweiger, H. F., Scharinger, F., Wiltafsky, C., and Galavi, V. (2009). A multilaminate framework for modelling induced and inherent anisotropy of soil. Geotechnique 59, No. 2, pp. 87–101.

Analytical and numerical investigation of the subgrade modulus for raft and pile-raft-foundations

A. Kirsch
ILF Beratende Ingenieure, Feldkreuzstraße 3, A-6063 Rum bei Innsbruck, Österreich
E-mail: ansgar.kirsch@ilf.com

Abstract

It is common practice in structural engineering to idealise the soil-structure interaction between a foundation and the underlying soil with a modulus of subgrade reaction k_s. A comparison of existing analytical/empirical approaches for the determination of k_s for a raft foundation showed a reasonable amount of scatter with differences of more than 100%. Therefore, these approaches were compared to two- and three-dimensional finite element calculations by way of an example of a raft foundation on stiff silt/clay. The results indicate that results of analytical settlement calculations are in reasonably good agreement with the numerical results for the given example.
The comparison of additional calculations for pile and pile-raft foundations showed a surprising inconsistency between a 2D axi-symmetric model and a full 3D model. Further investigations are necessary to study the reasons in more detail.

Introduction

At the interface between geotechnical and structural engineering it is common practice to use the Winkler model [10] to idealise the interaction between soil and structure. This model, which dates back to the 19th century, replaces the soil by a system of mutually independent, closely spaced and linearly elastic springs. Soil is a continuum which can transmit shear stresses, its behaviour is nonlinear, non-elastic, stress-dependent, anisotropic and heterogeneous. But despite all its unrealistic simplifications, the Winkler model is still frequently used in engineering practice.
The main parameter of the model is the modulus of (vertical) subgrade reaction k_s. This modulus is defined as the ratio between (vertical) stress, σ, at a given point underneath a foundation and the corresponding settlement, u, at this point:

$$k_s = \frac{\sigma}{u} \tag{1}$$

It is very important to underline that the modulus of subgrade reaction is a parameter describing the soil-structure interaction and *not* a soil constant. It depends, among other parameters on the following factors (cf. [3]):

- Layering and nature of the soil below the foundation
- Foundation geometry, i.e. shape and dimensions
- Foundation stiffness and stiffness of the superstructure
- Nature and size of the applied load
- Distribution of loads on the foundation
- Time effects, e.g. due to consolidation and creep

It becomes clear that as the stress and settlement between arbitrary points underneath a

foundation vary, also the value for k_s must vary.
A lot of research has been done to derive formulas for the determination of a numerical value for k_s. And despite the long existence of the model and its widespread use, there is still some fundamental disagreement on the determination method.
Basically, methods are available to determine the modulus of subgrade reaction from field tests, from theoretical and empirical correlations and from numerical studies.
This article compares several of the proposed methods by way of an example calculation, excluding methods which make use of field test results. Moreover, the determination of k_s for a pile-raft-foundation is discussed.

Analytical and empirical methods for the determination of k_s

Example problem
For the study of the modulus of subgrade reaction, a raft foundation with dimensions of 40 m x 50 m and an embedment depth of 3 m (on average) was considered (Figure 1). It lies on an inclined stratum of silt and clay with a thickness of approx. 10 m and is rather soft. Below this layer there is a stratum of non-cohesive sandy gravel with boulders, which has a high stiffness. Some material parameters for the model materials are summarised in Table 1. Groundwater was considered at a depth of 4.0 m below foundation level.

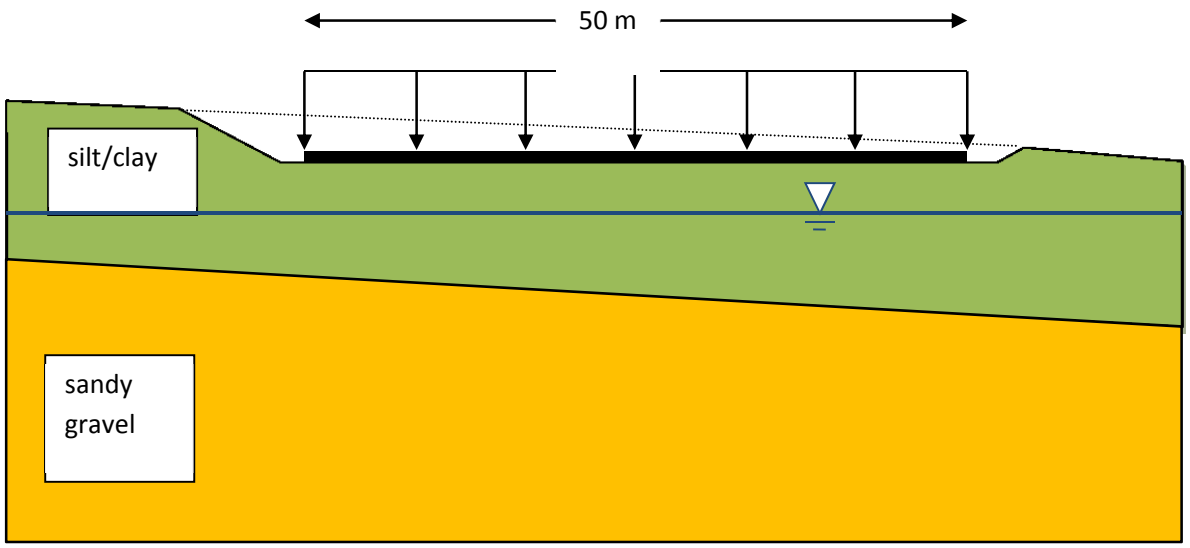

Figure 1: Geometry of the example

Table 1: Material parameters

parameter		unit	silt/clay	sandy gravel	structural fill
self-weight	γ	[kN/m³]	20	21	21
stiffness modulus	$E_{s,loading}$	[MN/m²]	10	100	75
	$E_{s,unloading}$	[MN/m²]	30	300	225

Poisson's ratio	ν	[-]	0.2	0.3	0.3
Friction angle	φ	[°]	22	37.5	35
Cohesion	c	[kN/m²]	10	1	1

The foundation plate was assumed to be 0.8 m thick. The foundation load was assumed to be evenly distributed with a value of 120 kPa. Moreover, the influence of a 1 m thick layer of structural fill below the foundation was taken into consideration.

Analytical and empirical approaches

In a first step, the modulus of subgrade reaction was determined for above mentioned situation with approaches by Biot [1], Vesic [9], Bowles [2], Goris [4], Meyerhof and Blaike [cited in [6]], Kopple and Glock [cited in [6]] and Selvadurai [cited in [6]]. Moreover, a settlement calculation for the given situation was performed according to ÖNORM B4431 (cf. also DIN 4019), taking the subsurface structure, the un-reloading behaviour and the position of the point of interest into account.

The results for an average stiffness modulus of 50 MN/m² (over the depth of influence) are shown in Figure 2. It becomes obvious that there is a large scatter of results, varying between 0.9 MN/m³ and 4.6 MN/m³. Most of the results lie in the range between 1 and 2 MN/m³.

It should be emphasized that these values are much lower than tabulated values: e.g. in Goris [4] for a medium plasticity clay a range of 15-30 MN/m³ is given, Bowles [2] quotes a minimum range of 12-24 MN/m³ for a clayey soil. The reason for this is probably that tabulated values only apply to very small foundations or serve as reference for the determination of the modulus of subgrade reaction from a plate load test, but they do not hold for large footings any more.

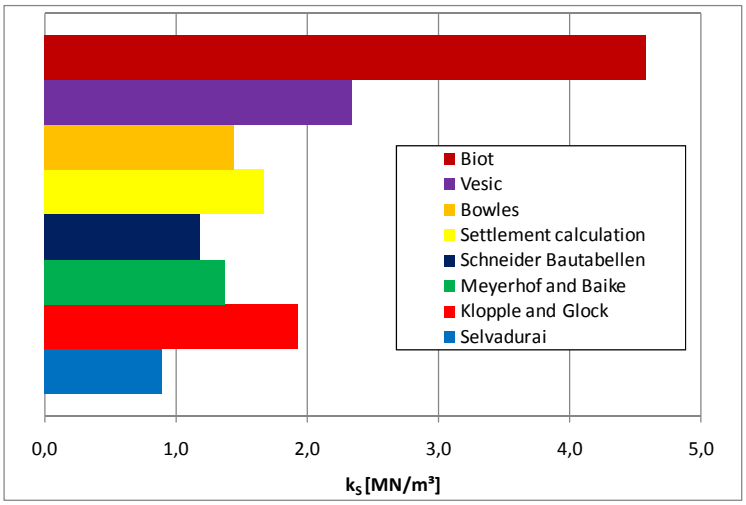

Figure 2: Results for analytical/empirical determination of k_s

Due to the large discrepancies among the analytical/empirical results and the unsatisfactory comparison to tabulated values, two- and three-dimensional finite element analyses were performed for the raft foundation.

Numerical determination of k_s with 2D- and 3D-FE calculations

One possible solution to determine the modulus of subgrade reaction is to perform finite element calculations and put the resulting stress between foundation plate and soil settlement into relation, according to formula (1). To investigate also the influence of the three-dimensional nature of the problem, both 2D- and 3D-Finite Element calculations were performed.

Numerical models and analysis steps

The 2D analyses were performed with the geotechnical FE-software PLAXIS. The plane strain model consisted of 775 15-noded triangular elements and considered the longitudinal section of the foundation. For the 3D investigation, the package PLAXIS 2010-3D was used. In that case, the model consisted of approx. 60000 tetrahedral elements with 10 nodes each.
The use of interface elements allowed to read out easily contact stresses between soil and foundation plate as well as the settlements of the plate.
In both cases an advanced hardening soil model was used for the soil types. The foundation plate was modelled with a linear-elastic plate element.
Different investigation phases were applied: after an initial step to establish geostatic equilibrium, excavation of the construction pit was simulated, followed by installation and loading of the foundation plate. Optionally, a homogenisation layer of structural fill was considered below the foundation plate.

Parametric study

Apart from the comparison between numerical and analytical results, the influence of the following factors on the subgrade modulus was investigated:

- Thickness of the raft foundation (between 0.6 and 1.0 m)
- Stiffness of the upper layer (between 10 and 100 MN/m²)
- Construction of 1m thick homogenisation layer (or not)

Results

The results were evaluated for the longitudinal section of the raft, cutting through the centre of the foundation. Figure 3 shows a comparison of 2D-, 3D-FE calculations as well as the determination of k_s with a standard settlement calculation for three chosen points across the foundation.

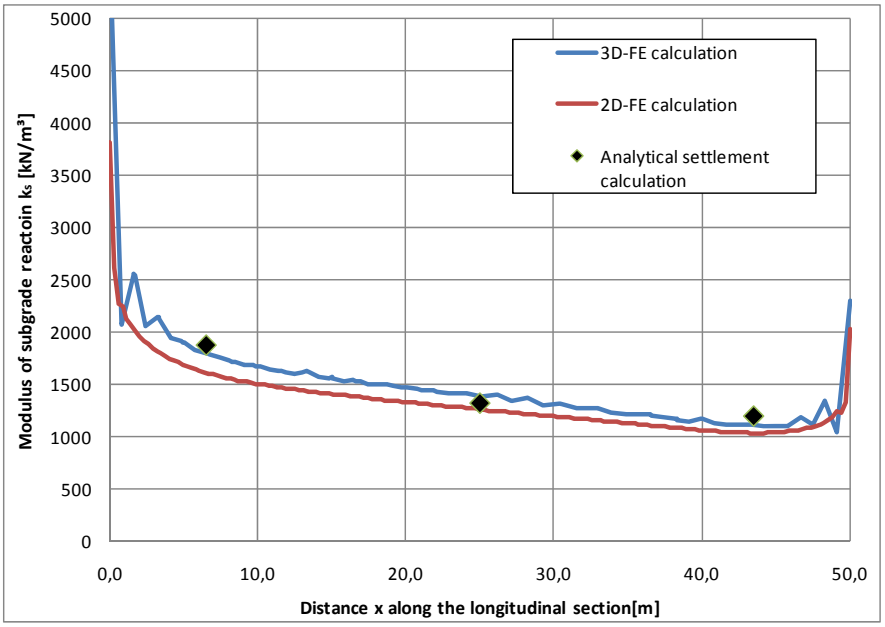

Figure 3: Distribution of k_s along the longitudinal section of the foundation (t = 0.6 m, E_s = 10 MN/m², no structural fill below foundation)

The distribution of k_s along the longitudinal section is not constant. This is due to the different degree of unloading for different points along the cut (inclined topography). In addition, the sharp increase of k_s towards the edges is attributed to stress concentrations at the edges.

It becomes obvious that the 2D- and 3D-FE results do not differ significantly from each other for the given problem. Also the analytical results, derived from standard settlement calculations, show a very good correlation to the numerical results (Figure 3). The range of values for k_s lies between approx. 1 and 2 MN/m³, thus supporting the range of values derived from the analytical/empirical approaches (cf. Figure 2).

Moreover, the following conclusions can be drawn from the calculations for the given example:

- The thickness of the foundation plate has a negligible influence on the k_s-values.
- The crushed stone layer below the foundation increased the modulus of subgrade reaction by on average 10 to 30%.
- As expected, the stiffness of the upper soil layer has a big impact on the value of k_s. E.g. for the centre of the foundation the values increased from approx. 1500 kN/m³ (for E_s=10 MN/m²) to 6000 kN/m³ (for E_s=100 MN/m²).

Extension of the analyses to pile-raft foundation

In order to evaluate the changes of the system behaviour, if piles are installed below the foundation, additional three-dimensional Finite Element analyses were performed. These analyses were performed with both, axi-symmetric 2D-simulations with PLAXIS as well as full 3D-simulations with PLAXIS 2010-3D.

Geometry and input parameters
For the pile-raft foundation piles with a diameter of 80 cm and a spacing of 3.75 m were considered. The length was varied between 10 and 14 m. The soil parameters were identical to those used in the previous stage.

Axi-symmetric model
For the axi-symmetric model a so-called unit-cell approach was considered (cf. [7]). In that case the diameter of the problem domain is chosen in a way that the zone of influence of one single pile is equivalent to that in the field. The boundary conditions of the model represent an infinitely large pile group. The raft was modelled with a plate element with rotation fixities at each end.

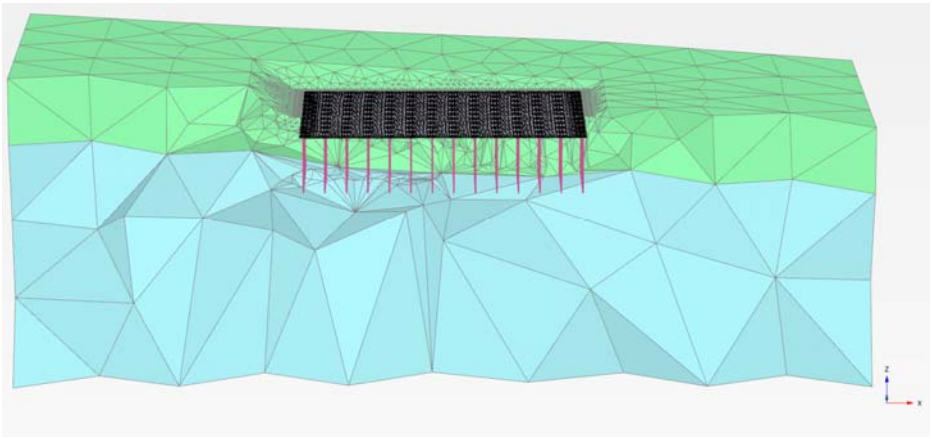

Figure 4: 3D-FE model for the piled foundation

Full 3D model
In order to assess also the effects of the position of the piles in a group, an overall number of 154 so-called embedded-piles were added to the 3D model (Figure 4).

Results
The results of the axi-symmetric model showed that the modulus of subgrade reaction virtually dropped to zero underneath the plate ($k_s \approx 25$ kN/m³ instead of 1500 kN/m³), whereas the area below the pile cap showed moduli in the order of 10,000 to 12,000 kN/m³.
The same conclusion holds, if only one layer of homogeneous soft soil was applied for the whole problem domain (stiffness of 10 MPa). This means that, for the given example, the bedding reaction below the raft of the foundation is negligible in any case.
The simulations with a full 3D model performed differently. In that case the zones below the pile caps also showed a significant increase in bedding reaction between 10,000 and 15,000 kN/m³, but the modulus immediately below the raft remained virtually unchanged.
Further investigations and variations are necessary to identify the reasons for such a different behaviour in the numerical models, which is also not in agreement with published ratios between $k_{s,pile\text{-}raft}$ and $k_{s,raft}$ (cf. e.g. [5]).

Conclusion

The comparison of existing analytical/empirical approaches for the determination of the modulus of subgrade reaction for a raft foundation showed a reasonable amount of scatter with differences of more than 100%. Therefore, these approaches were compared to two- and three-dimensional finite element calculations by way of an example of a raft foundation on stiff silt/clay. The results indicate that results of analytical settlement calculations are in reasonably good agreement with the numerical results for the given example.
The comparison of additional calculations for pile and pile-raft foundations showed a surprising inconsistency between a 2D axi-symmetric model and a full 3D model. Further investigations are necessary to study the reasons in more detail.

Acknowledgements

The support of my colleagues Christoph Pletzer and Vlastislav Trunda is thankfully acknowledged.

References

[6] Biot, M.A. (1937). Bending of infinite beams on an elastic foundation. J. Appl. Mech. Trans., ASME, Vol. 59, pp. A1-A7.
[7] Bowles, J.E. (1997). Foundation analysis and design, 5th ed., McGraw-Hill, New York
[8] DIN Deutsches Institut für Normung e.V. (2003). DIN-Fachbericht 130, Wechselwirkung Baugrund/Bauwerk bei Flachgründungen, Beuth Verlag, Berlin
[9] Goris, H. (ed.) (2008). Bautaubellen für Ingenieure, 18th ed., Werner Verlag, Köln
[10] Hanisch, J., Katzenbach, R., König, G. (eds.) (2002). Kombinierte Pfahl-Plattengründungen, Ernst & Sohn, Berlin
[11] Sadrekarimi, J., Akbarzad, M. (2009). Comparative study of methods of determination of coefficient of subgrade reaction, EJGE, Vol. 14, pp. 1-14.
[12] Schweiger, H.F., Gäb, M. (2006). FE-Simulation von Baugrundverbesserungen – Möglichkeiten und Grenzen, Christian-Veder-Kolloquium 2006, pp. 139-154.
[13] Terzaghi, K.V. (1955). Evaluation of coefficient of subgrade reaction. Géotechnique, Vol. 5, No. 4, pp. 297-326.
[14] Vesic, A.B. (1961). Beams on elastic subgrade and Winkler's hypothesis. Proc. 5th Int. Conf. on Soil Mech. Found. Eng., Paris, Vol. 1, pp. 845-850.
[15] Winkler, E. (1867). Die Lehre von Elastizität und Festigkeit. Dominicus, Prague

Comments on the State of Art of Design of Pillar Systems in Mines

Horst Wagner[1] and Hannes Blaha[1]

[1] Chair of Mining Engineering and Mineral Economics, Montan-University Leoben,

Franz-Josef-Straße 18, A-8700 Leoben, Austria

E-Mail: Horst.Wagner@MU-leoben.at

Abstract

Pillars are essential elements in underground mines. The design of pillar systems requires knowledge of the strength of and load acting on pillars. Because of size pillar strength can in most instances not be determined experimentally. Development of empirical strength formulae is discussed. Some of widely used formulae are compared. Rock mass strength estimate is the most critical parameter. Different approaches are compared. Advances in numerical methods are briefly mentioned. Pillar load is displacement controlled and requires detailed knowledge of mine and pillar stiffness and position of pillar in the mine. Often pillar load is estimated on basis of tributary area concept which applies to very specific situations. Associated problems are discussed. Use of numerical models to estimate pillar loads is recommended, particularly in mining situations involving small mining spans.

Introduction

Pillars are essential structural elements of most underground mining systems. Their role is to protect essential mine infrastructure or to support overburden rock strata in extraction areas. Typical examples are shaft protection pillars, barrier pillars against inflow of water in mining areas and support pillars in extraction areas such as in room and pillar mining.

Pillar failures have been the cause of many mine accidents and mine disasters. Probably the most severe of which was the failure of several thousand coal pillars at Coalbrook coal mine in South Africa in 1960 resulting in the death of 437 miners,[1]. Large regional pillar failures have occurred in potash mines in Central Germany triggering mine tremors with magnitudes in excess of 5 on the open-ended Richter scale.[2].

Following the Coalbrook mine disaster a systematic long-range research program into pillar behavior was initiated by the South African government in 1963 and later continued by the South African Chamber of Mines. Much of the understanding of the behavior of pillars systems stems of this pioneering work. In Central Germany systematic research into the behavior of salt pillars was conducted by the International Bureau for Rock Mechanics of German Academy of Science in Leipzig. Despite all these and other efforts and the advances that have been made pillars continue to present a considerable risk in underground mining.

Rock Mechanics Aspects of Pillar Systems

Design of pillar systems centers around two issues, namely the strength and the load acting on pillars. The pillar system comprises of the pillar, the interface between pillar and surrounding rock mass, and the local and regional mining situation. In addition geological factors such as nature of immediate and regional rock strata, mechanical properties of rock strata, degree of rock jointing and fault systems are important factors influencing and controlling pillar system behavior.

Pillar load is the result of a statically indeterminate system and depends on external stress field, stiffness of mining system and stiffness of pillar itself and, except for some idealized cases, can be determined only by means of complex numerical analysis, [1].

Pillar strength

Pillar strength depends on the strength of pillar material, degree and orientation of rock jointing, frictional properties of contact area between pillar and surrounding rock strata, creep properties of pillar, loading rate and geometry of pillar, i.e. length, width and height of pillar. Pillar strength cannot be determined directly because of the forces involved and the disturbance of the pillar by the experimental process. For these reasons pillar strength is determined by means of back analysis of actual pillar performance in mines..

Empirical pillar strength formulae

Without doubt the most comprehensive and reliable state of knowledge of pillar strength exists in the area of coal pillars. The reasons for this are the systematic research on coal pillars following the Coalbrook coal mine disaster on the one hand and the fact that every year several hundred thousand pillars are created in room and pillar mining operations. Some of the difficulties mentioned above have been overcome by Salamon and Munro by analyzing a number of failed and intact pillars in South African coal mines using advanced statistical methods [3]. This work resulted in the following well known and widely applied pillar strength formula for square coal pillars:

$$S_p = 7{,}2 * \frac{W^{0,46}}{H^{0,66}} \qquad (1)$$

Where S_p…….pillar strength (MPa)

W…….pillar width (m)

H…….pillar height (m)

For rectangular pillars (L, W) an effective pillar width, W_{eff}, can be defined as follows [4, 5]

For $W/H=R<3$ $\quad W_{eff} = W$

For $W/H= 3<R<6$ $\quad W_{eff} = \left\{\frac{2L}{L+W}\right\}^{\left(\frac{R-3}{3}\right)} * W$

For *W/H=R >3* $W_{eff} = \frac{2*L*W}{(L+W)}$ (2)

Pillar strength formula (1) which is valid for pillars with *R=W/H) <4* has been extended by Salamon to cover squat pillars [4].

For *W/H=R>5* $S_p = \frac{18,7}{V^{0,0667}} * \left\{0,237 * \left[\left(\frac{R}{5}\right)^{2,5} - 1\right] + 1\right\}$ (3)

The above pillar strength formulae have been applied successfully in a number of coal mining countries and have acquired statutory status in South Africa.

As far as the strength determination of hard rock pillars is concerned the situation is less advanced. The reasons for this are the varying geological conditions, the wide range of strength values of hard rock formations, the less clearly defined frictional properties of the contact area between pillar and surrounding rock and the lack of comparable mining conditions. In recent years a number of papers have been published in connection with the strength and design of hard rock mine pillars [6, 7, 8, 9, 10, 11]. Table 1 gives an overview of some strength formulae for hard rock pillars. Three different types of formulae can be distinguished, namely power laws, linear relationships and others. Within the limitations of this presentation only the first two will be discussed.

Tab. 1: Summary of some of the published pillar strength formulae (after Martin & Maybee; Gonzalez-Nicieza et al [12, 13])

Formula/author	α	β	a	b	c	σ_c (MPa)	Rock type
$S_p = c * \sigma_c * W^{\alpha} * H^{\beta}$							
Salamon & Munro	0,46	-0,66			0,24	30	Coal
Hedley & Grant	0,50	-0,75			0,58	230	Quartzites
Von Kimmelmann et al	0,46	-0,66			0,49	94	Metasediments
Potvin et al	1	-1			0,42	various	Canadian shield
$S_p = c * \sigma_c(a + b * R)$							
Krauland & Soder			0,778	0,22	0,35	100	Limestone
Sjöberg			0,78	0,22	0,30	240	Limestone/Skarn
Lunder & Pakalnis			0,680	0,52κ	0,44	-	Hard rocks

κ in the Formula by Lunder & Pakalnis take the influence of confinement on pillar strength into account.

The pillar strength formulae address two main issues, namely the in situ strength of pillar material, i.e. rock mass strength, and the effect of confinement caused by pillar geometry on pillar strength. The parameters α and β, and a and b describe the influence of pillar geometry on pillar strength while the parameter c accounts for rock mass factors such as jointing and frictional properties on pillar strength. The variation in numerical value of parameters which describe

influence of geometry on pillar strength within each group of pillar strength formulae is relatively small with the exception of Potvin et al and to a lesser degree Lunder and Pakalnis.

In assessing the above pillar strength formulae it has to be born in mind that these are based on analysis of pillars with width to height ratios smaller than four and often smaller than two and do not cover the strength of squat pillars.

The rock mass parameter c varies between 0,24 and 0,58 and accounts for most of the strength differences. While the value of c is known for specific situations the challenge is to predict it for new situations. The differences in c values are largely due to existing discontinuities in the rock mass, i.e. number, orientation and frictional properties of discontinuity surfaces. All commonly used rock mass rating systems pay more attention to these parameters than to the actual strength of rock material. In general the rock mass rating deteriorates with joint density and smoothness of joint surfaces and joint alteration.

A basic shortcoming of most rock mass rating systems is that while providing a general indication of rock mass quality they do not provide a direct measure of rock mass strength [15, 16]. Sheorey [17] has published a rock mass strength formula based on RMR values.

$$\sigma_{rm} = \sigma_c * e^{\frac{RMR-100}{20}} \tag{4}$$

Applying Sheorey's rock mass strength estimate it is found that the published „c"-values fall in the RMR-range of 70 to 90 which appears reasonable.

Another widely used approach in rock mass strength determination is based on the Hoek-Brown failure criterion in combination with the Geological Strength Index; GSI.

$$\sigma_1 = \sigma_3 + \sigma_{ci}\left\{m_b * \frac{\sigma_3}{\sigma_{ci}} + s\right\}^a$$

$$m_b = m_i * exp\left\{\frac{GSI-100}{28-14D}\right\}$$

$$s = exp\left\{\frac{GSI-100}{9-3D}\right\}$$

$$a = \frac{1}{2} + \frac{1}{6}\left\{e^{-GSI/15} - e^{20/3}\right\} \tag{6}$$

$$\sigma_{c(RM)} = \sigma_{ci} * s^a$$

$$\sigma_{t(RM)} = -\frac{s * \sigma_{ci}}{m_b}$$

Where σ_{ci}……uniaxial compressive strength of intact rock
m_i…….parameter describing rock type ($4<m_i<32$)
D…….Disturbance factor describing effect of rock excavation ($0<D<1$)

Table 2 summarizes the strength estimates using the rock mass strength formulae of Sheorey and Hoek-Brown. It is seen that the differences between the Sheorey (RMR) and Hoek-Brown GSI(D=0) strength values are smaller than the effect of disturbance factor on GSI-strength estimates. Furthermore it will be observed that all published c values fall in the rock mass rating range above 60, i.e. good to excellent rock masses.

Table 2: Comparison between nominal rock mass strength values based on the Sheorey and Hoek-Brown rock mass strength criteria.

RMR/GSI	**Strength(RMR)**	**Strength GSI_{D0}**	**Strength $GSI_{D0,5}$**
20	**0,018**	**0,001**	**0,001**
40	**0,050**	**0,033**	**0,017**
60	**0,135**	**0,107**	**0,068**
80	**0,368**	**0,329**	**0,263**
90	**0,607**	**0,574**	**0,513**
100	**1**	**1**	**1**

As the RMR and GSI ratings cannot be compared directly it is necessary to first examine the relationship between the two rating systems. Based on numerous comparisons the following relationship between the RMR_{89} values and the GSI values have been found.

$$GSI = basicRMR_{89} - 5 + (-R_w + 15) \qquad (7)$$

Where R_w …….Correction for water situation in rock mass (R_w =15 for dry conditions)

For comparable rock masses it is found that strength values in the area of interest based on the Hoek-Brown – GSI approach are between one third and one quarter lower than the Sheorey strength values.

A basic weakness of rock mass strength values based on rock mass rating systems is that the effects of orientation on strength are inadequately accounted for. This is particularly critical in the case of slender pillars. Esterhuizen [18] has shown that the effects of orientation of joints on pillar strength diminish with increasing with to height ratio of pillar. These findings have been confirmed by numerical studies [19]. Critical parameter is the joint orientation in the direction of minimum pillar width. In the case of one dominant joint direction it is advisable to employ rectangular pillars oriented such that the long side of pillar is oriented in the dip direction of joint. Square pillars are the most unfavorable pillar geometry in such cases.

The differences in strength increase with width- to- height ratio are largely due to differences in frictional properties a the interface between pillar and surrounding rock strata. Low cohesion and friction values prevent build up of three dimensional state of stress in central portion of pillar

with adverse effect on pillar strength. Soft shale bands in pillars promote development of tension cracks and cause severe weakening of pillars. These effects are more severe in case of slender pillars (R<0,8) and can in the case of very low weak band strength ratios reduce pillar strength to one fifth of solid pillar [20,21].

Despite all efforts the assessment of pillar strength is still one of the critical areas of design of pillar systems. Advances in numerical methods such as the PFC-code by Itasca or the degradation model by Fang and Harrision [22] make it possible to gain deeper insights into the complex and progressive mode of pillar failure and to assess the effects of different rock and structural parameters on pillar behavior. However application of these approaches to real life mine pillar design is still at an early stage.

Pillar load

With very few exceptions pillar systems are displacement- and not load controlled systems. Pillar systems are statically indeterminate systems, i.e. the load acting on the pillar is influenced by the external stress field, the depth below surface, the composition and mechanical properties of rock strata, the mining geometry, the position of pillar within the mine and the geometry and deformation properties of the pillar. Pillar load has therefore to be determined separately for each case. However, practical experience shows that this is usually not been done. Instead use is made of the tributary area concept which is based on a load controlled situation. This concept has been developed for determining pillar loads in horizontal tabular mineral bodies situated at constant depths which have been extracted over very large areas employing a regular system of rooms and pillars. In this case each pillar has to carry the weight of the prism of rock which it supports [1, 4]. Since tributary area load concept applies to very large mining areas the effects of load re-distribution from the mined out area to the abutments of extraction area are not considered. Tributary area load constitutes the upper limit of pillar load. The problem frequently arises when small experimental areas are established to study pillar behavior and the latter is viewed in the light of tributary area load whereas actual pillar load is only a fraction because of redistribution of weight of overburden strata in the abutment areas [23, 25].

As a result pillar strength is grossly overestimated. On full production scale this can lead to disastrous pillar failures. On the other hand tributary area based pillar design in narrow mining areas can result in grossly overdesigned pillars and unnecessary losses in mineral substance. A most complex issue is the influence of mining geometry, i.e. dimension of the extraction area, and composition of overburden strata on the mode of pillar failure. Pillars are strain softening structures, that is up to the point of maximum strength they build up resistance to deformation. When strained beyond this point the resistance to deformation reduces. In the case of slender hard rock pillars the drop in resistance is very rapid, in the case of squat pillars the reduction in resistance is gradual. Whether the failure process of strain softening system is sudden and uncontrolled or gradual and controlled depends on the stiffness of loading system and the post-failure stiffness of pillar. The theoretical background to this complex problem has been studied in considerable detail by Salamon [24]. It is noteworthy that in Austria, because of small mining spans, a number of stable pillar failures have taken place which in other situations would undoubtedly have been violent. Again this aspect is often overlooked or not appreciated.

To account for many of the uncertainties governing pillar behavior and design of pillar systems extensive use is made of the concept of factor of safety, FOS. Depending on the importance of structure and consequence of failure nominal safety factors employed in pillar design range from 1,6 to 2,5[1, 4].

Conclusions

The apparently so simple mine pillars are complex structures with many intriguing and difficult to understand features. Shortage of time and space has allowed to deal with only the most basic issues.

In mining with often very large numbers of pillars and limited pre-mining geotechnical information extensive use is made of empirically derived pillar design procedures. Most critical is the estimation of rock mass strength as this is a key parameter in determining pillar strength. In recent years good progress was made in estimating rock mass strength using empirically derived rock mass classification systems. The drawback of these is that the complex rock mass behavior cannot be described adequately with one single parameter. To compensate for this high safety factors are recommended in pillar design. With adequate experience these can be reduced in time. Loading of mine pillars is a complex issue and often inappropriate use is made of the tributary area concept. This results in either overestimating pillar strength or overdesigning pillars with consequent loss in mineral substance. Use of numerical methods in assessing pillar loads is recommended particularly in alpine mining situations where mining areas tend to be small and mining geometries are irregular [25]. An area which requires considerable attention and research work is the effect of time on behavior of hard rock- and coal pillars.

References:

[1] Salamon M. D. G., Oravecz K. I. Salamon, M. D. G. and Oravecz, K. I. (1976). Rock Mechanics in Coal Mining. Chamber of Mines of South Africa, P.R.D. Series No. 198, 1976

[2] Bodenstein J., Minkley W., Staufenbiel W. (1998). Sicherungsmaßnahmen im stillgelegten Kalibergwerk Teutschenthal-Versatz mit betriebsfremden Stoffen. In: Proc, Depotech, Hengerer et al. Editors, Balkema-Rotterdam, pp. 203-211.

[3] Salamon M. D. G., Munro A. H. (1967). A study of the strength of coal pillars. J. S. Afr. Inst. Min. Metall. Vol.68, pp. 55-67.

[4] Wagner H. (1992). Coal pillar design in South African coal mines. In: Coal Pillar Design Workshop. 33rd US Rock Mechanics Symposium, Sante Fe, New Mexico.

[5] Galvin J. M. (1999). Private communication on effective pillar widths in Australian coal mines.

[6] Hedley D. G. F., Grant, F. (1972). Stope- and- pillar design for the Elliot Lake Uranium Mines. Bull.Can.Inst.Min. Metall., Vol. 65 pp. 37-44.

[7] Von KimmelmannM. R., Hyde B., Madgwick, R. G. (1984): The use of computer applications at BCL Limited in nplannining pillar extraction and design of mining layouts. In: Brown E. T., Hudson J. A., editors. Proc. ISRM Symposium: Design and Performance of Underground Excavation. London: British geotechnical Society, pp. 53-63.

[8] Krauland N., Soder, P. E.(1987). Determining pillar strength frommpillar failure observations. Eng.Min.J. Vol.8, pp. 34-40.
[9] Potvin Y., Hudyma M. R., Miller H. D. S. (1989). Design guide lines for open stope support. Bull. Can. Min. Metall. Vol. 82, pp.53-63.
[10] Sjöberg J. (1992). Failure modes and pillar behavior in the Zinkgruvan Mine. In: Tillerson, J. A., Wawersik, W. R. editors. Proc. 33rd US Rock Mechanics Symposium. Santa Fe. Rotterdam. A.A. Balkema, pp. 491-500.
[11] Lunder P. J., Pakalnis R. (1997). Determining the strength of hard rock mine pillars. Bull.Can. Inst. Min. Metall., Vol. 90, pp.51-55.
[12] Martin C. D., Maybee W. G. (2000). The strength of hard rock pillars. Int. J. Rock Mechanics &Min. Sci., Vol. 37, pp. 1239-1246.
[13] Gonzalez-Nicieza C., Alvarez-Fernandez M. I., Menendez-Diaz A., Alvaraez-Vigil A. E. (2006). A comparative analysis of pillar design methods and ist application to marble mines. Rock Mechanics and Rock Engineering. Vol. 36, pp.421-444.
[14] Esterhuizen G. S., Dolinar D. R., Ellenberger J. L (2008).: Assessment of stable and failed pillars in underground limestone mines. Min. Eng. 2008 Nov; 61(11):43-48.
[15] Bieniawski Z. R. (1989). Engineering rock mass classification. A complete manual for engineers and geologists in mining. In: J. Wiley, Civil and Petroleum Engineering.
[16] Hoek E., Brown E. T. (1997). Practical estimates o9f rock mass strength. Int. J. Rock Mech. Min. Sci., Vol. 34, pp. 1165-86.
[17] Sheorey F. R. (1997). Empirical rock failure criteria. A. A. Balkema, Rotterdam
[18] Esterhuizen G. S. (1995). Rock engineering evaluation of jointing in South African coal seams and its potential effect on coal pillar strength. In: Mechanics of Jointed and Faulted Rocks. Rossmanith. Editor. A.A. Balkema. Rotterdam. ISBN 90 5410 541 0. pp. 807-812.
[19] Zhou T. (2010). Study of mine pillar strength in different conditioins by numerical modelling with 3DEC. Project report. Chair of Mining Engineering. University of Leoben.
[20] Wagner H. (1987). Design and support of underground excavations in highly stressed rock. Proc. 6th Congress International Society on Rock Mechanics. Montreal, Canada.
[21] Esterhuizen G. S., Ellenberger J. L.(2007): Effects of weak bands on pillar stability in stone mines: field observations and numerical model assessment. Proceedings of the 26th International Conference on Ground Control in Mining, July 31 - August 2, 2007, Morgantown, West Virginia. Peng SS, Mark C, Finfinger GL, Tadolini SC, Khair AW, Heasley KA, Luo Y, eds., Morgantown, WV: West Virginia University, 2007, Jul; :320-326.
[22] Fang Z., Harrison J. P. (2002). Numerical analysis of progressive fracture and associated behavior of mine pillars by use of local degradation model. Trans. Int. Min. Metall. (Sect. A: Min techn.), The Institution of Mining and Metallurgy, pp. A59-A72.
[23] Blaha H., Wagner H.: Die Wechselwirkung von Versatz und Bergfesten beim „Post-pillar“-Abbauverfahren. BHM, 154. Jg. (2009), Vol 2. 60 – 66.
[24] Salamon M. D. G. (1970). Stability, instability and design of pillar workings. Int. J. Rock Mech. Min. Sci., Vol. 7, pp.613-31.
[25] Wagner H. (2003). The role of pillars in small underground mines. In: Intern. Conference on Safety and Environmental Aspects of Mining. Publ. of University of Miskolc. Series A. Mining. Vol. 63, pp. 89-103.

On the slope stability of alpine water-storage reservoirs in case of a damaged surface sealing

M. Schranz[1], A. Kirsch[1], Th. Marcher[1] und F. Preser[2]
[1] ILF Beratende Ingenieure, Feldkreuzstraße 3, A-6063 Rum bei Innsbruck, Österreich
[2] HTWK Leipzig/University of Applied Sciences, Fakultät Bauwesen,
Karl-Liebknecht-Str. 132, D-04277 Leipzig, Deutschland
E-mail: mathias.schranz@ilf.com

Abstract

Due to the increasing demand for artificial snow, ever increasing technical snow-making systems are planned and constructed in the alpine ski resorts. For that purpose also large storage reservoirs with dam heights of more than 15 m and storage capacities of 400,000 m³ are needed.
In most cases, flexible liners are used as inner impermeable barrier. To avert danger of dam collapse in case of a damage (e.g. of the surface lining), the Austrian authorities require that the reservoir is emptied within 3 days. This requirement leads to problems with the downstream water bodies, as these are often not capable to lead away the necessary amount of water safely. This can, in some cases, influence the feasibility of such a reservoir project in a negative way.
For that reason, the influence of a membrane leak on the slope stability of the reservoir earth dams was investigated by means of numerical, transient two-dimensional Finite Element calculations. In a parametric study the permeabilities of the dam materials were varied and the global slope stability evaluated for different time steps.
The calculation results indicate that, from a purely geotechnical point of view, an extension of the 3 day-period for emptying the reservoir is possible. Prerequisite for this extension is an efficient monitoring and control system of the storage facility.

Introduction

In the alpine ski regions there is an ever increasing demand for large water-storage reservoirs with volumes of more than 400,000 m³ and dam heights of more than 20 m to increase the capacity of the technical snow-making systems. Such reservoirs obviously pose a risk for the population due to their exposed positions and the high potential damage in the event of, e.g., a dam break. Therefore, the geotechnical proofs of stability of the earth dams are an essential condition for the permission to construct such a reservoir.
Usually, geomembrane sealings are used as water barriers. These sealings are combined with underdrain systems below the sealing to detect damages of the geomembrane as soon as possible. In such an event it is a mandatory procedure to rapidly drawdown the water in the reservoir within 3 days to a level that is non-critical from a geological-geotechnical point of view to minimise the risk of dam failure [1]. This extreme case must be considered in the hydraulic design of the whole reservoir system, because also the downstream water bodies must be capable to lead away the resulting amount of water safely.
This article analyses the impact of a membrane leak, which is not immediately detected, on the

stability of a reservoir earth dam. Results of transient two-dimensional Finite Element calculations will be presented, which also allow to assess the timely evolution of the safety factor η for different scenarios.

Possible failure mechanisms for water-storage reservoir with membrane sealing

General

From a geotechnical point of view a number of stability proofs have to be provided before a water-storage reservoir can be constructed. In general, superficial sliding, slope failure of the entire dam body, spreading of the dam toe and sliding of the whole dam can be distinguished.
Instabilities of earth dams are usually attributed to a loading in excess of the material's shear resistance. This happens if the virgin ground is not suitable for the construction of a reservoir dam, if the dam material itself is not suitable, if the construction procedures are inadequate, if loads due to self-weight or traffic loads are too high or if seepage forces or extreme impacts, such as an earthquake, occur.

Implication of membrane leaks and the resulting water loss

In case of a membrane leak, on the one hand, a geohydraulic failure of the dam body due to inner erosion („piping") is possible. In the close vicinity of the leak, water can seep into the earth dam, develop preferred seepage routes and, thus, continuously erode the dam material. On the other hand, failure of the downstream dam slopes is possible due to saturation of the dam material and destabilising seepage forces.

Risk management

Generally, suitable mitigation measures for the above mentioned risks due to a membrane leak should be considered in all phases of a reservoir project, i.e. design, construction and operation. Such mitigation measures are, e.g., a proper site selection, choice of suitable construction material, adequate construction methods and a well-defined monitoring and control system (visual checks plus automated warning devices). Prerequisite for a safe operation of a snow-making reservoir is that all components of such a monitoring and control system are used responsibly and checked on a regular basis.

Slope stability analysis in case of a large membrane leak

General

In case of a large membrane leak, the slope stability of a reservoir dam is highly influenced by the evolving seepage regime inside the dam body. Thus, sufficient knowledge of that regime, together with the stratigraphy of the subgrade and the dam as well as the permeabilities of the individual components, is essential to study the behaviour of a dam in the extreme case of a leak.
By way of an example the slope stability of the dam of an alpine snow-making reservoir in case of a large membrane leak is investigated in the following. Special emphasis is put onto the time-dependent evolution of the seepage through the dam, and, thus, the time-dependent evolution of global slope stability.

Geometry of the example problem

The investigated earth dam is partly founded on rock, partly on soil. The chosen geometry is shown in Figure 1. The downstream slope has an inclination of 1:1,8 (~29,05°), the upstream slope an inclination of 1:2,0 (~26,57°) against the horizontal. The maximum height of the dam is 16.70 m.

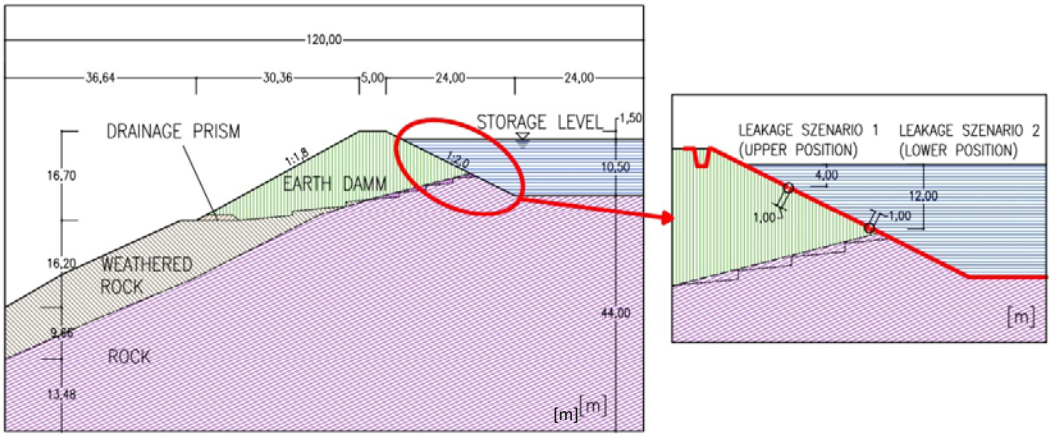

Figure 1: Investigated cross section

Calculation methodology

The stability calculations for the earth dam were performed with (uncoupled) two-dimensional Finite-Element calculations with the software PLAXIS. With this software package it is possible to analyse the transient flow of water into the dam body. Moreover, with the so-called φ-c-reduction technique, it is possible to evaluate the global slope stability of the dam for different time steps. For this example the following steps were chosen: 3 days, 6 days, 10 days, 20 days, 50 days, 100 days, 183 days, 366 days (1 year) and 1098 days (3 years).

To simulate the history of the construction, different calculation stages were applied: primary stress field, the construction of the dam body, application of traffic loads and simulation of the leak.

Model parameters

During the analyses the permeabilities of the subgrade and the dam material, as well as the location of the membrane leak, were varied (cf. Figure 1). For the seepage analyses three different parameter sets were defined, based on the Austrian code ÖNORM B 4422-1 (cf. Table 1):

For the earth dam isotropic permeabilities (parameter set 1) and anisotropic permeabilites (parameter sets 2, 3a and 3b) were applied. Due to the layered construction of the dam, it is likely that the vertical permeability is somewhat lower than the horizontal one, which was considered in parameter sets 2, 3a and 3b. Parameter set 3a differs from set 3b by consideration of a drainage prism at the toe of the dam, this prism being a constructional mitigation measure.

On the safe side, the size of the membrane leak was chosen to be 0.5 m. It was assumed that the leak is undetected in the first place – therefore, no drawdown was considered and the water table

within the reservoir remained constant. It should be mentioned that the performed calculations assumed plane strain conditions, which means that the infiltration was assumed over an infinite leak in longitudinal direction of the dam. Therefore, the speed of infiltration is overestimated by the chosen model with respect to a real membrane leak scenario.

Table 1: Chosen permeabilities for the subgrade and the dam material

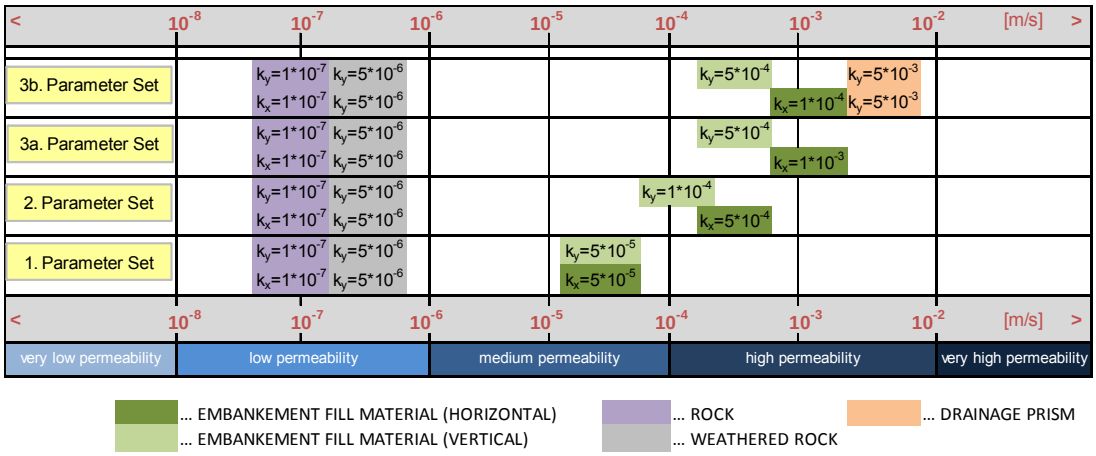

For the mechanical stability calculations a set of material parameters were fixed for all scenarios in the parametric study. The bedrock was modelled with a Mohr-Coulomb model, dam fill material, weathering zone and drainage prism were modelled with a higher-order Hardening Soil model. Global slope stability was assessed via a φ-c-reduction.

Calculation results

The results of the slope stability calculations are global safety factors η for the different scenarios and time steps (cf. Figure 2). According to the Austrian codes and standards a global safety factor of $\eta_{req} \geq 1.10$ is required for the extraordinary load case of a membrane leak.

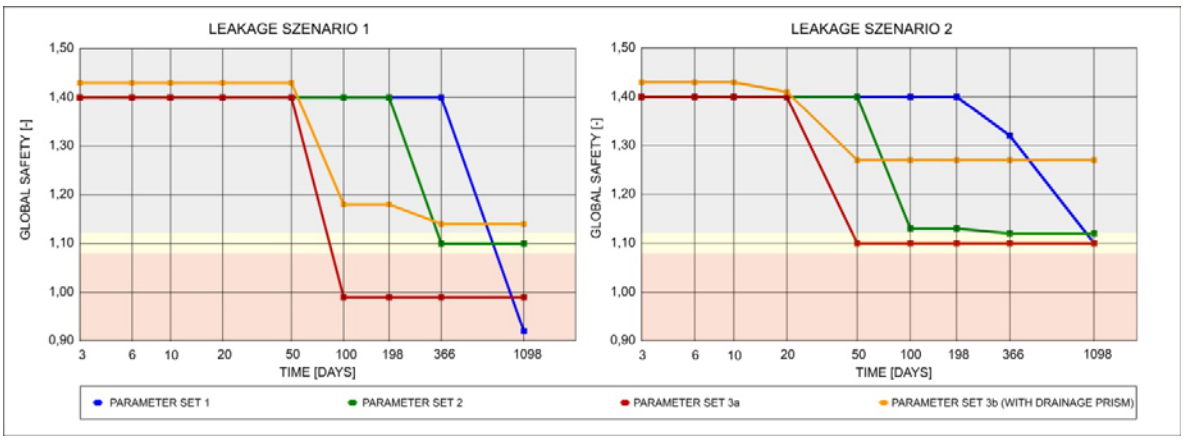

Figure 2: Results of the parametric study in terms of global safety factor η vs. time (left: leak at the top of the dam; right: leak at the bottom of the dam)

The calculations show that, for the investigated example, a leak of the membrane at the top of the reservoir dam influences η only after approx. 50 days. The obtained safety factor drops below the required one of $\eta_{req} \geq 1.10$ for parameter set 3a between 50 and 100 days, and for parameter set 1 after one year.
For a leak in the lower part of the dam, a first drop of η can already be observed after 20 days. Still, the calculated safety factor does not drop below the required one within the time period of 3 years for any parameter set.
The influence of the drainage prism can be seen when comparing the results of parameter sets 3a and 3b. For the given example, the increase in safety with a drainage prism amounts to approx. 16% on average.

Conclusion

From a geotechnical point of view, the performed numerical parametric study allows the conclusion that the required rapid drawdown within a time frame of 3 days is not necessarily justified in case of a large membrane leak. For the given example, a small drop in the computed safety factor could only be observed after 20 days. This conclusion holds for the seepage through homogeneous earth dams, the danger of piping though predefined zones of weakness was not considered in the analyses.

References

Amt der Salzburger Landesregierung, Abt. Wasserwirtschaft, in Zusammenarbeit mit dem Landwirtschaftministerium Österreich und den Bundesländern Niederösterreich, Oberösterreich, Steiermark, Kärnten, Tirol und Vorarlberg (2011): Beschneiungsanlagen - Leitfaden für das wasserrechtliche Behördenverfahren Band 1: Bewilligung und Überprüfung von Neuanlagen

Wasserrechtsgesetz 1959 idgF (WRG)

Striegler W. (1998): Dammbau in Theorie und Praxis, 2. Auflage, Verlag für Bauwesen, Berlin

Marcher Th., Wechsler H.G., Speckle A. (2010): A State of the Art Review: Design and Surveillance Practice of Water storage Reservoirs for Snow-Making Systems in the Alps. In: Proc. of the 8th ICOLD European Club Symposium, 2010, Innsbruck

Tate D. R.(2001): Piping Failure of the Poihipi Reservoir, Neuseeland

Seismic Stability of a Rock Wedge in the Abutment of an Arch Dam

M. Goldgruber, R. Feldbacher and G. Zenz
Institute of Hydraulic Engineering and Water Resources Management, Stremayrgasse 10/II, A-8010 Graz, Austria
E-mail: gerald.zenz@TUGraz.at

Abstract

It is shown by the fact of recent earthquakes that dam structures designed in accordance with the state of the art are safe structures. For such safe dam design it is necessary to account for the loading in an appropriate way together with the geotechnical site conditions. Based on these, the optimum layout of the structure can be found. For the dynamic loading of the dam structure intensive site specific investigations are needed. The interaction with the abutment is in most cases approximated by means of rigid body models.
To account for the dynamic interaction a more elaborated model is investigated based on calculations and results from the ICOLD "10th Benchmark Workshop on Numerical Analysis of Dams". For this the orographic left rock wedge in the abutment of the Luzzone Dam is discretized within a numerical arch dam model accounting for the wedge mass gravitational forces. Time histories of accelerations are applied and fluid structure interaction is accounted for with added mass approach compared against fluid elements.
The investigations on the stability are carried out within the finite element model and – with the time history of the dam thrust acting onto the wedge – with the Londe method. The results of the calculations are compared with respect to different distributions of the pore water pressure in the contact between rock wedge and underlying rock. It is to conclude that more sophisticated, realistic models show higher margins to entire system failure, which anticipates, that the existing model assumptions are conservative – as it is assumed.

Introduction

Dams are designed to withstand high horizontal loading. The loading occurs certainly and is bounded with the maximum reservoir water level with an additional increase in case of flood events. Very essential for the performance of the dam - apart from the constructive elements e.g. grout and drainage curtain – is the bearing capacity of the abutment. The ability for the abutment of carrying the load is based upon geotechnical investigations, careful judgement, design measures as well as an appropriate model underlying the analyses. Since the Malpasset dam failure due to the fact of unconsidered abutment behaviour at the time of design and construction the geotechnical aspect attracts high considerations. With the results of these investigations Londe - as scientist and engineer - is closely related. This method is based on rigid body stability considerations. Based on the geological site conditions the geometry of possibly formed wedges in the abutment is considered for block stability considerations. For this it is required to account for the rock material parameters as well as seepage conditions in the subsoil and the occurrence of water uplift pressure. By means of this method no redistribution of forces due to the abutment

flexibility is accounted for.

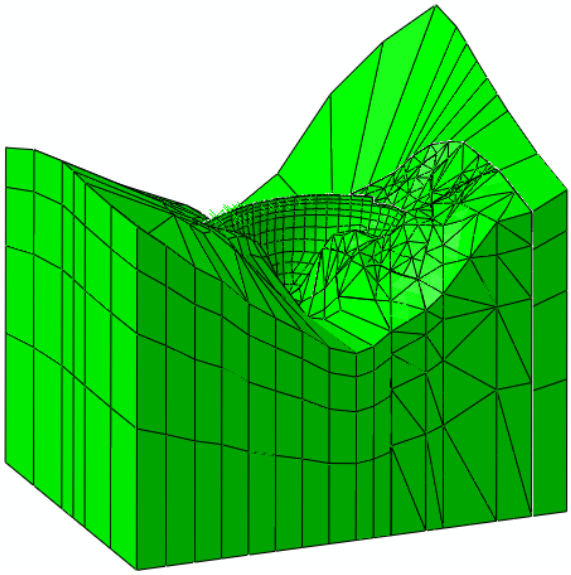

Figure 1: Luzzone Model

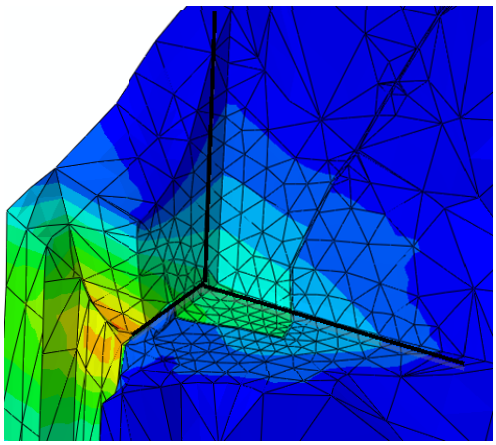

Figure 2: Pore water pressure in the joints

For dynamic earthquake analyses the time varying forces from the dam are transferred to the abutment and the wedge stability is calculated. The dynamically induced forces from the earthquake acting on the wedge are approximated with the free field accelerogram and the body mass of the wedge. The interaction of the wedge, the dam and the abutment based on their flexibility is normally not accounted for.

Within the Master Thesis [1] the entire system is discretized with finite elements; the rock wedge is coupled via contact to the surrounding. The reservoir, the dam and the wedge has proportional mass distribution for being excited during the earthquake. The analyses are carried out under linear conditions in a first step, to compare the results with the rigid body method. In further steps, the nonlinear behaviour in the contact surface due to sliding and its influence on the dam structure with a redistribution of stresses is considered.
To account for the overall stability of the wedge – as it is not appropriate under such conditions to calculate a factor of safety only – the parameters of the rock surface ($\varphi = 35°$, $c = 0$MPa) are reduced in steps until the numerical procedure can't converge any more.

Problem Setup - Abtument Stability

This study is aimed to evaluate under the scope of the Tenth Benchmark Workshop on Numerical Analysis of Dams -Theme C - the abutment stability of Luzzone arch dam under static and seismic loadings. At first the three dimensional model of the dam has been transferred for being applicable in the finite element program. With the FEM the interface forces between concrete dam and wedge are calculated for all required loading cases. The stability analysis of the given wedge is then evaluated by means of the Londe method.

The Luzzone dam is a double curved concrete arch dam which was initially built in the sixties. The dam was heightened within the ninetieths. The total height of the dam is 225 m.

Key Data

Height:
225m
Crest Length:
600m
Elevation:
1609m

Thickness base:
36m
Thickness crest:
4.5m

Reservoir Volume: 108 Mio. m^3

Figure 3a: Luzzone dam in nature

For the benchmark in the left bank of the dam are two geological joints. With these joints a wedge is defined and has a potential to slide under arch dam and uplift loading. To verify about this situation a stability assessment is necessary. The volume of the wedge has been estimated as 1.92×10^6 m^3.

It is to mention that in calculating the interface forces between dam and wedge, only the stiffness of foundation is considered its density is neglected. For this kind of analyses for the dam a massless foundation is considered. However, the mass of the wedge is considered later in the separated stability analyses.

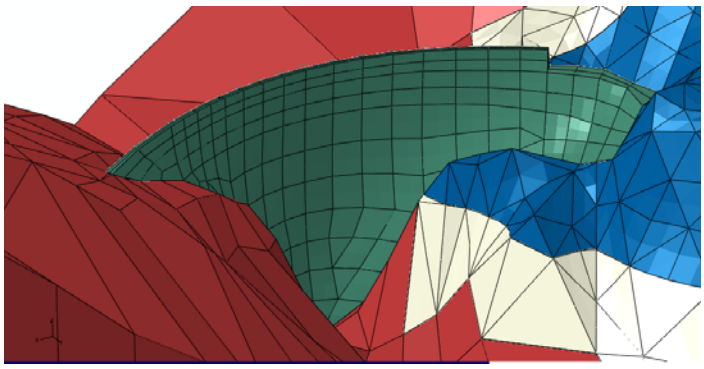

Concrete of dam
Density (ρ) = 2400 kg/m^3
Poisson ratio (ν) = 0.167
Modulus of elasticity (E) = 27 GPa
Rayleigh damping coefficients: α =0.6 and β =0.001

Foundation rock
Density (ρ) = 2600 kg/m^3
Poisson ratio (ν) = 0.2
Modulus of elasticity (E) = 25 GPa
Rayleigh damping coefficients: α =0.6 and β =0.001

Figure 3b: Luzzone dam in nature and finite element mesh

Londe Method

The Londe method for stability of rock slopes is used and some simplifying assumptions are made. The volume of the wedge is limited by intersections of three planes. This assumption is conservative as the natural surfaces are generally irregular. The wedge is considered as a rigid body and the geometry of the wedge is kept constant during application of the forces throughout the investigation.
Cohesion and tensile strength are neglected in the contact planes and therefore, it is supposed that the friction between surfaces is the only parameter that can resist sliding. It is supposed that the moments of the forces (provide not a constant stress distribution along the surface) have negligible influences and therefore will be ignored. The applied forces can be categorized as:

- Weight of the wedge

- The thrust force which is the resultant force at the dam wedge interface. This force is time dependent and its magnitude and direction will change by time.

- The forces due to uplift pore pressure: U1, U2 and U3 which are applied to the planes 1, 2 and 3 respectively- these forces do not change during investigation.

- Seismic forces due to applied earthquake: Three components of seismic forces are considered as the max, may and maz which m is the mass of the wedge and ax, ay are az are acceleration time histories which were defined earlier.

- The reaction of planes: due to applied forces, three reaction forces will develop on the planes (N1, N2 and N3). As mentioned before these forces can only be compressive. Tensile forces, which mean that the plane is open, are not acceptable and will lead to a different sliding mode respectively exclude sliding in the decoupling plane due to tensile forces.

Wedge alone

Wet area [m²]			Wedge			
Jh	J1	J2	Volume [m³]	Mass [kg]	Weight [MN]	tan 35°
28650	23300	7200	1,92E+06	4,99E+09	48970	0,70

Pore pressure [% of full]			Loading	Weight of Wedge [MN]			U on Jh [MN]	U on J1 [MN]			U on J2 [MN]			Driving Force	Stabalizing Force	SF
Jh	J1	J2		Gx	Gy	Gz	Uz	Ux	Uy	Uz	Ux	Uy	Uz			
100	50	50	SW+hyd	0	0	-48970	28110	900	10320	4830	-3370	600	850	11190	10630	0,95
100	50	50	SW+hyd+dyn	-2960	4330	-44730								16180	7660	0,47
50	50	50	SW+hyd	0	0	-48970	14050	900	10320	4830	-3370	600	850	11190	20470	1,83
50	50	50	SW+hyd+dyn	-550	6300	-46370								17480	18650	1,07
35	**35**	**50**	**SW+hyd**	**0**	**0**	**-48970**	**9840**	**630**	**7220**	**3380**	**-3370**	**600**	**850**	**8290**	**24440**	**2,95**
35	**35**	**50**	**SW+hyd+dyn**	**-550**	**6300**	**-46370**								**14500**	**22620**	**1,56**
35	35	35	SW+hyd	0	0	-48970	9840	630	7220	3380	-2360	420	600	7830	24620	3,14
35	35	35	SW+hyd+dyn	-550	6300	-46370								14720	22800	1,61

Wedge alone + dam thrust

Pore pressure [% of full]			Loading	Weight of Wedge [MN]			Uplift	Dam Thrust Force [MN]						Driving Force	Stabalizing Force	SF
Jh	J1	J2		Gx	Gy	Gz	Jh, J1, J2	Fx	Fy	Fz	Fres	alpha	beta			
0	0	0	SW	0	0	-48970	0	180	20	-4050	450	87,4	96,5	11	37090	3333
35	**35**	**50**	**SW+hyd**	**0**	**0**	**-48970**	**vide supra**	**-5480**	**-4680**	**-4650**	**8580**	**32,8**	**-130,5**	**8800**	**27690**	**3,15**
35	**35**	**50**	**SW+hyd+dyn**	**-6740**	**280**	**-46930**		**-9310**	**-770**	**-400**	**12730**	**18,3**	**-128,3**	**17570**	**26360**	**1,41**

Figure 5: Sensitivity Analysis - Wedge stability – Static / Dynamic Loading [2]

For wedge stability evaluation at first the three plane reaction forces are to be calculated by solving static equilibrium equations in three direction x, y and z, Figure 5-a. For this wedge geometry and applied forces, due to equilibrium condition and calculated plane reaction forces, eight cases are possible. Table 1 of [] shows all sliding failure mode.

The wedge stability safety factor of the dam during static loading and the earthquake is shown in Figure 5. The safety factor for a short period of time is less than 1, which means that the wedge would move during this time period. The concept of Newmark's method is used to calculate displacement of the wedge.

Results
One of the conclusions of the contribution by [2] was the following:
"Under the assumption of a rigid body wedge the analysis is carried out for dead weight, water loading and uplift. No variation of the earthquake acceleration along the valley is assumed. The uplift pressure at the wedge interface is very conservative, as it would never be the case that the entire planes are under full uplift.
With the help of FEM the wedge is suggested to be analysed as deforming body and with this the stability of the abutment. However, this assumption used normally, was out of scope of this benchmark. "
Based on this conclusion the analyses are carried out with the help of the finite element method.

Finite Element Analyses

Contrary to the model, which is used for the Londe – Method, the wedge is cut out of the underlying rock mass. The wedge has now a volume of $1.4*10^6$ m^3.
The wedge is not rigid anymore and discretized as a deformable body. The friction angle in the joints is set to 35° with neglecting the cohesion. To take the water into account for the added water mass under seismic loading, two different discretizations are used. At first, the water mass is modelled with the added mass technique according to Westergaard. Therefor a user subroutine is programmed, which calculates the mass per element surface. In contrast and for comparison reasons, the water is additionally modelled as a volume itself with the implemented acoustic elements in the program.

Additionally the pore water pressure in the joints and the grout curtain in the abutment of the dam are modelled to take the effect of uplift in account.

In total the system consists of 6828 elements and 34723 nodes.
The results show, that the analysis with the Westergaard added mass technique is permanently showing higher vertical and horizontal stresses in the cross-section compared to the model with acoustic elements. The difference between these two discretization methods of the added water mass is about 50 %. So it can be said that the Westergaard method is a more conservative one. The acoustic elements are showing the better results because of the more suitable modelling.

For the stability analysis of the wedge, the friction angle in the joints is reduced to a value for which the system collapses and the analysis doesn't converge anymore. That happens at a friction coefficient of 0.25, which relates to safety factor against collapse of 2.8.

System comparison

The differences of system discretization can be seen in the weight of the wedge, which differs by a factor of 1:0,725.

Modeling

First of all, the problem was, that there was no file, which allows modifying the geometry of the model. Due that, the surface of the rock mass, which is cut by the planes that define the wedge, had to be converted to a 3D modelling program. For this, the nodes of the surface where copied out of the "input – file" and imported into the program AUTOCAD. After the definition of the surface, the surface net was used to reconstruct the Volume of the rock mass in the program SOLID WORKS, where the wedge was cut out (Figure 7). The two parts, the wedge and the rock mass, were now imported into ABAQUS for meshing (Figure 8 and 9).

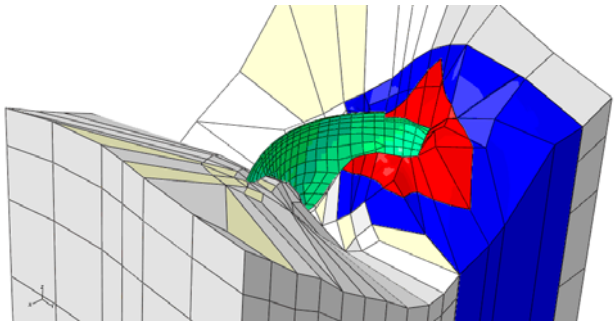

Figure 6: Final model

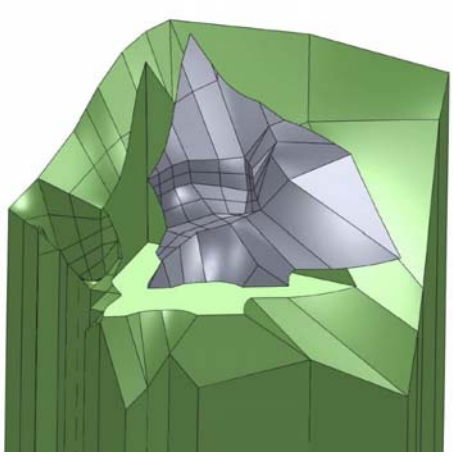

Figure 7: Model in SOLID WORKS

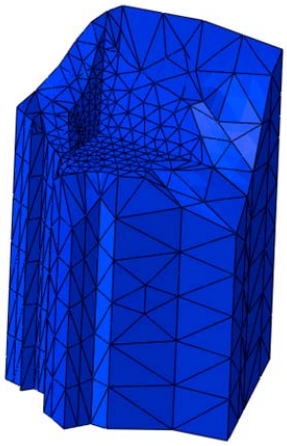

Figure 8: meshed rock mass in ABAQUS

To simulate the added water mass for seismic loading, in contrary to the Westergaard method the water is also modeled as acoustic elements, therefore a volume itself has to be generated. (Figure 10).

In the model, which is used for the Londe – Methode, the wedge itself is not disrcretized. The interacting forces between dam and wedge are summarized and used for the investigation of the stability after the analysis of the finite element model.

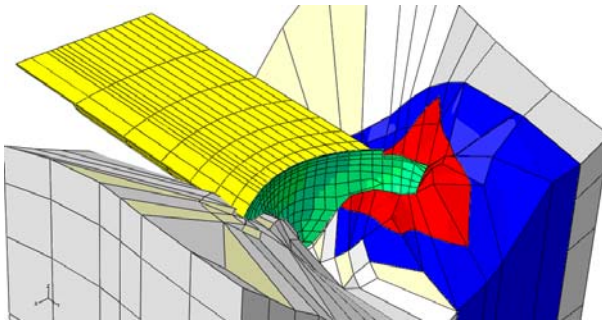

Figure 10: Acoustic elements model

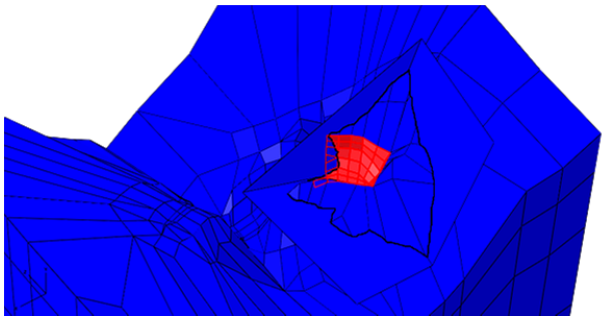

Figure 11: Londe – model

Conclusion

The finite element method is very well established for dam layout and design. It is a very appropriate method to account for stress distributions under usual, linear loading conditions. For calculating the ultimate bearing capacity under nonlinear system behavior the redistribution of forces within the system is required. This provides an additional advantage of the method. The redistribution of forces under nonlinear system behavior during earthquake excitation is used

herein to compare the results with the commonly applied Londe method based on rigid body investigated.

With the finite element method the calculated factor reduction leads to 2,8 – which could be seen as a kind of factor of safety. After the reduction of the friction angle tan(φ) from 0,70 to 0,25 the convergence could not be achieved any more, the sliding mode is becoming progressive.
With the rigid body model, the calculated factor of safety leads to 1,56 – until the wedge starts to slide. This consideration does not take into account the interdependence of deformation and stress distribution on the loaded structure and the wedge too. Between these two methods still a so called safety margin by 1,8 is inherent.

It can be concluded, that the – simplified – rigid body method used to carry out the abutment stability analysis under dynamic earthquake loading leads to a conservative factor of system safety. With a better system discretization and consideration of the load redistribution during the dynamic analyses the system is able to bear an even higher load. Under these circumstances the resistance can be additionally reduced by a factor of 1,8 compared with the rigid body method for wedge stability.

Acknowledgements

The support of Pöyry Energy Ltd to carry out the numerical investigations and the contributions to the ICOLD Benchmark Workshop by the research project “Design of Hydraulic Structures” is gratefully acknowledged.

References

[16] Goldgruber M. (2011). Numerische Untersuchung der Felskeilstabilität im Widerlager der Luzzone Staumauer bei Erdbebenbelastung. Master Arbeit, Institut für Wasserbau und Wasserwirtschaft, TU - Graz.

[17] Gilani S.M., R. Feldbacher, G. Zenz (2009). Stability of dam abutment including seismic loading; 10th ICOLD Benchmark Workshop, Paris 2009.

[18] Londe P. (1973). Analysis of the stability of rock slopes. In “Quarterly Journal of Engineering Geology and Hydrogeology”, Vol. 6, Issue 1, pp. 93-124.

[19] Newmark N.M. (1965). Effect of earthquakes on dams and embankments. In Geotechnique, “Milestones in Engineering”, Vol. 15, No. 2, pp. 109-129.

[20] Bathe K.-J. (2002). Finite-Elemente-Methoden, Springer –Verlag.

[21] Müller L. (1992). Der Felsbau, Teil 2 – Gründungen, Wasserkraftlagen, Stuttgart.

[22] Wittke W. (1984). Felsmechanik, Springer-Verlag, New York Tokyo.

[23] Zienkiewicz O.C., Taylor R.L. (2000). The Finite Element Method, Fifth edition, Vol. 1: The Basis, Butterworth-Heinemann, Oxford.

Numerische Modellierung des Verformungszustandes hochbelasteter Abbauwerkzeuge von Tunnelbohrmaschinen

T. Bumberger[1], M. Entacher[1] und R. Galler[1]
[1] Lehrstuhl für Subsurface Engineering, Erzherzog-Johann-Straße 3/III,
A-8700 Leoben, Austria
E-mail: subsurface@unileoben.ac.at

Kurzfassung

Die Einwirkungen auf Abbauwerkzeuge (Disken) von Tunnelbohrmaschinen werden im Allgemeinen über eine Gesamtvorschubkraft abgeleitet. Dadurch ergibt sich bei üblichen 17“-Disken ein Wert für die Anpresskraft von etwa 250 kN. Um die stark oszillierende Charakteristik der Diskenkräfte genau erfassen zu können, ist ein Ansatz über die Gesamtvorschubkraft jedoch nicht ausreichend.
Ein Messtechniksystem, das die drei Kraftkomponenten (Anpresskraft F_A, Rollkraft F_R, Seitenkraft F_S) jeder einzelnen Diske abbildet, ist aufgrund widriger Umgebungsbedingungen an der Ortsbrust und komplizierter Verformungszustände des Bohrkopfes schwierig umzusetzen.
Im Rahmen dieses Vortrages werden dreidimensionale numerische Berechnungen präsentiert, die den Verformungszustand einer Diske und der umgebenden Stahlkonstruktion detailliert abbilden. Mit Hilfe dieser Vorstudie kann es gelingen, ein serienmäßig einsatztaugliches Messtechniksystem für die Erfassung der Einwirkungen an Disken zu entwickeln.

Einleitung

Funktion einer Tunnelbohrmaschine

Tunnelbohrmaschinen (TBM) dienen dem Auffahren von Tunnels im Hartgestein (vgl. Abbildung 1). Zur Verspannung der Maschine werden Gripper gegen die Tunnellaibung gepresst. Anschließend drücken Vorschubzylinder den rotierenden Bohrkopf gegen die Ortsbrust. Der Bohrkopf ist mit zahlreichen Abbauwerkzeugen, den sogenannten Disken, bestückt. Sie rollen mit einer hohen Anpresskraft über der Ortsbrust ab und lösen dadurch das anstehende Gestein.

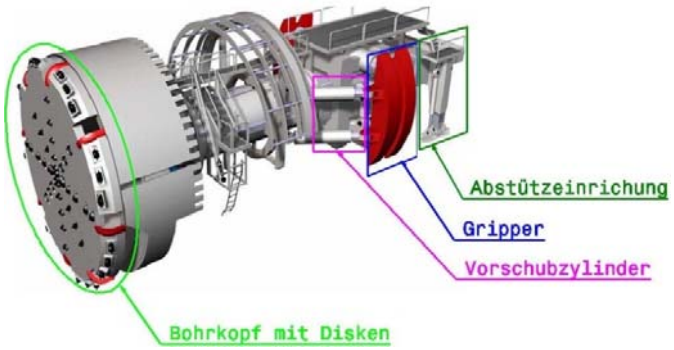

Abbildung 1: Aufbau einer offenen Tunnelbohrmaschine (Herrenknecht)

Die Kräfte, die auf eine Diske wirken sind noch nicht genau bekannt. In Großversuchen wurden Diskenkräfte bereits erfolgreich gemessen (Samuel and Seow, 1984; Zhang et al. 2003). Das für

den serienmäßigen Einsatz vorgesehene Mobydic-System (Beer, 2009) enthält vielversprechende Ansätze, konnte sich nach Kenntnis der Autoren allerdings noch nicht ausreichend durchsetzen.

Aufbau und Lagerung einer Diske

Abbildung 2 zeigt ein Schnittmodell sowie eine CAD-Schnittansicht einer 17“-Diske. Sie ist aus folgenden Bauteilen aufgebaut: Achse (Position 1), bundseitiger und gewindeseitiger Deckel (Pos. 2 und Pos. 9), zwei O-Ringe (Pos. 3), Dichtungen (Pos. 4), zwei vorgespannte Kegelrollenlager, bestehend aus Lagerinnenring (Pos. 5), Lageraußenring (Pos. 6) und dazwischen liegenden Wälzkörpern, Rollengrundkörper (Pos. 7), Sicherungsring (Pos. 8), welcher den aufgeschrumpften Schneidring (Pos. 12) gegen Ablösen sichert, Verschlussschraube (Pos. 10) sowie einem Sicherungsblech (Pos. 11).

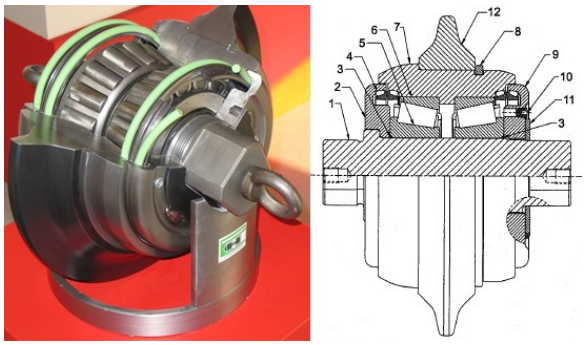

Abbildung 2: Ausstellungsstück 17“-Diske (links, Herrenknecht), CAD-Schnittansicht (rechts, Frenzel, 2010)

Abbildung 3 zeigt die Lagerung einer Diske in einem monolithisch gefrästen Gehäuse (Pos. 3), welches mittels einer umlaufenden Schweißnaht an der Außenseite des Bohrkopfes und an den Stützblechen (Pos. 5) in den Bohrkopf eingeschweißt wird. Die Diske liegt nicht direkt im Gehäuse, sondern auf einem austauschbaren Zwischenstück (C-Stück, Pos. 4). Sie wird über das sogenannte Wedge-Lock-System, einem Keil (Pos. 6) und einer Schraube (Pos. 2) fest verspannt.

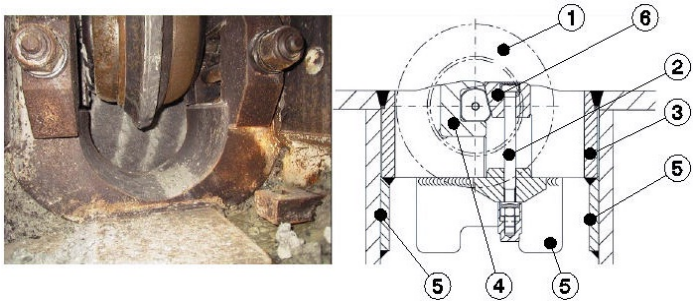

Abbildung 3: Einbau einer Diske im Bohrkopf einer TBM (Herrenknecht)

Modellbildung

Ziel der Modellbildung

Das Ziel der Modellbildung ist die wirklichkeitsnahe Darstellung des Spannungs- und Verformungszustandes einer Diske und des dazugehörigen Gehäuses, um in weiterer Folge mögliche Positionen von Sensoren für in situ-Messungen der Diskeneinwirkungen ermitteln zu können. Es werden zahlreiche verschiedene Lastfälle untersucht, die in einer vertretbaren Zeit

berechnet werden sollen.
Aufgrund der dreidimensionalen Einwirkungen (Anpresskraft F_A, Rollkraft F_R und Seitenkraft F_S) ist eine dreidimensionale Berechnung erforderlich, Symmetrieeffekte können im globalen Modell nicht ausgenützt werden.

Modellierung der einzelnen Bauteile
Die Modellierung der einzelnen Bauteile erfolgte in Abaqus CAE 6.10. Nachdem die Platzierung der Sensoren nicht an der Diske selbst, sondern in den Auflagerbereichen geplant ist, wurden in der Modellierung der Diske einige Vereinfachungen akzeptiert.
Schneidring, Rollengrundkörper und Kegelrollenlager werden als ein Bauteil betrachtet. Die Kegelrollenlager sind stark vorgespannt und haben somit eine nahezu linear-elastische Kennlinie. Der Fehler durch ein falsches Materialgesetz ist somit vernachlässigbar. Durch die fehlende axiale Lasteinleitung aufgrund der Geometrie der Lager entsteht eine kleine Ungenauigkeit, die gegenüber einer stark steigenden Rechenzeit bei Definition von komplizierten Kontaktbedingungen in Kauf genommen wird.
Die Kräfte werden in drei Komponenten (x-, y- und z-Richtung) aufgeteilt und als Punktlast auf ein starres Kreissgement aufgebracht. Dadurch werden eine flächige Krafteinleitung in die verformbaren Teile des Modells gewährleistet und extreme Spannungsspitzen vermieden.
Zahlreiche Bauteile sind aufgrund ihrer Funktion für die Modellierung vernachlässigbar. Dazu zählen die beiden Deckel, der Sicherungsring, das Sicherungsblech, die O-Ringe, die Dichtungen sowie die Verschlussschraube. Das C-Stück, welches zwischen Gehäuse und Diske liegt, wird mit einer Schraube in Position gehalten, welche in der Simulation nicht berücksichtigt wurde.
Der Spannkeil und die dazugehörige Schraube des Wedge-Lock-Systems werden durch äußere Kräfte ersetzt. Die genaue Vorspannkraft ist den Autoren nicht bekannt, sie wurde mit 150 kN angenommen (entspricht einer Zugspannung im Schraubenschaft von etwa 200 MPa). Eine Änderung der Vorspannkraft verändert die Ergebnisse linear, die qualitative Richtigkeit der Ergebnisse ist somit gewährleistet. Die äußeren Kräfte wurden unter Annahme eines Reibungskoeffizienten von $\mu = 0{,}15$ anhand einer überschlägigen Rechnung bestimmt (vgl. Abbildung 4).

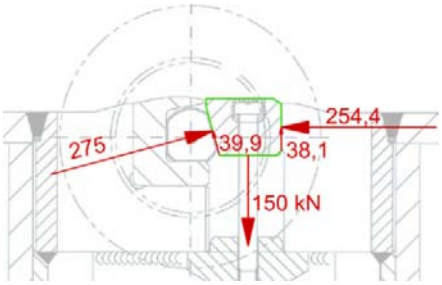

Abbildung 4: Reaktionskräfte am Spannkeil durch Schraubenvorspannung (μ=0,15)

Um eine gleichmäßige Lasteinleitung sicherzustellen, wurde ein „rigid shell“ (starres Schalenelement) mittels „tie constraint“ (keine Relativverschiebung zwischen den Kontaktflächen) auf die Lasteinleitungsfläche aufgebracht und mit Einzelkräften belastet. Durch die äußeren Kräfte verformt sich das Gehäuse um ca. 0,04 mm in vertikaler Richtung. Daraus ergibt sich – bei einer Schraubenlänge von 400 mm und einem Durchmesser von 30 mm – eine Verringerung der Vorspannkraft wie folgt: $\Delta\varepsilon = 0{,}04 / 400 = 0{,}0001$; $\Delta\sigma = 200.000$ MPa x

0,0001 = 20 MPa; daraus folgt ΔF = 20 x 706,5 mm² = 14,13 kN. Das entspricht einer Verringerung der Vorspannkraft um etwa 7%, die bei der gewählten Vorgehensweise vernachlässigt wird. Eine genaue Modellierung des Spannkeils inklusive aufwändiger Kontaktbedingungen wäre zeitintensiv und würde die Rechenzeit stark erhöhen.

Kontaktbedingungen

Bei sämtlichen in Interaktion stehenden Flächen wurden die Kontaktbedingungen als „General Contact" mit der Bedingung „Hard Contact" in der Normalenrichtung definiert, welche das gegenseitige Durchdringen der in Berührung stehenden Flächen verhindert. Für Kontakte in tangentialer Richtung wurde ein Reibungskoeffizient von $\mu = 0{,}1$ gewählt.
Die Position der Diske in den C-Stücken in axialer (seitlicher) Richtung ist nicht eindeutig definiert, sie wird erst durch die Verspannung des Keils bestimmt. Diese undefinierte Lage könnte bewirken, dass der Achsabsatz am Gehäuse ansteht und somit eine Kontaktnichtlinearität erzeugt. Nachdem dieser Zustand quasi zufällig ausgelöst wird, ergibt es keinen Sinn ihn in der Simulation zu berücksichtigen. Das Superpositionsprinzip verliert durch diese Nichtlinearität seine Gültigkeit, deshalb könnte dieses Phänomen auch messtechnisch mit vertretbaren Mitteln kaum berücksichtigt werden.

Randbedingungen und Einwirkungen

An jene Stellen, an denen das Gehäuse an den Bohrkopf angeschweißt ist, wurden die Verschiebungen in die drei Raumrichtungen gesperrt.
Als äußere Kräfte wurden eine Anpresskraft F_A, eine Rollkraft F_R und eine Seitenkraft F_S aufgebracht. Die Verspannung des Wedge-Lock-Systems wurde ebenfalls als äußere Kraft modelliert. Abbildung 5 zeigt die Randbedingungen und Einwirkungen des Modells.

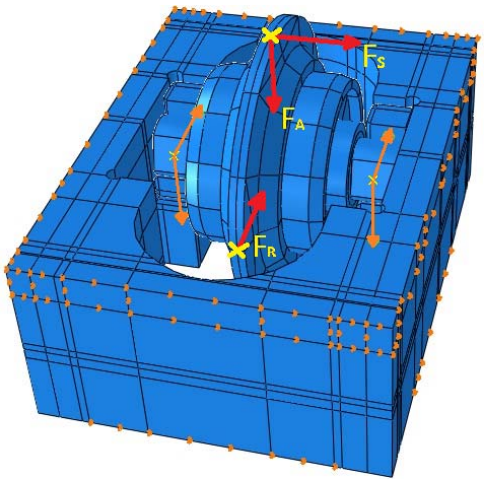

Abbildung 5: Randbedingungen und Einwirkungen im Modell

Aus Versuchen ist bekannt, dass die Belastungsfrequenz einer Diske im Bereich von wenigen Hertz liegt (Samuel and Seow, 1984). Aufgrund der hohen Systemsteifigkeit kann man daher davon ausgehen, dass die Diske Belastungen sehr direkt an das Gehäuse weitergibt und eine dynamische Belastung in der Simulation daher nicht berücksichtigt werden muss, um das gewünschte Resultat zu gewährleisten.

Elementwahl und Vernetzung
Die einfachste Vernetzungsmöglichkeit in Abaqus CAE ist die freie Vernetzung mit Tetraederelementen. Im Modell wird jedoch eine strukturierte Vernetzung (vorgegebene Elementgeometrien) mit Hexaederelementen angestrebt, um den Verzerrungszustand bei vertretbarer Elementzahl möglichst genau abbilden zu können. Die Bearbeitungszeit des Modells steigt dadurch sehr stark an, weil zahlreiche Partitionen erstellt werden müssen.

Submodellbildung
Submodelle bieten die Möglichkeit den Ausschnitt eines Modells in stark reduzierter Zeit zu berechnen. Zunächst wird ein Gesamtmodell mit relativ grober Vernetzung gerechnet. Danach wird ein Teil des Modells weggeschnitten und an der gesamten Oberfläche die Verschiebungen bzw. Spannungen aus dem Globalmodell eingeprägt. Anschließend wird der verbleibende Teil fein vernetzt und neu berechnet. Die Rechenzeit wird dadurch erheblich reduziert.

Ergebnisse

Berechnungsergebnis Gesamtmodell und Submodell
Abbildung 6 zeigt den Verlauf der Mises-Spannungen anhand eines Schnitts durch das Gesamtmodell. Die äußeren Kräfte betragen für alle folgenden Abbildungen F_A= 400 kN, F_R= 70 kN, F_S= 10 kN.

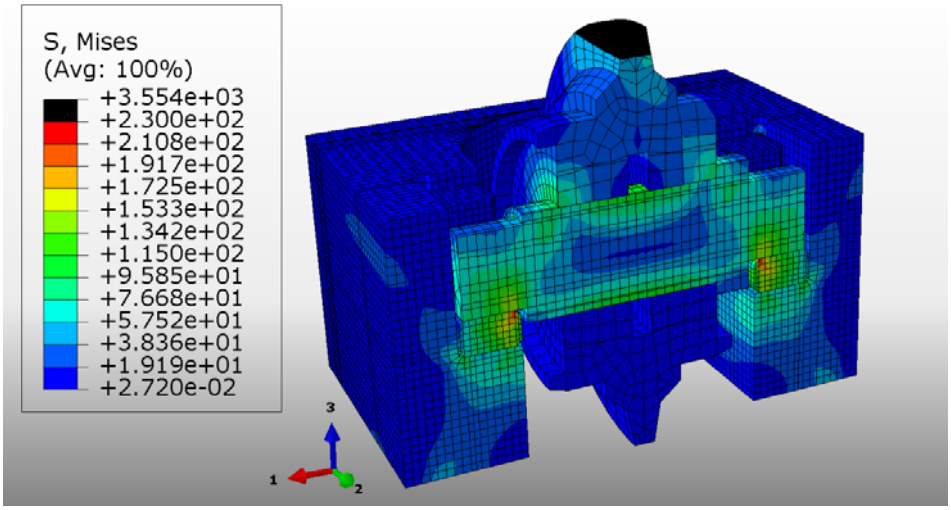

Abbildung 6: Mises-Spannungen des durchgeschnittenen Gesamtmodells

Abbildung 7 zeigt den Verlauf Mises-Spannungen im Auflagerbereich.

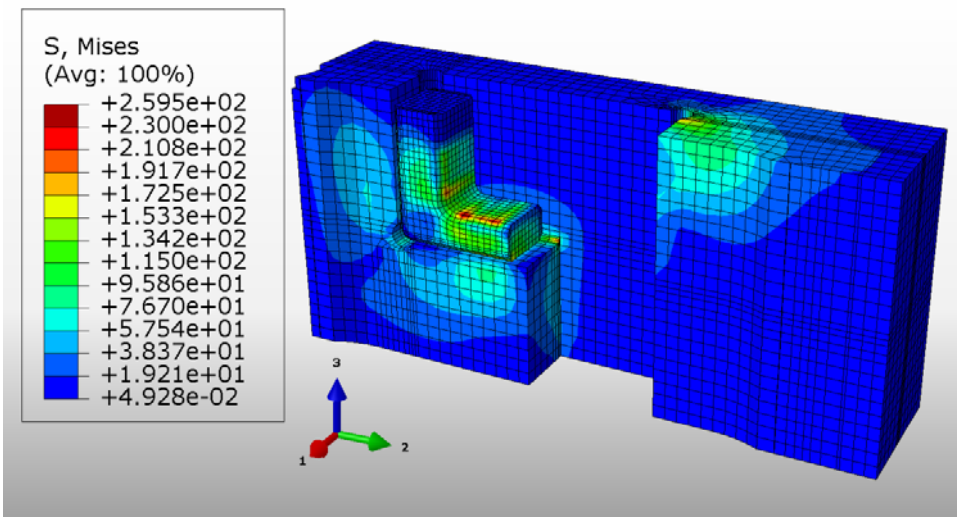

Abbildung 7: Mises-Spannungen im Auflagerbereich

Modifikationen des Gehäuses

Mithilfe der vorgestellten Ergebnisse können jene Stellen identifiziert werden, an denen große Spannungen auftreten. In weiterer Folge ist es möglich, das Gehäuse zu modifizieren, um Stellen zu schaffen, an denen Sensoren angebracht werden können und die Auswirkungen dieser Modifikationen auf den Spannungszustand zu untersuchen. Abbildung 8 zeigt die Ergebnisse einer möglichen Modifikation.

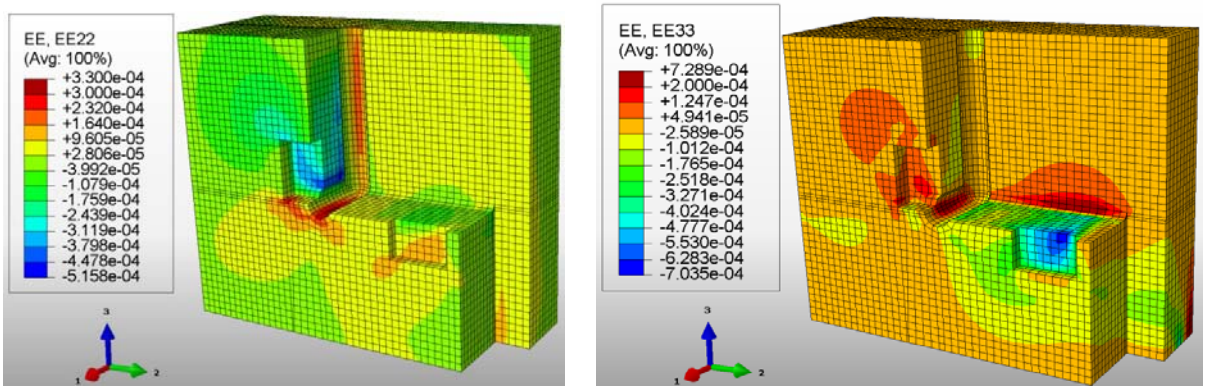

Abbildung 8 : ε_{22} (links) und ε_{33} (rechts) des bearbeiteten Gehäuses

Diskussion und Ausblick

Für die Entwicklung eines Messtechniksystems, welches imstande ist Diskenkräfte in situ zu messen, wurde als Vorstudie eine FE-Simulation mit dem Programmpaket Abaqus CAE durchgeführt.

Die Modellbildung erfolgte unter zahlreichen Vereinfachungen, die aus Sicht der Autoren nur unwesentlichen Einfluss auf das Ergebnis haben, die Rechenzeit jedoch drastisch verkürzen.

Die aufgebrachten Lasten sind statisch, wobei gezeigt wurde, dass die auftretenden Spannungen deutlich unter der Fließgrenze eines üblichen Baustahls liegen. Modifikationen des Gehäuses zur Platzierung von Sensoren sind daher möglich ohne einen Verlust der Tragfähigkeit zu riskieren. Einschränkend muss dazu gesagt werden, dass keine Aussage über die Dauerfestigkeit getroffen

werden kann. Der Ansatz von statischen Lasten im Gegensatz zu den realen, stark oszillierenden Einwirkungen kann aufgrund der hohen Systemsteifigkeit der Diske und des Gehäuses in Kauf genommen werden.
Abaqus erwies sich als sehr gut geeignet für die Aufgabenstellung. Mit der Möglichkeit Submodelle zu erstellen konnte beispielsweise sehr viel Rechenzeit gespart werden.
Die Grundlage für die erfolgreiche Implementierung eines Messtechniksystems im Labor und in situ wurde geschaffen.

Danksagung

Die Autoren bedanken sich bei den Mitarbeitern des Lehrstuhls für Allgemeinen Maschinenbau und bei Prof. Antretter vom Institut für Mechanik der MU Leoben, die durch ihre Unterstützung wesentlich zum Gelingen der Arbeit beigetragen haben. Großer Dank gilt außerdem der Fa. Herrenknecht für informative Fachgespräche und die verwendeten Bilder.

Quellenverzeichnis

Beer, G. (editor, 2009) “Technology Innovation in Underground Construction.” *Institute for Structural Analysis*, Graz University of Technology, Graz

Frenzel, C. (2010) “Verschleißkostenprognose für Schneidrollen bei maschinellen Tunnelvortrieben in Festgesteinen.“ *Münchner Geowissenschaftliche Abhandlungen* (15), Verlag Dr. Friedrich Pfeil, München

Samuel, A.E, Seow, L.P. (1984) “Disc Force Measurements on a Full-face Tunneling Machine.” *Int.J.Rock.Mech.Min.Sci. & Geomech. Abstr.* Vol.21, No 2, 83-96

Zhang, Z.X., Kou, S.Q., Tan, X.C., Lindqvist, P.-A. (2003) “In-situ Measurements of Cutter Forces on Boring Machine at Äspö Hard Rock Laboratory, Part I.” *Rock Mech. Rock Engng. 36 (1), 39-61*

Anforderung an die Modellbildung bei Finite-Element-Berechnungen – 2D versus 3D

Stefan Wachter und J. Martin Hohberg
IUB Ingenieur-Unternehmung AG, Thunstraße 2, CH-3005 Bern, www.iub-ag.ch
E-Mail: info@iub-ag.ch

Abstract

Die Leistungsfähigkeit heutiger Rechner und die modernen Geotechnikprogrammpakete ermöglichen die Berechnung großer 3D-Modelle mit einer sehr hohen Anzahl an Freiheitsgraden. Dies hat zur Folge, vermehrt 3D-Berechnungen als Standard einzusetzen, obwohl speziell gewählte 2D-Modelle wegen ihrer größeren Auflösung aussagekräftiger sein können und dank kürzerer Rechenzeiten mehr Variantenstudien erlauben. Der folgende Beitrag zeigt anhand eines Kavernenbeispieles, wie selbst im dreidimensionalen Bereich einer Kavernenstirnwand eine zweidimensionale Näherung eingesetzt werden kann und welche Konsequenzen bezüglich Arbeitsaufwand und Ergebnisqualität zu erwarten sind.

Einleitung

Numerische Kontinuumsberechnungen erlauben nicht nur die Erfassung der Wechselwirkung zwischen Baugrund und Bauwerk, konstruktiver Details und realistischer Materialgesetze, sondern auch den Einbezug des räumlichen Tragverhaltens. Daher stellt sich zu Beginn der Durchführung geomechanischer Berechnungen unter Verwendung der Finite-Element-Methode (FEM) die Frage nach Ansatz der Dimensionalität. Ist eine zweidimensionale geometrische Modellierung ausreichend oder muss ein hochwertigerer dreidimensionaler Ansatz, der generell mehr Aufwand erfordert, gewählt werden. Der Arbeitskreis "Numerik in der Geotechnik" der Deutschen Gesellschaft für Geotechnik formulierte 1991 dazu folgende Empfehlung [1]:

> "Die erste Stufe, ein geotechnisches System in ein Berechnungsmodell abzubilden, besteht in der Wahl des geometrischen Modells. Zunächst muß untersucht werden, welche geometrischen Vereinfachungen des i.a. räumlichen Systems möglich sind. Im Hinblick auf Rechnerkapazität, Aufwand der Datenaufbereitung, Datenkontrolle und Übersichtlichkeit sollte versucht werden, nur die wesentlichen Einflüsse im Berechnungsmodell abzubilden. Insbesondere ist das System auf Symmetrien und auf ausgeprägte Hauptbeanspruchungs-richtungen zu untersuchen. In vielen Fällen genügt ein ebenes oder rotationssymmetrisches Modell."

Demnach obliegt es dem Ingenieur, den Ansatz in Abhängigkeit der projektspezifischen Randbedingungen, modelltechnischen Möglichkeiten und des gegenüber dem Bauherren vertretbaren Aufwandes im Kosten-Nutzen-Spannungsfeld zu wählen. Dabei muss neben der ggf. realitätsnaheren Erfassung der Gegebenheiten [z. B. 2] die Fehleranfälligkeit und der Aufwand der Datenaufbereitung bzw. Auswertung [z. B. 3] einer 3D-Simulation gesehen werden.

Anhand des Beispieles der Stirnwand einer Großkaverne [z. B. 4] werden im Folgenden die Vor-

und Nachteile eines 2D-Modells unter Verwendung bewusster Modellvereinfachungen gegenüber eines entsprechenden 3D-Modells ausgeführt.

Fallbeispiel

Die modellierte Stirnwand ist 45.0 m hoch und 30.0 m breit. In einer homogen und isotrop angenommenen Felsformation (Standfeste Zone) verläuft schräg eine Schwächezone (Gebräche Zone) mit reduzierten Steifigkeits- und Festigkeitseigenschaften. Als konstitutives Modell wird vereinfacht die idealplastische Grenzbedingung nach MOHR-COULOMB eingesetzt [5]. Das verwendete FE-Programm Z_SOIL.PC [6] erlaubt auch im zweidimensionalen Fall die Berücksichtigung aller drei Hauptspannungen über getrennt eingebbare Seitendruckbeiwerte. Die folgende Tabelle zeigt typische Kennwerte, die unter der angesetzten Überlagerungshöhe (bewusst) nennenswerte plastische Zonen erwarten lassen.

[12] Tabelle 1: Charakteristische Eingabewerte für Kontinuum

Kennwert			Standfest	Gebräch
Raumgewicht	γ_k	[kN/m^3]	27	27
Elastizitätsmodul	E_k	[GN/m^2]	10	2
Reibungswinkel	φ'_k	[°]	40	35
Kohäsion	c'_k	[MN/m^2]	1.0	0.3
Querdehnzahl	ν	[-]	0.20	0.20
Zugfestigkeit	f_{tk}	[MN/m^2]	0	0
Seitendruckbeiwert	K_0	[-]	0.50	0.50

Als Sicherungselement wird nur die Ankerung modelliert. Dazu werden ungespannte Stabanker mit einem Durchmesser von 36 mm diskret eingebaut. Die Längen werden im standfesten Fels mit 8.0 m und im gebrächen Fels mit 12.0 m angesetzt. Das mittlere Ankerraster beträgt 1.5 x 1.5 m, was an der Stirnwand die Größe der Kontinuumselemente vorgibt. Zur Simulation des Verbundes werden die Anker in 1.0 m lange Teilabschnitte unterteilt und an den Zwischenknoten schlupflos mit dem Kontinuum verbunden.

Der Ausbruch erfolgt in acht Etappen (Kalotte und sieben Strossenetappen) ohne Unterteilung in Kavernenquerrichtung. Die Anker werden nach einer anfänglichen Gebirgsvorentspannung üblicher Größenordnung aktiviert.

Das 3D-Modell ist 100.0 x 200.0 x 220.0 m groß und besteht aus rd. 35'000 Kontinuumselementen sowie 570 Ankern in der Stirnwand. Das 2D-Modell folgt dem Längsschnitt der Kaverne in Stirnwandmitte. Die Abmessungen des Modells entsprechen denen des 3D-Modells. Dafür sind rd. 2'800 Kontinuumselemente und 30 Anker erforderlich.

Der etappenweise Ausbruch wird algorithmisch dadurch realisiert, dass die entfallende Elementgruppe durch äquivalente Knotenkräfte ersetzt wird, die allmählich reduziert werden. Indem im 2D-Modell diese Stützkräfte am First und in der Sohle nicht vollständig, sondern zonenweise bis zu einem definierten Anteil reduziert werden, kann die Gewölbetragwirkung quer zur

Stirnwand ansatzweise simuliert und das Tragverhalten dem Tatsächlichen angenähert werden. Damit ist sichergestellt, dass im 2D-Modell in Längsrichtung der Kaverne keine unrealistischen Biegemomente im Hangendem bzw. Liegendem auftreten. Die Reststützkräfte müssen vorgängig bestimmt werden, entweder auf der Basis von Schätzwerten oder über eine vereinfachte 3D-Vergleichsberechnung an einem Referenzmodell. Der Aufwand dafür ist dank einfach gewählter Diskretisierung (vereinfachte Geometrie, keine Ankerung) sowie Ausbruch in einem Schritt kleiner als die Durchrechnung des vollen 3D-Modells und kann für elastisches Verhalten erfolgen.

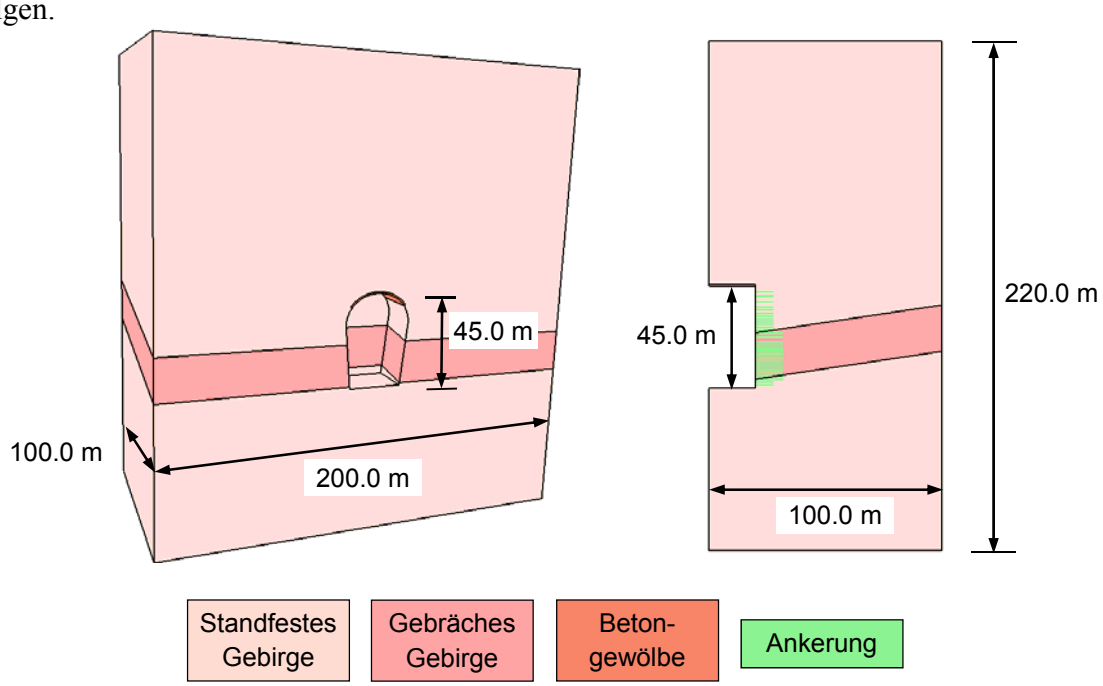

Bild 1: 3D-Modell (links) und 2D-Modell (rechts)

Berechnungsergebnisse

Nachfolgend werden die Ergebnisse des 2D-Modells mit denen des detaillierten 3D-Modells verglichen. Dazu werden die plastischen Zonen, die horizontalen Verschiebungen der Stirnwand und die Ankerkräfte im Endzustand betrachtet.

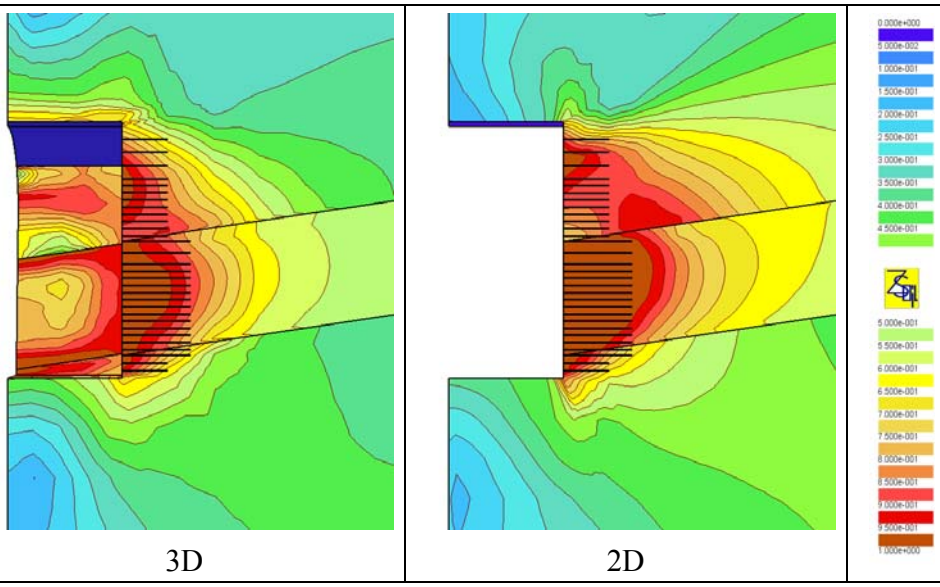

3D 2D

Hinweis: Plastische Zonen entsprechen Zonen mit Wert 1.0. Zonen mit < 1.0 sind elastisch.

Bild 2: Plastische Zone

Das 2D-Modell zeigt erwartungsgemäß eine stärker ausgeprägte Beanspruchung des umliegenden Gebirges, da die Spannungsumlagerung nur in den frontal bergseitigen Bereich der Stirnwand möglich ist und diejenige in die Kavernenparamente bzw. -eckbereiche nicht erfasst wird. Dementsprechend ist die plastische Zone der 3D-Berechnung wesentlich geringer ausgedehnt. Im 3D-Modell überspannen die Anker den Bereich der Gebirgsplastizierungen, im 2D-Modell nicht. Entsprechend größer sind im 2D-Modell auch die horizontalen Verschiebungen. Ihr Maximum ist rd. 40 % größer als im 3D-Modell.

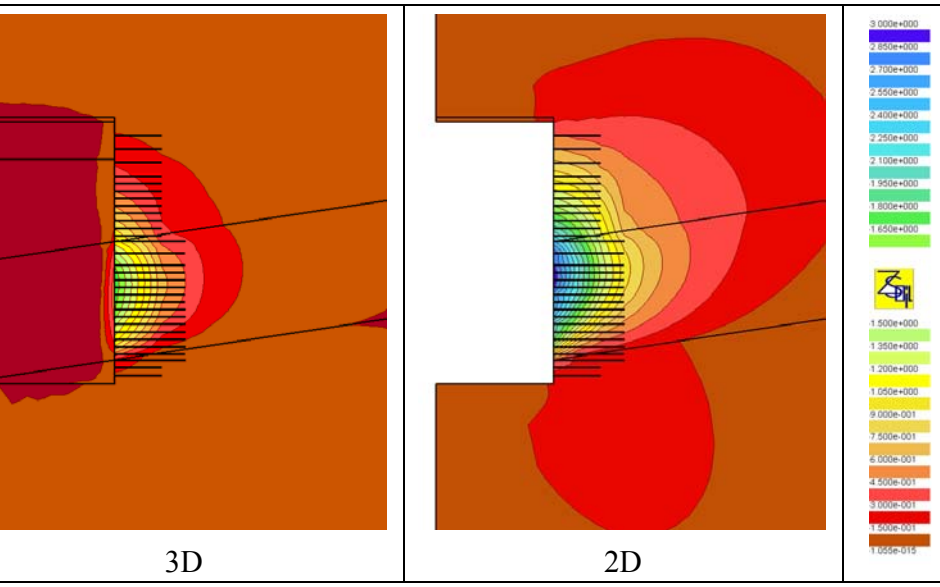

3D 2D

Hinweis: Positive Verschiebungen sind zum rechten Seitenrand orientiert.

Bild 3: Horizontale Verschiebungen [cm]

Die maximale Ankerkraft beträgt im 2D-Modell A_k = 420 kN, im 3D-Modell A_k = 260 kN, also nur rd. 60 %. Der innere Tragwiderstand wird in beiden Berechnungen nicht erreicht.

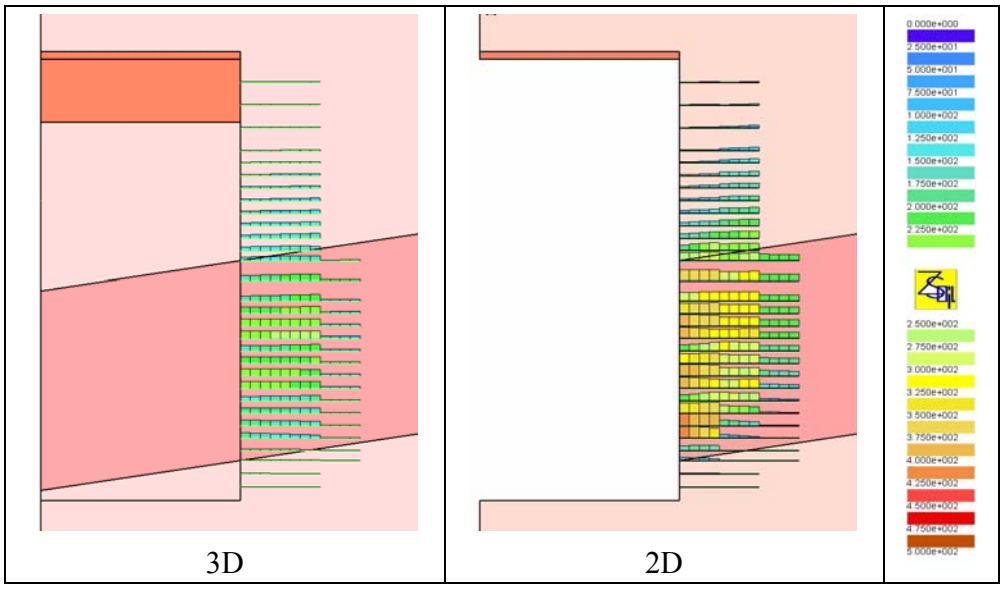

Bild 4: Ankerkräfte [kN]

Bewertung

Die Bewertung soll zunächst modelltechnisch auf Basis der Eingabe und der Berechnungsdauer erfolgen. Dazu gibt die folgende Tabelle die Anzahl der Elemente, der Knoten und Unbekannten des Gleichungssystems sowie die Rechenzeit an. Der Aufwand zur Erstellung der Modelle soll hier nicht quantitativ einfließen, da er stark von den Möglichkeiten der einzelnen Programmsysteme und dem Bearbeiter abhängt. Doch dürfte die Eingabezeit des detaillierten 3D-Modells mindestens um den Faktor 10 größer sein. Die technischen Betrachtungen am 2D-Modell beinhalten nicht den erforderlichen Aufwand für das Referenzmodell zur Festlegung der Reststützkräfte.

[13] Tabelle 2: Modelltechnische Gegenüberstellung

	3D	2D	3D : 2D
Anzahl Kontinuumselemente	35'190	2'840	12 : 1
Anzahl Stabelemente	5'776	304	19 : 1
Anzahl Knoten	44'848	3'256	14 : 1
Anzahl Unbekannte	108'538	5'680	19 : 1
Rechenzeit	4.23 h	0.06 h	71 : 1

Die modelltechnische Gegenüberstellung belegt deutlich den Mehraufwand des 3D-Modells. Es ist insbesondere die Rechenzeit zu beachten. Während die 2D-Berechnung innerhalb weniger Minuten abgeschlossen ist und somit zur Auswertung zur Verfügung steht, sind bei der 3D-

Berechnung nur wenige Iterationsläufe je Arbeitstag durchführbar. Des Weiteren bedingt das Mehr an Information aus dem 3D-Modell einen wesentlich höheren Auswertungsaufwand. So schlummern ggf. wichtige Resultate (im Extremfall unentdeckte Netzfehler) im Inneren des Modells, die von außen nicht unmittelbar ersichtlich sind und durch Freischneidung erst sichtbar gemacht werden müssen. Weiterhin erlaubt die 2D-Modellierung aufgrund des geringeren Aufwandes und der kürzeren Rechenzeiten eine kleinmaschigere Netzgenerierung. Das mittlere Elementvolumen im Bereich der Stirnwand beträgt im 2D-Modell rund die Hälfte jenes des 3D-Modells.

Die inhaltliche Auswertung soll unter zwei Gesichtspunkten erfolgen. Zum einen gilt es, mit den Modellen für die Randbedingungen und die vorgesehenen Sicherungsmittel den Nachweis der Gesamtstandsicherheit (soweit im Kontext des Teilsicherheitskonzeptes möglich) zu erbringen. Zum anderen kann mit einem FE-Modell das Spannungsverformungsverhalten analysiert, daraus ein entsprechendes Optimierungspotential abgeleitet oder das zu erwartende Verformungsbild, beispielsweise zur Festlegung von Melde- und Alarmwerten während der Ausführung, prognostiziert bzw. rückgerechnet werden. Diese Aspekte werden hier unter dem Begriff der Systemanalyse zusammengefasst.

Bezüglich der Gesamtstandsicherheit kann für beide Modelle festgehalten werden, dass auf charakteristischem Niveau infolge der numerischen Konvergenz der Berechnungen ein Gleichgewichtszustand gefunden ist. Damit lässt sich argumentieren, dass unter Vernachlässigung des Sicherheitsniveaus die Standfestigkeit als nachgewiesen gilt. In diesem Punkt führen beide Modelle zu einem gleichwertigen Ergebnis, wenn auch mit unterschiedlichen Ausnutzungsgraden.

Im Punkt der Systemanalyse überwiegen die Vorzüge des 3D-Modells. Die stärkere und weiter ausgedehnte Mobilisierung der Festigkeit im 2D-Modell führt zu höheren Beanspruchungen, größeren Verformungen und einer größeren Ausnutzung der Ankerung. Für die mögliche Anforderung einer Verankerung über die plastizierte Zone hinaus ergibt sich aus dem 2D-Modell ein erheblicher Zuschlag bei den einzubauenden Ankermetern. Überdies ist mit dem 2D-Modell keine Optimierung der Ankerung in Stirnwandbreite möglich. Die Überschätzung der Verschiebungen im 2D-Modell ist nachteilig für die Festlegung von Melde- und Alarmwerten, wenn auch aus praktischer Sicht der Unterschied der Verschiebungen in Bezug auf die Abmessungen der Kaverne und Unsicherheiten, die aus der im Allgemeinen großen Spannweite der geotechnischen Kennwerte (z.B. Elastizitätsmodul) resultieren, als gering einzustufen ist.

Schlussfolgerung

Die Gegenüberstellung zeigt, dass ein 3D-Modell unstrittig zu genaueren Ergebnissen führt, sofern ein ausreichender Detaillierungsgrad erreicht wird und programm- oder rechnerspezifische Randbedingungen, beispielsweise maximal mögliche Elementanzahl, zu keinen Einschränkungen führen. Anders als im Fallbeispiel können sehr große 3D-Modelle mit einem hohen Abstraktionsgehalt auch das Gegenteil bewirken, nämlich infolge zu vieler Vereinfachungen zu Minderkenntnissen führen. Dem genaueren Analysepotential stehen der deutliche Mehraufwand in der Modellierungs- und Auswertungsarbeit sowie die längeren Rechenzeiten, die häufig nur wenig Raum für Variantenstudien lassen, gegenüber.

Eine empfehlenswerte Vorgehensweise ist im Kontext der Projektphasen bzw. der Problemstellung zu sehen und in einem statischen Konzept frühzeitig festzulegen. Da in frühen Projektphasen meist Variantenstudien und Sensitivitätsanalysen zur Konzeptfindung bzw. Vorbemessung im Vordergrund stehen, sind hier 2D-Modelle unerlässlich. Zur Begleitung der Ausführung von Großprojekten, das heißt nach Festlegung der endgültigen Abmessungen, des Bauprogramms usw., kann ein detailliertes 3D-Modell empfehlenswert sein, um beispielsweise interaktive Einflüsse zu erfassen. Alle Berechnungsansätze sollten aber frühzeitig in einem statischen Konzept festgelegt werden, da 2D-Modelle um später ergänzte, lokale 3D-Modell an speziellen Knackpunkten meist effizienter und aussagekräftiger sind als verwässerte globale 3D-Modelle am Gesamtsystem.

Persönliche Erfahrungen zeigen, dass geometrische Änderungen in den Randbedingungen, beispielsweise in den Bauteilabmessungen oder im Verlauf geologischer Störzonen, zu erheblichem Änderungsaufwand führen, um ein 3D-Modell entsprechend zu modifizieren. Unvorhergesehene Änderungen in der Stratigraphie oder die Spannweite der geotechnischen Kennwerte können zudem zu wesentlich größeren Unterschieden in den Berechnungsergebnissen führen als die Dimensionswahl.

Literatur

Meißner H., (1991). Empfehlungen des Arbeitskreises Numerik in der Geotechnik, Deutsche Gesellschaft für Erd- und Grundbau e. V. Geotechnik, Jahrgang 14, S. 1 – 10.

Vermeer P.A., Bonnier P.G., Möller S.C. (2002). On A Smart Use of 3D-FEM in Tunneling. Proceedings of the 8th International Symposium on Numerical Models in Geomechanics (NUMOG VIII), Rome, A.A. Balkema Publishers, Lisse, S. 361 – 366.

Potts D., Axelsson K., Grande L., Schweiger H., Long M., (2002). Guidelines for the use of advanced numerical analysis. Thomas Telford, London.

Giesecke J., Mosonyi E., (2009). Wasserkraftanlagen. 5. Auflage, Springer, Heidelberg.

Chen W. F, Mizuno E., (1990). Nonlinear Analysis in Soil Mechanics. Elsevier, Amsterdam.

Zimmermann T., Rodriguez C., Dendrou B., (1988). Z_SOIL.PC: A program for solving soil mechanics problems on a personal computer using plasticity theory. Proceedings of the 6th International Conference on Numerical Methods in Geomechanics, Innsbruck, Balkema, Rotterdam.